INVESTIGATION INTO THE ROBUST MODELLING, CONTROL AND SIMULATION OF A TWO-DOF GIMBAL PLATFORM FOR AIRBORNE APPLICATIONS.

Buhle W. Bujela

A dissertation submitted to the Faculty of Engineering and the Built Environment, University of the Witwatersrand, Johannesburg, in fulfilment of the requirements for the degree of Master of Science in Engineering.

Johannesburg, 2013

Declaration

I declare that this dissertation is my own, unaided work, other than where specifically acknowledged. It is being submitted for the degree of Master of Science in Engineering in the University of the Witwatersrand, Johannesburg. It has not been submitted before for any degree or examination in any other university.

Signed this _____ day of _____ 2013

_____

Buhle W. Bujela

Abstract

The Council for Scientific and Industrial Research's Sensor Science and Technology discipline has developed a multi-sensor camera (which consist of ultraviolet, infrared and visual lenses) capable of diagnosing HV/MV power transmission lines for hot/cold spots, corona effects and visual defects of conductors, towers and pylons. This camera is planned to be mounted on a double-gimbal platform, which will be suspended on a rotary-unmanned aerial vehicle for the autonomous inspection of power transmission lines. The work presented in this dissertation focuses on the robust modelling and control of the gimbal assembly. The purpose of this is to ensure smooth and jitter-free motion of the gimbal against mechanical vibrations, sensor and actuator noise, and disturbances so that the images that are captured by the camera are not distorted. The work encompasses modelling the gimbal using the Lagrangian theory and applying Proportional Integral Derivative control,Ziegler-Nichols tuning and Integral Square Error, Integral Absolute Error, Integral Time Square Error, Integral Time Absolute Error tuning techniques, robust H_∞, Quantitative Feedback Theory and Model Reference Adaptive Control to stabilise the assembly against the aforementioned disturbances and parametric model uncertainty. The results obtained indicate favoritism towards the frequency domain robust control algorithms over the standard Proportional Integral Derivative controller, even when it is auto-tuned.

This thesis is dedicated to all the Bujela family members*, especially* Busisiwe *and* Thandeka*, for their understanding and patience through this very intense and monumental time in my life. A very special appreciation goes to* Sizanobuhle Lissa Ngidi *for her love, inspiration and unconditional support.*

Acknowledgements

The author would like to convey his profound gratitude to Mr Roel Stolper (*UAV Project Director at CSIR-SST*) for the opportunity to pursue a post graduate career with the CSIR; Nattele Maistry (*very very good friend and close colleague*) for her invaluable contribution and recommendations; Prof. Anton van Wyk, Prof. Brian Wigdorowitz and Dr. Otis Nyandoro for their assistance and constructive feedback and Dr Ali Shahdi (*CSIR*) for his time and suggestions.

Contents

List of Figures

List of Tables

Chapter 1

Introduction

The Sensor Science and Technology (SST)[1] research and development practice within the Material Science and Manufacturing (MSM) discipline in the Council for Scientific and Industrial Research (CSIR) group, in South Africa, has been developing a multiple sensor camera for the diagnosis of medium to high voltage power distribution/transmission lines for defects. The multi-sensor camera has already been developed, built, tested and commissioned. It is called the MultiCam and it is capable of detecting corona effects (observed in the ultraviolet spectrum), hot/cold spots (observed in the infrared spectrum) that occur as a result of broken connections, cracks in insulation, pollution deposits and material deterioration and any visual defects such as corrosion (observed through the day-light lens). This technology is aimed at being used by electric power utility companies, such as ESKOM and CITY POWER in South Africa, to inspect their power line pylons for structural damage. Research [2–10] discusses how important and useful power line maintenance is and highlights some of the methods implemented to recover essential qualitative and quantitative information regarding the condition of the power line conductors, insulators, pylons, steel members, and the tower structure. The pylon is a ceramic/polymer/glass insulator mounted on a cross-arm at the top of a power line structure (steel or wood pole) to support the uninsulated transmission/distribution conductors.

Current methods for inspecting power transmission lines involve holding the camera by hand and walking by foot (foot patrol), climbing and also by using a large-scale helicopter to fly over the power lines while holding the camera by hand and performing the inspection. Two problems are identified with these approaches. The first is that it takes too long with foot patrol and the inspecting individuals/crew begin to experience fatigue which compromises the results. The second issue is that to hire a commercial/military helicopter with the pilot on an hourly basis cost a lot of money, and it is approximately R16 000 for the helicopter plus the pilot. To controvert this approach, SST has now developed a miniature rotary unmanned aerial vehicle (R-UAV) to conduct the surveying of these power lines. The R-UAV is to have a two degree of freedom inertially stabilised platform (gimbal) which holds the MultiCam sensor camera and is

[1] Appendix E contain a list of all the abbreviations which are used throughout the entire dissertation

mounted underneath the R-UAV. SST intends the R-UAV with the gimbal and the camera to be fully autonomous.

1.1 Background Information

An extract from an on-line South African business report published on the 16 November 2012 that ESKOM's unplanned outages rose up to 5 480 Megawatt (MW) on November 15 from an overwhelming 4 443 MW on November 12 [11]. On the other hand, South African citizens are still being requested to save at least 10% of their power consumption in their households. The key to mitigating the problem of unplanned outages is to perform preventative maintenance; however, this requires sufficient knowledge of the status of the power lines so that maintenance can be planned ahead.

ESKOM supplies approximately 95% of South Africa's (SA) electricity and, on the global side, it supplies more than 40% of Africa [12]. Some more facts, the peak demand forecast for 2012 averaged at 31 232 MW while the available capacity sat at 32 629 MW, which only leaves a margin of 4.3%, and note that international norms is to have a margin of 15% [11]. Many blackouts occured in the Western and Northern Cape (2005-2006) and country wide (2007-2008).

Imagine a situation where one is able to inspect HV/MV power lines autonomously by simply pressing a button, which results in a UAV flying through the power line and capturing images. When it has completed this task the UAV comes back home. The following subsections provide a brief overview of the gimbal platforms that will be used to mount the camera sensor to be used for inspection purposes.

Inertial Stabilised Platform (ISP) systems have existed for more than 100 years and they are primarily utilised for pointing single or multiple (array) sensors, telescopes, cameras, and weapon systems. The application of these ISP systems has ranged across all sorts of available moving vehicles such as satellites and submarines, and they have even been applied on some hand-held and ground mounted devices. *Figure 1.1* depicts just a few of the applications of ISP devices which include surveillance, target tracking [13], missile guidance, gun-turret control, communications, astronomical telescopes and hand-held cameras[14]. The project has similar functionality to the depicted applications.

Examples of these applications include the Hubble space telescope being designed and implemented as a gyro-stabilised ISP, which is intended to point at distant stars and galaxies to within a few milliarcsec and hold the optical axis steady to a fraction of the angle to avoid blurring the magnified image. In other instances ultraviolet (**UV**), infrared (**IR**) and visible cameras are usually constantly pointed and maintained in a stable position by ISPs on ground vehicles,

Figure 1.1: Inertial Stabilised Platform applications

aircraft, ships and spacecraft for diverse missions such as scrutinizing military targets, mapping and providing high-resolution imaging for environmental surveys. Other more specialised ISPs are installed on vehicles to stabilise and point communication antennas and pencil-beam laser communication devices.

The ISP electromechanical design configuration is complex and diverse. It consists of an assembly on which, bearings, and motors called a gimbal to which a gyroscope or a set of gyroscopes can be attached. The payload, which may include a camera sensor, for stabilisation is generally mounted directly on the gimbal assembly in some configurations while, in others, mirrors or other optical elements are mounted on the gimbal and the payload-sensor is fixed to the vehicle. Typically, the pointing and stabilisation of a gimbal involves the control of its degrees of freedom in two or more axes in the Cartesian plane, and this is why most gimbal applications require at least two orthogonal gimbals. However, it is usually better to have more than two gimbals to provide additional degrees of freedom or to achieve better isolation from the host vehicle. The weight of an ISP is completely dependent on the size of the payload being suspended onto it; also the size and weight of the ISP increase as the number of gimbal axes are introduced. The main requirements for ISPs are to hold or control the line-of-sight (LOS) of one object relative to another object or inertial space. This LOS can be the centre of the field of view (FOV) of a telescope, or the orientation in which a sensor is pointed.

In essence, a gimbal is a device that can allow for the LOS of a stabilised object to be rotated and controlled while a gyroscope (gyro) is an instrument that is used to measure rotational motion in inertial space.

1.1.1 Performance Concepts

Stabilisation Requirements

Generally, an ISP attempts to prevent the payload sensor from rotating in inertial space; however this may not be sufficient, depending on the application. It may be necessary to control the sensor system in a specific manner if the goal is to obtain a clear image of a certain target object by holding the image steady within the sensor FOV without concern for the aim-point. Sometimes, if a different application that concerns a beam, such as a laser range finder, is to be directed at the target, then in this particular instance it may be crucial to hold the target exactly at the centre of the FOV, while very small amounts of high-frequency rotation or jitter might be inconsequential. In other projects it may be necessary to control both the jitter and the aim-point [13–16].

Configuration of LOS Control

It is very common to configure the ISP control system such that it has a high-bandwidth rate loop inside a lower-bandwidth pointing or tracking position loop. This method entails rejecting high-frequency disturbances and controlling the LOS, and the pointing and tracking loops are employed to remove the lower-frequency parallatic motion which includes any bias or drift in the ISP rate loop [14].

Principle of Operation

Many approaches exist for stabilising the LOS of a payload sensor such that it does not rotate relative to the inertial space; however the most used approach by design engineers is mass stabilisation [14]. The very basis of mass stabilisation is an acknowledgment of Newton's first and second laws of motion, but applied to rotational motion. Newton's first law asserts that a body does not accelerate with respect to an inertial frame unless a torque is applied; Newton's second establishes that if a net torque τ is applied to a homogeneous rigid mass that has a moment of inertia J, then the body develops an angular acceleration α as follows.

$$\tau = J\alpha = J\ddot{\theta} \tag{1.1}$$

This means that in order to prevent the object from rotating with respect to inertial space, all that has to be done is to ensure that the applied torque turns to zero. However, this becomes very difficult to accomplish when one considers that there are many sources of torque disturbances,

which can act on the gimbal mechanism and eventually cause excessive motion or jitter of the LOS[14]. Another aspect of interest is a means for controlling the object so that rotational motion can be achieved in response to an input command. This is the reason why instruments such as rate or displacement gyros are usually mounted on the object in order to measure the inertial rotation about the axes that require stabilisation and control. The gyro is implemented in a closed-loop servo system that acts against the disturbance and at the same time allow the object to be controlled from external command inputs.

The Importance of Bandwidth

In order to build a convincing insight into the properties of a complicated realistic system it is necessary to approximate it with an idealised system and analyse the characteristic response and transfer function, paying particular attention to sensitivity-to-disturbance and error qualities. The most indicative parameter used to predict the performance of a control system on its ability to follow command inputs and compensate for disturbance torque is the closed-loop bandwidth. The standard definition of bandwidth is the frequency with which the closed-loop frequency response drops to 0.707 (70.7%) of its DC value. The measure of how well the system is able to track an input command is evaluated by looking at the rate-command following error and it is reduced by a factor that is approximately proportional to the closed-loop bandwidth. The closed-loop bandwidth is also used to determine the disturbance rejection ratio, which is a performance characteristic of how well the system is able to reject disturbance torque[14].

The torque disturbance rejection ratio for Type-II control system design is approximately proportional to the squared inverse of the closed-loop bandwidth, but this is only for disturbances whose frequency content is below the closed-loop bandwidth. The dynamic characteristics of various components in the loop, such as gyroscopes and the actuators, are the ones which determine the loop bandwidth. Torsional mode response of the physical structure plays a role, but it is more prominent in a larger system[14].

1.1.2 Structural Consideration

The most challenging aspects in ISP design pertain to the consideration of structural interactions and it is quite easy for these interactions to dominate the performance if they are disregarded in the design and planning phase. There are three aspects to be considered that involve all of the components attached to the system. These are the structural characteristics of the payload, the gimbal axes and support mechanism. To commence, let us define the structural mode which should be thought of as a shape and a particular frequency at which the structural shape resonates. It's important to take note that the structural shape and frequency of a

mode is a function of the structural stiffness, damping and mass distribution. However, the amplitude of the response depends on the amplitude and spectrum of the vibration input that causes the mode to respond. The various structural dynamics to be considered and tested are introduced in the following subsection. A rigorous discussion on the mechanical composite camera gimbal construction is detailed in the research conducted in [17], and it provides comprehensive structural and material considerations for the gimbal.

Some of the important aspects of the gimbal are briefly discussed below.

Bending Impacts

The first thing to be considered is the displacement of the LOS as a result of the bending in the gimbal and payload, which can be caused by base-motion vibration and torsional responses to the gimbal actuators. This type of displacement motion of the LOS is often not sensed by the gyros, while other portions that can be sensed generally occur at frequencies that are above the frequencies that can be dealt with by the servos[14].

A very common attenuation procedure that is implemented in design practice for the LOS motion due to the bending of the mechanical structure is to stiffen the mechanical structure. However, this method alone does not suffice and other alternative design approaches are explored such as fast-steering mirrors that can be used to measure the rotational displacement and then compensate for the motion. In other instances, such as satellites that need to perform as ISPs, the main source of vibration comes from the servo actuators and to mitigate this action engineers employ precision reaction wheels to prevent the actuators from reacting against the sensitive structure. Sometimes base-motion is the main reason for the vibration; a method that is adapted to mitigate this is to provide an active or passive vibration isolation system to attenuate vibration inputs[14].

Torsional Servo Impacts

This effect pertains to the interaction between the structure and the stabilisation control. Even though this effect is completely independent of the dynamic environment, it can limit the bandwidth of the control system, which inherently affects the system performance. The resonances typically demonstrate large peaking by factors as much as 15 to 25, and as a result this can limit the loop bandwidth to 1/10 or less of the first major resonant frequency. Once again, the first approach to improve this situation is to stiffen the structure in order to modify the relevant structural transfer function. The difficulty of not being able to achieve enough stiffening makes it necessary to introduce one or more notch filters in the feedback control system to attenuate the loop gain in the vicinity of the resonance[14].

While this may prove to solve the problem of achieving sufficient stiffening, the notch filter adds another problem to the situation by adding phase lag to the loop and this limits the system bandwidth to less than about 1/3 of the first torsional resonance in spite of the filtering. As the gimbal rotates, the modes also shift in the gimbal system and this leaves the filter inactive. Many methods that involve input shaping and fluxure control are available and very well documented for controlling torsional modes in structures. However, they are very difficult to implement to the complex high-frequency modes that are typically encountered in ISPs[14].

Mounting Compliance Impacts

The mounting compliance effect is similar to the previous torsional servo impacts discussion in the sense that it involves the interaction between the control system and the structural platform on which it is mounted. However, it has no impact on the design and/or performance of the inertial stabilisation control system. On the other hand, it can severely limit the bandwidth of any positioning or pointing system that relies on feedback from the sensors that measure relative motion between the gimbal and the base structure. The gimbal actuators react against the physical structure on which they are mounted and this causes them to deflect. This deflection can be sensed by the gimbal transducer. Methods for improving the effects of this interaction include stiffening the torsional response of the mounting structure, applying notch filters in the pointing servo system and adding mass to the stationary gimbal structure[14].

1.2 The Problem Statement

Gimbal platforms are used extensively for many applications, from PTZ security cameras to the weaponised military UAVs. They are currently being adapted for surveillance purpose applications such as rescue missions, dam inspections and power line inspections. The environment in which the system operates (UAV + gimbal) is very dynamic and unpredictable to a point that the control system struggles to maintain stability and the smooth operation of the system. Extensive wind gust causes mechanical vibrations in an unpredictable manner; these vibrations effectively behave as disturbances on the system since they may alter certain commanded motions.

The complete system (helicopter + camera + gimbal platform) is exposed to all sorts of wind and rough weather conditions; also the system is subject to vibrations generated by the engine of the miniature helicopter. As a result of these issues, the system becomes unstable and difficult to control. The current method of control makes use of a hand-held RC controller and a ground pilot to control both the helicopter and the two Degree Of Freedom (DOF) gimbal.

Simply stated, *camera shake* degrades images. The main challenge is maintaining the camera

gimbal system in a particular position and orientation with reference to the ground while the helicopter is in motion or hovering to perform the inspection. In addition to this, the gimbal needs to be capable of following a specific motion trajectory for a certain type of transmission line configuration in order to inspect and diagnose the power line accurately. The coordinate system selection is important as it needs to somehow include the space coordinates and GPS coordinates of the helicopter and the transmission lines, because the helicopter UAV will rotate around the power line. The controller to be used to realise the full autonomy of the system is an autonomous flight control system (also known as an autopilot). It has been noticed that most commonly used autopilots in the industry make used of PID (proportional integral derivative) control principles to control the system; this is because classical PID has been tried and tested and has been found to be very easy to implement and tune [18].

The other challenge that PID controllers commonly experience is selecting the best tuning techniques. The tuning basically means determining the most appropriate gains which yield the desired output from the system given a particular input [19–27]. Various methods exist for tuning PID controllers, the most common being manually tuning the controller parameters, but no study has been conducted to present a comparison of the different approaches especially applied on the gimbal platform for UAV applications.

This then means that there is a requirement for a controller or control algorithm that ensures that the system performs all the commanded actions within the required time frame while rejecting all unwanted signals, disturbances and noises. Even more than this, the system is required to adapt to all the unpredictable changes that may occur while in flight.

The unwanted behavior from the external world affects the image quality of the camera. This is because the camera begins to experience jitter and distortion/blur. The reader is reminded that the main objective of this application is to be able to obtain visual images of whatever is being inspected so that the electrical engineer, or in other applications the rescue mission chief, can make a decision on what actions need to be taken. Any unwanted external influences that are not dealt with impede the operation of the system, and thus impact on the final decisions.

This challenge with unwanted disturbances can be categorised as follows: there is the robust stability aspect and the robust performance. To guarantee both, or a satisfactory balance of the two, all disturbances and noise signals from the sensors need to be rejected and/or suppressed. The other problem that most researchers do not realise is that mechanical assemblies are constantly changing and being reproduced in smaller dimensions and weight; however, this then requires that the control engineer be hired to re-programme the controller so that it works with the new platform specification (inertia, weight, dimensions, etc.) and this is an additional exorbitant unnecessary cost. Also, many of the standard control algorithms that are being widely used implement constant gains or constant parameter transfer functions. These are Proportional Integral Derivative (PID) and Linear Quadratic Regulator (LQR), to name a few.

Robust control algorithms have been developed and motivated by problems experienced by UAVs during testing and deployment; however, these algorithms have not been applied in gimbal platform control. The reason is because many of the robotic engineers or researchers perceive the control as simply being able to command/drive the servos/motors to rotate in a certain direction at a particular speed and at a particular angle.

The algorithms that have been tested by researchers on UAV platforms include but are not limited to LQR, Linear Quadratic Gaussian (LQG), H_2, H_∞, Quantitative Feedback Theory (QFT), advanced self tuning techniques for PID, Neural Networks and adaptive control [28].These algorithms have not been extensively implemented on the gimbal control problem.

1.3 Overview of Intended Airborne Inspection Procedure

Conventional inspection methods for power lines include the foot patron and climbing inspection [4]. The disadvantage that comes with foot patrol is that little qualitative information is obtained relating to the condition of the insulators, fittings and steel members higher up the tower structure. While climbing inspection can provide greater detail concerning the condition of the structure, however, it comes at a greater cost and inconvenience owing to safety and electricity supply isolation. For example, when dealing with a dual circuit tower, it is necessary to de-energise and inspect each tower separately, which makes it necessary to return to the same tower on two separate occasions in order to climb and inspect each side. The airborne inspection procedure that is implemented by ESKOM is illustrated in *Figure 1.2*, and can be explained as follows, the helicopter lifts off from the ground and flies to a pre-defined location around the power line tower to hover while video images are being taken of the power line pylon. Bearing in mind that the the field of view (FOV) of the MultiCam camera sensor is relatively small (10°), the helicopter will have to travel around the power line tower in order to obtain different views around the power line. This is also done in a very neat and safe manner so that zero contact is maintained with the MV/HV power line cables. The development and deployment of UAVs for power line inspections is an interesting area of research for many researchers [7–10, 29–36] who investigated the development of a robotic system for the maintenance and inspections of power lines using brachistochrone motion to move along the power line.

The research in [37] elaborates on the sightline for the camera when being applied in overhead power line inspection. The concerning principal difficulty is the degradation of the images captured by the camera as a result of the motion of the camera sightline. These researchers recommend optical stabilisation of the order of 100μr for satisfactory inspection detail. One of the problems with having a camera operator on board a manned helicopter to control and stabilise the sightline is that the operator soon suffers from fatigue and becomes disoriented and loses the object being inspected. This leads to difficulty in identifying which section of the

power line is in view and, in some cases, the operator can be affected by airsickness.

Typically, the complete transmission/distribution network will be inspected by foot patrol on a four-year cycle. Also, helicopter patrols are performed on a four-year cycle; however, they are alternated every two years with the foot patrol. This effectively means that a line will be inspected by one method or the other every two years.

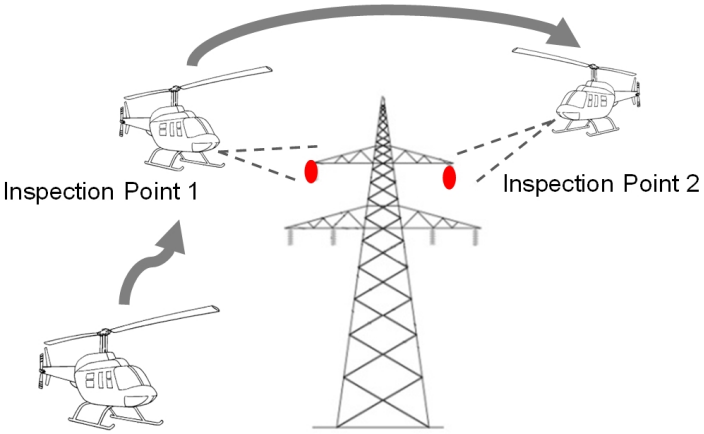

Figure 1.2: Eskom inspection protocol.

The images taken by the camera are presented in *Figure 1.3*. From the visual lens all visual defects can be observed, and through the infrared lens all hot/cold spots can be viewed while the corona effects are observed through the ultraviolet lens. These images and saved videos are then used by the engineer post inspection for analysis so that a decision is taken on whether maintenance is necessary and which type. This is beyond the scope of this study.

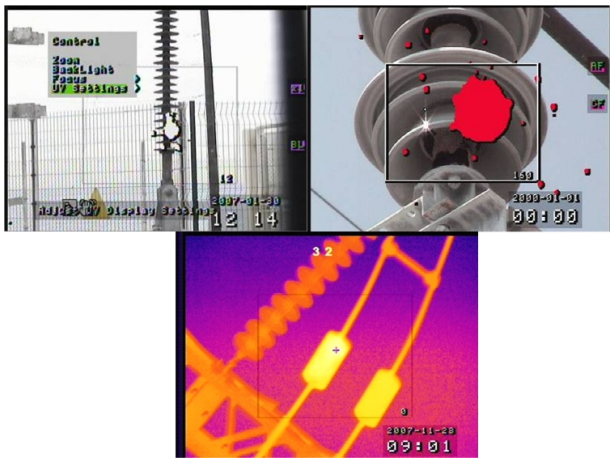

Figure 1.3: Three views from the camera sensor, visual, infrared and ultraviolet spectrum

Figure 1.4 presents a Computer Aided Design (CAD) drawing of the 110 cc petrol motor (located on the nose) that is rated at 11.2 Hp helicopter with the 2-degree-of-freedom gimbal(hanging

between the two legs) suspended. The details of the helicopter falls outside the scope of this study.

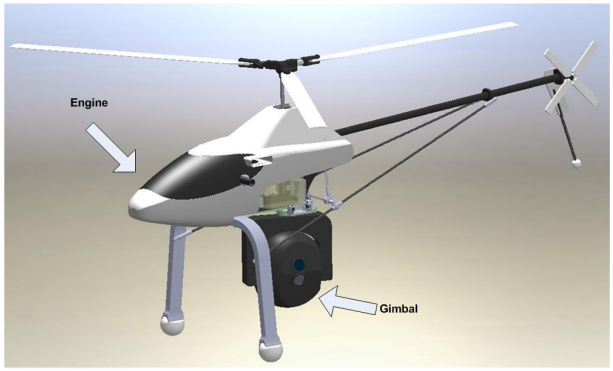

Figure 1.4: Artist impression of the helicopter and the suspended gimbal platform

The camera sensor that has been developed, commissioned and commercialised at the CSIR is shown in *Figure 1.5*, and it is this camera which is held by the gimbal platform and rotated.

Figure 1.5: Commercialized MultiCam camera sensor.

In closing, consider this very interesting projection which is a product of some of the team debates, the future of inspection protocols might involve inspections shown in *Figure 1.6*. However, can you imagine the life policy cover that will have to be taken for the men performing the inspection? This form of inspection is rather unrealistic; a more accurate forecast would be to replace the human being with a robot, since we are approaching a man-machine universe.

1.4 Problem Scope

With a project of this magnitude it is very important to narrow down and explicitly define the scope of research at a master's degree level. The work that is currently being researched by SST at the CSIR involves developing an algorithm to be used in conjunction with an autonomous flight control system for the helicopter and the attached two-DOF gimbal platform to inspect the high voltage power transmission lines. The algorithm would also need to provide additional stabilisation against vibrations on the platform and excellent disturbance rejection performance

Figure 1.6: Futuristic view of inspections performed on power line pylons.

characteristics. Some control mechanism would also be required to ensure that the system follows the commands from the algorithm and to maintain stability at all times. Sensors are a huge necessity since in order to practically realise the feedback control loops fully, the outputs and disturbances have to be measured and fed back to the input to minimise the error and improve performance.

The scope of this study is limited to the algorithm development and control of the inertially stabilised two-degree of freedom gimbal platform. As mentioned earlier, the purpose of the gimbal is to navigate the mounted camera so that accurate images of the transmission lines can be captured. The possible motions available from the gimbal are the pan rotation (rotation along the z-axis) and tilt rotation (rotation along the y-axis). The user specifications for the camera are set out below.

With the aid of a certified pilot and a ground control station, the inspection crew should be able to view the transmission line conductors, pylons and towers in the computer workstation for analysis of the defects. The images they are looking for are observed in the ultraviolet spectrum for corona effects and in the infrared spectrum for hot spots, broken/loose connections, cracks in the insulation and pollution deposits. The algorithm will be implemented in a microprocessor, which will then be attached to the main autopilot hardware through a USB port connection or an RS-232 port so that it can be executed within the main control loops during flight.

The technical specifications of the gimbal hardware platform and the camera are summarised in *Table 1.1*.

Table 1.2 summarises the gimbal platform specification

From the technical specification presented in *Table 1.2*, the following control specifications can

Table 1.1: Camera technical specifications

MultiCam Camera Specifications	
Description	**Specification**
Dimension	275 mm(ℓ) × 155 mm (h) × 165 mm (w)
Mass including battery	2.7 kg
UV Spectrum	**UV Spectrum**
Focus range	2 m to ∞
Image type	Monochrome video CCIR
Sensitivity	$8\times\ 10^{-18}\ Watts/cm^2$
Field of view	8° Horizontal × 6° Vertical
IR Spectrum	**IR Spectrum**
Image type	Uncooled Microbolometer
Sensitivity	50 mK
Range	0 - 250 deg
Field of view	8° Horizontal × 6° Vertical
Visible Spectrum	**Visible Spectrum**
Image type	Colour video, Full function
Field of view	8° Horizontal × 6° Vertical
Gain	Automatic or normal for back-light suppression

Table 1.2: Gimbal platform technical specifications

Gimbal Specifications	
Description	**Specification**
Stabilisation	$<$ 200 μm
Azimuth freedom	360° continuous
Elevation freedom	+10° to -110°
Payload mass, including camera and electronics	$<$ 9 kg
Dimension	700 mm(ℓ) × 460 mm (h) × 475 mm (w)
Modes of operation	Stabilisation, Stow and Shutdown mode
Frequency for the man-machine interface	433 MHz

be derived and the autopilot and associated algorithm and control loops have to adhere to the following specifications in order for stable performance to be achieved:

- The typical minimal mechanical stabilisation angular movement to be opted for is in the range 10-100 μrad.
- Minimum Pan/Tilt speed available of 0.05 deg/*sec*.
- Maximum Pan/Tilt speed available of 360 deg/*sec*.
- Pan range of 360° continuous.
- Tilt range of +10° to -110°.

The aforementioned control specifications will allow for the high quality of images to be recorded by avoiding jitter and distortions. The level of complexity on this project is high and as a result the work on the helicopter control and gimbal control has been split between two master's studies (conducted by the researcher and a colleague from University of Johannesburg (UJ)), as depicted in *Figure 1.7*. This study presents work that has been carried out on the gimbal platform alone.

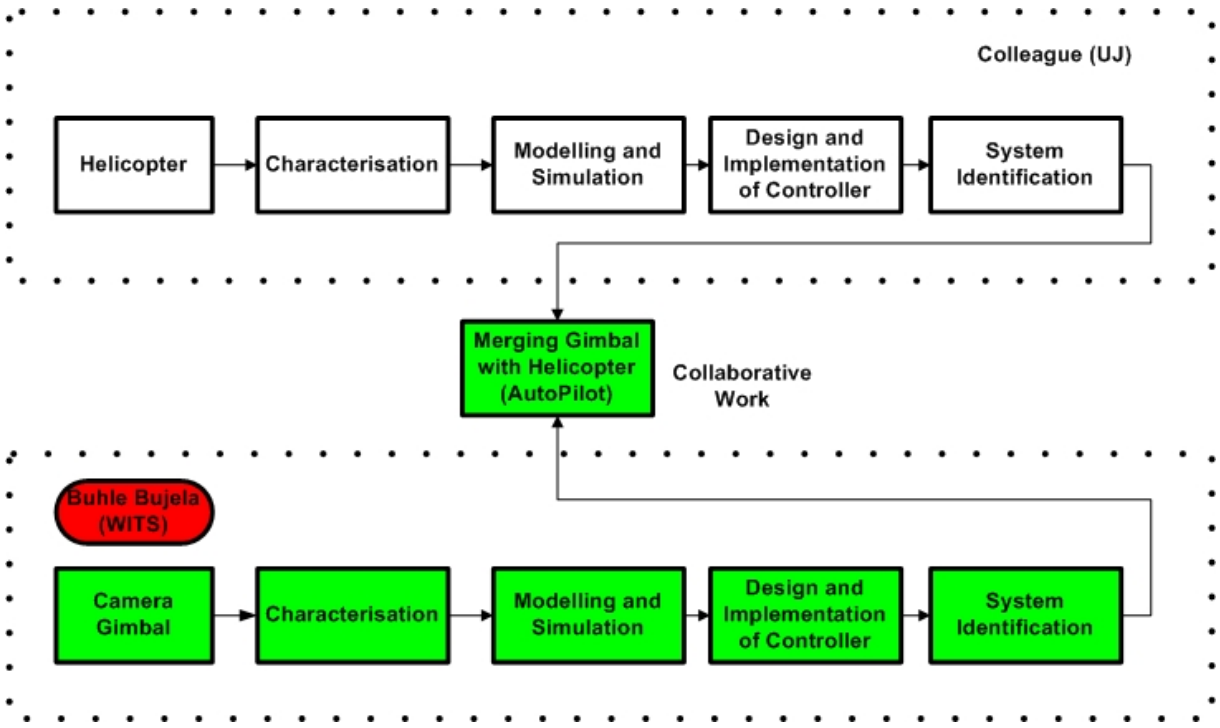

Figure 1.7: Work division for the UAV masters project

1.5 Research Objective

The research objective is to model a two-DOF gimbal platform using two different methods so that they can be compared to one another for verification purposes and to verify consistency. The one method needs to be an analytical method (such as Lagrange) and the other method needs to be a physical system-based approach (such as a CAD drawing of an actual system and translating it into a workable model in simulation).The analytical method is the main method of interest, and the physical system-based approach model is intended for visualisation aid and performance verification.

The second objective is to design a PID controller for the plant model, and control it as a regulator or tracking problem. In other words, the objective is to ensure that the plant (2-DOF gimbal with camera) system either locks on a pre-defined rotational position/velocity or tracks a reference trajectory. The important features here are how fast the system rises to the command, how long it takes to hold or lock on the location, by what fraction does it jump beyond what it is required to do and lastly the steady state error (difference between commanded position and actual position). The choice for PID is motivated by the fact that most autopilots use the PID structure in their control algorithms, and also because it is a tried and tested benchmark control which is used by 95% [38] of the industry. The next step is to apply auto-tuning algorithms to tune the control gains of the PID controller. This is required because manually tuning the PID controller is achieved by trial and error, which is very time consuming. Also, it is not robust because it is not able to cope with the dynamic environment since it has to be tuned off-line. By implementing an auto-tuning mechanism on the PID controller, off-line tuning is essentially mitigated and the controller is made more robust at the same time.

The third objective is to design robust control algorithms and apply them to the gimbal plant, and compare the robustness and performance to the former control approach. The reason for robust controllers is that they are able to cope with a dynamic environment since they are designed specifically to cater for the unpredictable nature of the environment. The robust algorithms to be tried are H_∞, QFT and adaptive control. The robust control algorithms are also compared against each other and the best one is recommended.

The final objective is to verify and validate the performance on a physical platform and test concepts such as repeatability, precision and disturbances.

1.6 Thesis Statement

In light of the above, the *thesis* of this work is that the robust modelling and control of a two-DOF gimbal platform can guarantee superior robustness and performance of the system in the presence

of disturbances and noise signals so that clear and useful images can be obtained on the mounted camera sensor. This robust design approach is necessary because the helicopter to which the gimbal platform will be mounted is unstable with many identified mechanical vibrations at various modes and wind forces that act on the system. The gimbal suspension system acts as a damping mechanism to reduce/eliminate the effects of these forces and associated mechanical vibrations on the camera sensor so that it can take images while in smooth operation.

1.7 Research Approach

To commence the research a thorough literature review was conducted on UAVs, inertially stabilised platform modelling, and control techniques to gain a global insight into the overall system and its behaviour. The various approaches were scrutinised until a more suitable and optimal solution was found. A mathematical representation of the system was developed and all the associated parameters were investigated to discover methods of how to measure and quantify them. Once the equations were ready, a model was developed and implemented on **Matlab**, using several toolboxes from **Simulink** so that the system could be simulated and preliminary results analysed.

The gimbal platform to be modelled is presented in *Figure 1.8*, and it is mounted as a suspension mechanism on the helicopter. This is how the complete system is intended to look when it flies over transmission lines. Once a satisfactory model of the gimbal was obtained a controller for the system was investigated and implemented. Initially a conventional basic PID controller was implemented and then improved during simulation and analysis of preliminary results.

More robust controllers such as the H_∞ were implemented and compared to the PID performance characteristics.

1.8 Constraints and Assumptions

In this section the three relevant constraints identified and assumptions made during the course of this project are listed and discussed.

1.8.1 Constraints

The constraints identified during the project regarding the inspection of power lines using visual cameras are as follows:

Figure 1.8: R-UAV with the camera gimbal attached

1. ESKOM regulations prohibit the helicopter and/or UAV from getting closer than 10 m to the power line tower, conductor and pylons. This is to prevent any possible Interference with the continuity of the electrical supply to ESKOM customers.

2. The camera field of view (FOV) is 10°. This is how the CSIR team decided to design the camera based on their limited resources.

3. There is no image/frame grabber mechanism with computer terminals for image feedback; this could be useful for tracking a point in space.

1.8.2 Assumptions

After reviewing the first constraint, adapted from ESKOM guidelines for power line inspections, the need for range tracking was dismissed. To elaborate further, when tracking point objects using cameras in space, range becomes an important factor for the following reason: the farther away the object is, the smaller the angle that needs to be moved by the gimbal platform; however, the closer the object, the larger the angle to be travelled.

Other assumptions that were made are:

1. The camera settings do not form part of the control algorithm, since these are left for the engineer's discretion.

2. The control algorithm being designed is independent of the control algorithm for the helicopter (this is part of another research project).

3. The control algorithm serves two purposes, one is robust stabilisation against external influences and the other is robust performance to satisfy the specifications.
4. The space coordinate integration will be handled by the autopilot algorithms.
5. The airspeed is constant.
6. The average wind speed and direction are known.
7. The altitude of the highest point in the power line tower is known and constant.
8. The gimbal platform structure is rigid, not flexible.
9. Joint axes are orthogonal.
10. Static friction is neglected and viscous friction is linear.

1.9 Delineation and Limitations

The delineation and limitations of this study are as follows:

- This study does not deal with the modelling and development of control algorithms for the helicopter UAV; this is a subject of another concurrent study.
- This work does not include the integration of the gimbal control algorithm with the autopilot.
- This work does not include the image processing of the videos/photographs obtained by the MultiCam camera sensor. The author is fully aware that to improve the tracking ability of the system, one would use the point pixels captured by the camera sensor as feedback and move the gimbal based on what is seen by the camera. However, the camera that is available and being used in the research group does not possess such capabilities.
- The author is also aware that when dealing with tracking objects based on the image pixels received from the frame grabber of the camera sensor, range distance often becomes a concern. This is because the closer the object is, the larger the angle that the gimbal platform has to move, and the farther away it is, the smaller the rotational angle to be moved. As stated above, this is not dealt with in the study.
- This study does not include a modal analysis of the gimbal mechanical platform.
- This work does not include a detailed method of producing the CAD mechanical drawing of the gimbal system; the drawing is simply borrowed from a colleague and acknowledged accordingly.

- This study does not include any flight test results obtained from the group project, as they are not relevant.
- The official group project gimbal could not be used for any verification and validation tests because it is an outsourced assembly and can only be driven (controller) via a pre-configured radio controller. It also has no feedback mechanism for angular position or velocity.

1.10 Success Criteria

For the project to be accomplished successfully, the following procedure needed to be carried out. An analytical model of the gimbal had to be derived and modelled on a computer simulation software, **Matlab**, and its parameters understood. A control algorithm had to be derived and tested on the gimbal plant for both robustness and performance.

When the gimbal platform can be commanded to lock on a particular position/location or follow a pre-defined trajectory, while rejecting all disturbance and suppressing all noise signals from the sensors, then the project can be considered a success. This performance will be measured by assessing the time response and frequency response for the rise time, overshoot, settling time, peak time and steady state error.

A final criterion is that a method be proposed for the system to be verified and validated on the hardware in real time to check consistency and repeatability of the algorithm.

1.11 Contribution to Academia

The originality of the work presented in this dissertation stems from applying the robust modelling and control algorithms in a gimbal platform application, since this has not been carried out before as can be seen from the highly detailed Institute of Electrical and Electronics Engineers (IEEE) literature review conducted by M.K Masten and J. Hilkert, both in 2008 [13, 14].

1.12 Dissertation Outline

The organisation of the dissertation is as follows: Chapter 2 contains detailed literature review on the application of gimbal platforms. A background on the deployment of gimbal platforms on UAV surveillance applications is also provided in this chapter. A literature review is provided

on the control algorithms used, and these are the PID controller plus its associated auto-tuning algorithms, H_∞ controller with the associated tuning weights, QFT and adaptive control.

Chapter 3 discusses the methodology which is followed throughout the research and the resources (software and hardware) that were used to successfully complete the research.

Chapter 4 presents the modelling of the actuator mechanism, the gimbal platform and the sensor mechanism. The modelling of the gimbal is divided into two approaches: the analytical representation which follows the Lagrangian design approach, and a physical system-based modelling approach.

Chapter 5 discusses the controller design and implementation for the PID controller and its associated auto-tuning algorithm, H_∞ control, QFT and adaptive control. The performance measure characteristics such as the speed, acceleration, accuracy and resolution, are discussed in this chapter. Concepts such as robustness and model uncertainty are also presented when the robust control algorithms are introduced.

Chapter 6 presents an analysis of all the results obtained from the model and control simulations. A detailed comparison of these results is also presented and some preliminary conclusions are drawn. A thorough critique of the results is presented, with all the trade-offs listed, and recommendations and suggestions for future work provided. The proposed experimental set-up for the verification and validation of the control algorithms is presented here.

Chapter 8 highlights some of the critical conclusions reached from the modelling and control simulation results

Supplementary information is contained in the appendices. Appendix A compares all the available advantages and disadvantages of the actuators, transmissions and sensors, while Appendix B presents the detailed Lagrangian analytical modelling of the gimbal platform. Appendix C discusses the project management aspect of the study while Appendix D discusses the financial considerations and overall cost of the project.

Chapter 2

Literature Review

2.1 Introduction

UAVs, rotary [39] or fixed wing, are useful for a variety of applications that range from civilian to military [40]. These applications extend to known and unfamiliar [41] terrain, where gimbals or inertial stabilisation platforms [16] and their extensions play a critical role. Gimbal stabilisation and control has always been a concern for many applications [42–44]. This includes the film and broadcast industry, where cameras are intended to capture moving objects and small disturbances affecting the camera when it is in motion can cause images to be blurry and jumpy [45]. In 1976 the Steadicam was introduced by the Cinema Products Corporation; this is a pan only inertial stabilisation gimbal platform with no gyros and it is generally strapped to the camera man for horizontal motion.

2.2 Previous Work

The complex exploration of UAVs in indoor applications has been the subject of investigation for many researchers. B. Michini in 2009 [46] particularly investigated the modelling and adaptive control of these platforms specifically autonomous ones which are subjected to the constraints imposed by indoor environments. Hald et al. [39] present a detailed discussion on the modeling and optimal control of an autonomous helicopter.

Griffin and Beach [47] discusses a gimbal test stand to be used to facilitate the development of autonomous robot helicopters. They present an indoor gimbaled flight test bed. The motivation for their work came as a result of the limitations posed by the free flight tests that are required to be performed outdoors for Radio Controlled (RC) helicopters. The first limitation is weather condition, and the second is the primary requirement for a skilled (in some countries licensed) pilot at all times, and even then it is still possible to experience unavoidable crashes. Their

gimbal test stand has three-DOF motion, the yaw, pitch and roll, which satisfies rotational motion for any helicopter. An important observation is made regarding the singularity of the joints; this is also referred to as the *gimbal lock singularity* and it occurs when two joints become collinear, making one of the joints redundant and reducing the degree of freedom of the system. This is something to look out for during the design stage.

A few patents [48, 49] were discovered during the literature review, which concern the gimbal platform being used as a stabilisation for sighting devices for vehicles or simply as an optical inertial system. Yonemoto et al. [50] presents an additional practical application for an obstacle detection and collision warning system for UAV civil applications. Their application is for power transmission lines and they use a colour camera and an infrared camera to develop the system.

Gimbal platforms and their motor drive configuration have been the subject of investigation for a number of years by many researchers such as Bederson et al. [51], who investigated the pan-tilt configuration which would result in a system which is fast, accurate, small and inexpensive. The investigation paid close attention to the actuators. It should be noted that during the early 90's, very few companies manufactured and sold (off-the-shelf) two-axis gimbals for computer vision applications.

Another key factor, which is explored in [52] by Otlowski, is the mass properties and how they affect the stability of gimbaled imagery platforms. Otlowski et al. mention that when the centre of gravity (CG) of a gimbal platform is not coordinated properly (*aligned*) with the torque motor axes, then all the undesired moments developed under vibrations due to the dynamic environment will disturb the stabilisation control. This then affects the pointing accuracy and ultimately causes imagery jitter in the camera. Stabilisation is achieved when the CG is aligned. They note that the best method to deal with this issue is by implementing physical balancing of assemblies, as it transcends all other stabilisation methods, since they are compensation techniques. When it is implemented in the correct way it allows the designer the advantage of managing the mass and power budget by utilising smaller torque motors.

A relevant application is presented in [53] by Tiimus and Tamre, which demonstrates a valuable design process as follows. The process commences with the basic underlaying concepts, then its design and modelling. From there it splits into two components: prototyping and a bidirectional connection to troubleshooting and re-designing. Finally the last step is the testing phase which involves a connection by a bidirectional arrow. For their system they use gyros with Attitude and Heading Reference System (AHRS) for the UAV, DC geared motors with integrated incremental encoders and modular ultra high resolution miniature incremental encoders for the three-axis camera gimbal platform. It is noted that the two main aspects concerned with motion control and which have similar tasks are position feedback and position reference data. Feedback provides the actual position of the mechanism and reference data indicates where the mechanism needs to be. Gimbal lock is stressed as something to be avoided. The authors also note the main sources

of vibrations from the helicopter are the main rotor, tail rotor, electric motors and transmissions.

The Swedish Defense Research Agency (FOI) [54] presents an image processing geared sensor management architecture for UAV infrared/Electro-Optic (IR/EO). Its gimbal platform is used as an experimental geo-referencing sensor platform. It is identified in this literature that the gimbal control is divided into two major groups: scanning and tracking. In scan applications, the gimbal is controlled to point at desired coordinates, which are expressed in either a global or local reference frame. In tracker applications, the objective is to keep a number of targets in the camera FOV simultaneously or switch between targets that are not simultaneously in the same view. It is noted that they chose to model the gimbal platform using the Lagrange approach. The work that is presented by Broilo [55] represents recent and similar research into the subject of gimbal modelling and control for aircraft applications. His work is, however, not very analytically driven in terms of the derivation of the equations governing the model of the gimbal, and the control laws chosen do not add a lot of robustness into the system.

The full details of the modelling and control of the IR/EO-gimbal utilised for UAV surveillance and reconnaissance applications is presented in the Skoglar's masters thesis [56]. The Signal Processing for moving IR/EO Sensors (SIREOS) projects, which is conducted at the Swedish Defense Research Agency, is concerned with the development of a sensor system that consists of an infrared and video sensor and an integrated navigation system to be used in conjunction with a UAV. The Agency's sensor system is mounted inside a four-axis gimbal platform, which is then suspended in a UAV. They define a gimbal as being a device which makes it possible for the sensors to point in any desired direction.

The Agency's gimbal consists of two outer joints and two inner joints; the outer joints which, are motor driven, represent the pan and tilt rotations. Inside the outer axes, they then mount the camera sensors in a two-axis inner gimbal. The main reason for this is to damp out and prevent high frequency mechanical vibrations from reaching the cameras and causing blur in the images. Note that they used digital encoders to measure the pan and tilt rotational angles and optical angle sensors to measure the angles of the inner gimbal mounting the cameras.

A dynamic kinematic model of the gimbal is presented and it is based on the robotic kinematic manipulator modelling theory such as forward, inverse and differential kinematics. The Denavit-Hartenberg (D-H) convention is also used to derive the dynamic differential equations for the system in conjunction with the Lagrange approach. In the thesis, Skoglar goes through a very detailed method for the development of the gimbal trajectory planning. This is necessary because he is considering multiple applications such as scanning and tracking. He then develops the gimbal trajectory planning algorithm to transform the different reference signals from applications to a camera orientation reference signal that can be used as the input to the gimbal platform controller.

He observes that that the gimbal system is a multi-variable system; however, to simplify the control implementation he assumes that the control of the two outer joints is *decoupled*. This then allows him to view each actuator to influence one specific degree of freedom; in other words, the systems are simplified to single-input single-output (SISO) type systems. The coupling effects, if any, are then viewed as external disturbances to the system under control consideration. Another possible approach for dealing with coupling effects is to apply a feedforward compensator torque based on the knowledge of the dynamics.

A note is made regarding the anti-windup phenomenon when applying the PID controller for his regulator controller. This phenomenon characterised by the output signal taking too long to reach the reference signal, and it is caused by the control input being sometimes saturated. The integration of the gimbal plus UAV was not undertaken here and, although acceptable results were obtained via the PID controller, it lacked robustness. This is also seen from his conclusions.

Two-axis-gimbaled cameras have been applied in a vast area of applications; Monda et al. [57] discuss one particular application concerned with the development of a framework for ground target localisation and tracking in a riverine environment using a UAV that mounts this gimbal. The method employed is localising the object from the target object pixel coordinates in the images which are captured by the camera. One of the useful assumptions made is that since the UAV is operating in a riverine environment, the altitude of the target on the water is known and taken to be constant (0 if at sea level). This then solves the problem of dealing with range ambiguity when trying to localise or track non-collaborative targets over unknown terrain. In their application the authors used a UAV that has a GPS-IMU autopilot, which is similar to the Cloud Cap Technology Piccolo, essentially to relate the measured visual pixel coordinates of the target object to the aircraft position and orientation. Suffice to say that they had the luxury of state-of-the-art camera technology with feedback and an autopilot infrastructure to be able to track moving objects.

Research conducted by [58–69] discusses a similar application where a nose-mounted two-axis camera which is capable of pan and tilt motion is attached to a UAV and used for the observation of ground targets. These studies also applied the same assumption regarding the altitude of ground targets, which is taken to be constant. In their application, of UAVs for airborne surveillance, they develop a flight path guidance algorithm for the UAV to optimise target exposure on the camera field-of-view. These studies note that while the actuators installed on the camera may be fast enough to keep up with the UAV motion, the limited range of the camera angle leads to the target moving out of sight. Its also mentioned that target exposure is affected by wind and the relative position of the sun can lead to glare and image overexposure. To mitigate this, it is suggested improving the effects of wind by commanding a sideslip angle and avoiding image overexposure by keeping the UAV between the sun and the target. They also apply an autopilot system for inner control loops of the UAV and gimbal, which then allows

them to focus on the design of the path-following algorithm.

The aforementioned applications utilise image processing techniques to track or localise ground objects by using a pan-tilt gimbaled camera suspended on a UAV. Another such application is presented in Sharp et al. [70] which extends the degree-of-freedom by using a Pan/Tilt/Zoom (PTZ) camera to design and implement a real-time computer vision system for a rotor-craft UAV to land onto a known landing target. They used the Yamaha R-50 helicopter, and customised vision software to estimate the pose (position and orientation) and speed of the UAV relative to the known landing target. It is also noted that they too used a state of the art frame grabber (*Imagenation PXC200*), camera (*Sony EVI-D30*) and navigation system with superior software for low level control of the UAV and gimbal platform.

The Georgia Tech UAV Lab actually has a very similar project that it is running using its in-house developed UAV helicopter (GTMax) [71], which is based on the Yamaha R-max airframe. Its UAV has a nose-mounted Pan/Tilt/Roll camera gimbal, as presented by Jakobsen and Johnson [72]. The controller has three modes of operations: it can keep the camera at a fixed angle with respect to the UAV, it can also make the camera point in the helicopter UAV velocity vector and lastly it can track a specific location. The project's specific focus is on imaging algorithms for tracking moving targets, obtaining live visual feedback while in flight, and automating landing on moving platforms.

The Lab has a very light weight gimbal platform which it purchased from *Neural Robotics*. To drive the respective gimbal axis of rotation the researchers used the *Hitec* servos [73], modified to take velocity as command inputs. The gimbal system axis of rotation is configured in the following manner: there are no limitations on the rotational angle for the pan axis, the roll axis is limited to between -100° and $+100^{\circ}$ and the tilt axis is limited to -90° to $+90^{\circ}$. For the measurement of angular rotational motion the incremental encoders from *US Digital* were used. It is noted that the velocity commands are given at a rate of 50 Hz, and the angles are being read at the same rate. They use an integrated navigation system to estimate the UAV's position, and attitude which are needed when the controller orders the camera to point at a specific location.

It is interesting to note that they chose to use a PID control algorithm to implement the low level part of the control, and its output is the velocity command to each servo motor. They also make a valid note that the payload experienced by each servo motor is different from the others in their rotational axis. The load experienced by the pan axis motor is much larger than that of the other motors, and this is because the other gimbal axis (tilt and roll) form part of the payload, since they are contained inside.

The aspects which link the GTMax [71] project to this study are their gimbal, servos, encoders and control system. It is noted that instead of building their own gimbal, the GTMax researchers

decided to opt for a light weight, inexpensive off-the-shelf gimbal solution. Light weight allows for ease of control using easily accessible motors without many demands in terms of power requirements and torque. The researchers have a total of 24 cables which are fed through a slip ring for the three servos, three encoders and the video camera. The slip ring allows for an unlimited number of rotations about the pan axis. One should be aware that depending on where the servos are mounted, they can create limitations for the rotation of the other gimbal axis.

The research engineers also chose to use the JR 8311 Hitec servos, one for each axis of rotation. These servos offer a maximum of 130 oz/in and a maximum speed of $0.18s/60°$. The conventional servos accept position as an input; however, it is noted that in their application they decided to modify the servos to accept velocity as an input instead. It is also noted that by setting a suitable gear ratio on the gimbal/motor, a desirable speed can be achieved for any of the rotational axes. Their pan axis is capable of a maximum speed of rotation of 80 deg/s, while the tilt is 40 deg/s and the roll is 29 deg/s.

The encoder chosen to use is the *H1* encoder from *US Digital*. This encoder has a resolution of 1024 CPR and X1 decoding is used. Encoders operate in the following manner: they output signals on three channels, A, B and *Index*. Channel A and B provide quadrature codes used to determine turn direction and calculate encoder shaft position. The Index channel outputs one pulse for each encoder revolution.

As mentioned before, the choice of control law that is implemented is a PID, and it takes care of the velocity signal to the servos. However, the researchers do not deal with model uncertainties and disturbances explicitly through the control design and implementation. A self-tuning PD controller has also been investigated by Shiino et al. [74] which is based on the generalised minimum variance control law for the computation of the PD parameters, and it was applied to the three-axis gimbal platform which mounts a camera. They used the least square method to estimate the system parameters of the gimbal. Kawada et al. [75] proposes a data-driven PD control algorithm for the gimbal with considerably good learning efficiency compared to standard neural network and genetic algorithm methods. The PD parameters are updated based on a database which is generated using the generalised minimum variance control (GMVC) algorithm, and the researchers were able to verify the results by performing experiments on their gimbal platform.

The approach that is presented in this study takes the route of dealing with model uncertainties, sensor noises and disturbances at the design stage of the controller.

Gimbal modelling [43, 44, 76–79] is a very important aspect of the project, as discussed in Singh et al. [80] in which the main focus is on a well-designed gimbal assembly to reduce jitter and optimise the line-of-sight so that at least the control system can be made much simpler and less

robust. The attenuation is achieved via the structure and bearings. Particular attention is paid to resonance, friction and inertia.

2.2.1 Gimbal Control

Seong et al. [28] present the approach of robustly controlling the gimbal platform through the application of the Linear Quadratic Gaussian with Loop Transfer Recovery (LQG/LTR) control approach to a two-axis (pitch and yaw axis) gimbal assembly. They were able to show that their relative stability is better than a lead-PI controller. In their gimbal analytical model, they chose to ignore the effects of the spring constant, since it affects the system only at low frequencies. Their primary reason for doing this was to convert the system to a proper minimum phase type. Hernandez and Alamia [81] take the approach of using the SimMechanics toolbox in Matlab to design a stabilising controller for a ball joint gimbal mirror.

Khodadadi et al. [82] examine the robust control and modeling of a 2-DOF inertial stabilized platform. They begin with an uncertain linear model for the inertial stabilization platform (ISP), which consists of a 2-DOF gimbal that is attached to a moving vehicle. The modelling aspect of the platform is simplified by implementing a linear-doubted model. Their justification for this is that the linearity allows for linear classic controllers to be used in the implementation phase to reduce and minimise costs. They introduce uncertainty in the model parameters to account for the non-linear nature of disturbances, friction, cable restraint and noise. Uncertainty also makes the dynamic model more realistic and practical. They only apply a PI controller with some feedforward robust compensator enhancer to reject the disturbances on the stabilisation control loop.

The next section provides a brief introductory overview of some of the issues regarding to the deployment and applications of UAVs. This helps to contextualise the extent to which the gimbal platform can be used in UAV surveillance application and what challenges need to be anticipated regarding regulation and certification.

2.3 UAV Application

A wide array of potential applications exists for robots that have the level of mobility offered by flight. The military applications of aerial robotics have been recognised ever since the inception of powered flight, and they have already been realised to sometimes spectacular effect in surveillance, target, and even strike missions. The range of civilian applications is even greater and includes remote sensing, disaster response, image acquisition, surveillance, transportation and delivery of goods.

The challenges faced by aerial robots span several and distinct fields, which include state regulations, man-machine interface design issues, navigation, safety/reliability, collision prevention, and take-off/landing techniques. The size of aerial robots can considerably influence their flight dynamics, and small aerial robots can end up looking considerably different from their larger counterparts. Similar to their manned counterparts, aerial robots may enjoy diverse propulsion systems and operate over large speed ranges.

Aerial robots must be equipped with reliable position and actuation equipment so as to be capable of controlled flight, and this constitutes a non-trivial requirement prior to conducting research.

2.3.1 Background

Robert Michelson is largely credited for the development of the term *aerial robotics*, which captures a new class of highly intelligent, small flying machines. However, its roots can be traced as far back as the beginning of the 20^{th} century, together with the birth of aviation. The word *aerial robotics* can have several meanings. It could mean *robotic flying machine*, which is a mission-independent, platform-oriented concept. However, it could also mean *robotics that use flying machines*, which is a platform-independent, mission-oriented concept. Finally, it could mean a combination of the above definitions, which provide a description of the robotic platform, together with its robotic mission. In aerospace terminology, robotic flying machines are commonly referred to as *unmanned aerial vehicle's* (UAVs), while the entire infrastructures, systems and human components that are required to operate such machines for a given operational goal are often called Unmanned Aerial Systems (UASs).

Samuel P. Langley's *Number 5*, in 1896, was the first successful powered flight which was unmanned, presumably to reduce risk to the pilot and to allow a smaller and less expensive vehicle (reasoning that is still used today). However, this was still not a definite aerial robot which can be simply defined as a system capable of sustained flight with no direct human control and able to perform a specific task.

This leads us immediately to the Hewitt-Sperry automatic airplane, which was developed before and during World War I. The airplane's purpose was to act as a flying torpedo, carrying on-board *intelligence* to sustain flight over long periods of time without human intervention. Such intelligence was provided by a complex system that involved gyroscopes mechanically coupled to the airplane's control surfaces so as to stabilise the vehicle. It must be noted that current literature suggests that the vast majority of current, operational aerial robots are *fixed-wing* aircrafts, and they tend to be present at all altitudes.

2.3.2 Possible Applications of Aerial Robots

A summary of the categories in which most popular applications are found is:

- Remote sensing - such as pipeline spotting, power line monitoring, volcanic sampling, mapping, meteorology, geology and agriculture, as well as unexploded mine detection;
- Disaster response - such as chemical sensing, flood monitoring, and wildfire management;
- Surveillance - such as law enforcement, traffic monitoring, coastal and maritime patrol, and border patrol;
- Search and rescue - in low-density or hard-to-reach areas;
- Transportation - including small and large cargo transport, and possibly passenger transport;
- Communications - as permanent or ad-hoc communication relays for voice and data transmission, as well as broadcast units for television or radio;
- Payload delivery - firefighting or crop dusting; and
- Image acquisition - for cinematography and real-time entertainment.

2.3.3 Current Challenges in UAV

There are six major challenges facing the application of UAV in the industry for commercial purposes. These are outlined below.

Regulation and Certification

A big challenge to the success of aerial robots is doubtlessly their acceptance by certification authorities. Indeed, the operation of aerial robots is currently significantly limited by regulation constraints. This is due to the complex set of regulations put in place by national agencies (e.g., the Federal Aviation Administration in the US, the National Air Traffic Services in the UK, or the Direction Generale de l'Aviation Civil in France), whose aim is to maintain very high levels of safety for air traffic. The rapid pace of change and related lack of standards among aerial robotic systems and how they are used have led to their slow acceptance by regulation agencies. However, with the help of other organisations, such as the Radio Technical Commission for Aeronautics (RTCA), regulatory agencies have moved forward towards establishing rules for the routine operation of aerial robots; such rules include the ability of aerial robots to see and avoid or sense and avoid other traffic, thus emulating human pilots.

The maturation of aerial robots which will lead to their everyday use in populated areas will require the development of more reliable components, defined maintenance procedures, formal training programmes, and the automation of emergency procedures (such as the forced landing process).

In general there is lack of legislation that is drawn up specifically for UAV operation [6]. The understood restriction is that UAVs should be operated within sight of a ground based pilot. The Australian Civil Aviation Safety Authority (CASA) has progressed in implementing UAV specific legislation. Ingham et al [83] highlight aspects which need to be investigated for the certification of UAVs in SA airspace; they also discuss the work which has been done by other governments in the hope that SA can learn from them and expedite the process.

Human-Machine Interfaces

The pilot interfaces used for manned aircraft have evolved continuously since the first manned aircraft. The standards that exist today directly benefit safety and operator costs by minimising operational errors and training time when transitioning between aircraft model types. The challenge arise when considering the complex need for autonomy, mission capability, operator skills, and the desire to have single operator-controlled multiple aircraft.

Navigation

Figuring out absolute and relative position is a central issue for aerial robots. Systems that overly depend on the global navigation satellite system (GNSS) infrastructure lack resilience and tolerance for a shortage of positioning services, whether such a shortage originates from the system itself or from the particular robot configuration (in cluttered environments such as cities). The challenge for researchers is to develop navigation technologies that allow aerial robots to operate without manned external navigation infrastructure, to handle the situation when it is not available.

Agile Flight and Fault Tolerance

Nearly every aircraft in operational use today has been challenged to fly far beyond its flight envelope during flight tests, especially during early flight demonstrations to clients/customers. The purpose of these demonstrations is not only to show the full capabilities of the vehicle but also to bring a sense of safety to the pilots that the aircraft is still able to perform well in adverse conditions. This includes operating well at unusual attitudes and under partial system failures

such as loss of actuation. Researchers and design engineers in this filed of study must develop automation systems that meet this need.

Obstacle Avoidance

The ability for a vehicle to manage its position away from obstacles represents a significant issue and a necessity for low-altitude operations in crowded environments. One of the key features of aerial robotics is their possibly high speeds, which challenge many existing sensor management and data processing algorithms, especially their ability to detect hard-to-see obstacles such as suspended cables quickly.

Aerial Robot Landing and Interaction with Other Vehicles

Owing to the finite endurance of aerial robots, landing and docking are particularly important to them. Docking becomes important for applications such as aerial refuelling. All operations involving close coordination and physical interaction between vehicles or between a vehicle and the ground require further research.

Several tasks require aerial robots to operate as a group, rather than as individual systems. This happens, for example, to create phased array antennas, or to perform object geolocation, or improve the quality of a surveillance service.

2.4 Conclusion

The literature which is relevant to the theory of UAVs, robotics, video surveillance applications, gimbal platforms and cameras has been discussed to provide a basis for the investigation being carried out in this study. The focus area is gimbal modelling and robust control that ensure good quality images can be obtained during power line inspections. UAV applications have been briefly highlighted.

Chapter 3

The Method

3.1 Outline

The purpose of this study is to model and robustly control the gimbal platform so that good stabilisation and reference tracking for the mounted camera can be achieved. In this chapter, the techniques and instruments that where used to complete this project in a satisfactory manner are discussed. Some of the limitations that where posed during the project are highlighted. The modeling technique used for the gimbal platform and the actuators is presented. The control approach taken for the gimbal is also presented with all the robust control algorithms.

Section 3.2 discusses the research design approach with all the techniques considered. Section 3.3 presents the methodology details and the implementation procedures of the techniques discussed in the aforementioned section. Aspects of the study such as the tools used to successfully complete the project, the limitations of the study and ethical considerations taken into account to carry out the study.

3.2 Research Design

The aim of the project was to drive the gimbal assembly which mounts the MultiCam multi-sensor camera effectively and with such ease and robustness that its mobility is unaffected by any activities within its neighbourhood. First and foremost, the need existed to find a mechanism that will be used to provide variable torque to the gimbal assembly so that it can rotate to any commanded location.

Appendix A presents a detailed discussion of the advantages and disadvantages of the actuator mechanisms that are commonly used in robotic applications. These include hydraulic, pneumatic and electromagnetic actuators. For this project, the DC motor was chosen as the preferred

actuator mechanism because of its simplicity, convenience and ease of implementation. A discussion of the transmission mechanisms is also included in this appendix and shows that, depending on the amount of torque required, one can use gears to amplify the generated torque to drive the gimbal mechanism. For the case of this project direct-drive was preferred because of its simplicity.

In order to develop a good control system and appreciate the kinematics of the gimbal assembly, a kinematic model is required. The Lagrange [84–86] dynamic approach was chosen as the preferred method to model the gimbal platform. The advantage of this technique is its usefulness for a rigid body [85]. The advantages of Lagrangian protocol is that it reduces the entire field of statics, particle dynamics and rigid body dynamics to a single procedure. This procedure involves the same basic number of steps regardless of the number of masses that are being considered; the number of constraints on the system and especially whether or not the constraints and the frame of reference are in motion; and the type of coordinates employed. The Lagrange equations are valid in any coordinates (that is inertial, non-inertial or a combination) which are suitable for designating the configuration of the system [85]. This advantage becomes evident when simplifying the kinematic equations derived for the representation of the gimbal platform.

Forces of constraints for smooth holonomic constraints are automatically eliminated and do not appear in the Lagrangian equation, since they may present difficulties. The Lagrangian method is largely based on the scalar quantities: kinetic, potential and virtual work. The designer must ensure that the vector nature of forces, velocities and accelerations are taken account of in the treatment of dynamic problems. It should be noted that the Lagrangian method is applicable to various fields other than dynamics, which highlights its diversity.

The physical system-based method, performed in SimMechanics [87], of modelling any dynamic system serves to allow superior visualisation of the dynamic behaviour of the system and allows for interpretive verification of the results.

The control algorithms that are used to achieve the required motion and stabilisation are (with the tuning algorithm for automated gain update), H_∞ control, QFT and adaptive control. The advantage of using PID control is that it is a well tried and tested control approach noted for its simplicity and ease of implementation for tuning the gains. The noticeable disadvantage is the general dependency on trial and error methods of updating the gains. For the tuning of the PID controller, the Ziegler-Nichols techniques are applied first to set the performance benchmark, and then the autotuning procedure is applied. The autotuning PID algorithms are Integral Absolute Error (IAE), Integral Square Error (ISE), Integral Time Absolute Error (ITAE), and Integral Time Square Error (ITSE). To implement these tuning algortithms the fminsearch algorithm is used. The advantage presented by these tuning techniques is the elimination of trial and error. The disadvantage of PID control in general is the lack of robustness.

The *fminsearch* [88] Matlab function tool implements an optimization algorithm, and in this context optimization referes to minimising an objective function. The algorithm is derivative-free and it works by finding the minimum of a scalar unconstrained multivariable function. In its search of a solution, it begins with an initial estimate. The algorithm is based on the Nelder-Mead (simplex) method. One of the shortfalls of this algorithm is that it is very sensitive to the initial iterate. This means that it can become stuck in a local minimum and get an answer that is non-sensible. As a means to provide a solution to this problem, when it does get stuck, one simply changes where they are looking and start looking somwhere else.

To introduce robustness in the control system and obtain robust performance at the same time, H_∞ control is applied. The advantage of the H_∞ control algorithm is that it takes into consideration the model uncertainty of the plant system and the relevant identified external influences affecting it such as disturbances and noise signals from the sensors [89]. The disadvantage in the implementation of this algorithm, is that one has to simultaneously satisfy the robust stability and robust performance of the system. This is a difficult task because often there is a trade-off between the two, and the design choices are based on the system requirements.

The next robust approach that was applied is the QFT control algorithm. The advantage of this control technique, once again, is that it provides robust performance and stability for dynamic systems. However, the disadvantage is that its successful implementation and use as a suitable controller depends on the qualitative knowledge of the designer. This is because the control is designed on a graphic user interface which presents a Nichols plot of the system performance [90]. The satisfactory performance of the controller depends on the experience of the engineer.

The last robust controller which was tried is the adaptive controller. In addition to providing robust performance, the advantage of this control technique is that it can adapt to the changing dynamics of the system. What separates the adaptive controller from the other robust control methods is that while those control methods contain constant gains of transfer functions with constant parameters, the parameters of the adaptive controller are not constant. The gains of the controller can be updated on-line while the system is in operation and, in other instances, the parameters of the model can also be updated through the use of a system identification tool. This is good, especially in cases where the system model is not too accurate because of the difficulty of modelling certain dynamic systems because its parameters can be better approximated while the system is operating. As the control law is based on the model, it too gets updated and better performance is achieved as a result.

3.3 Lagrangian Gimbal Modelling Method

In this section, the literature which was deemed relevant to the implementation of the modelling and control techniques is discussed. The general approach followed for the entire project is presented in *Figure 3.1* and the approach led to a successful model and control choice for the system. The final Lagrangian gimbal model is derived from robotic concepts where the gimbal assembly is treated as a manipulator. The underlying theory that is required for the understanding of the implementation of the modelling and control techniques is presented in the subsections that follow.

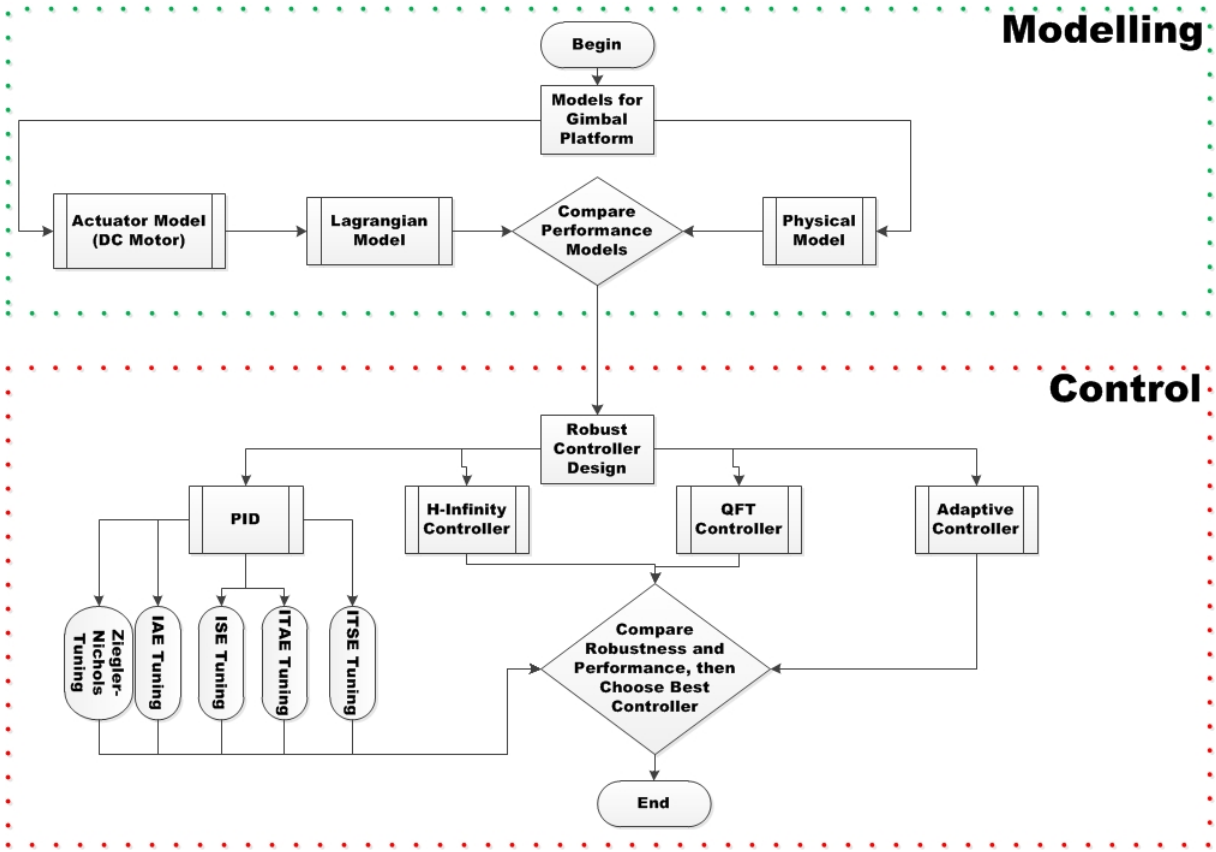

Figure 3.1: Gimbal modelling control design methodology

A varied spectrum of problems both theoretical and practical, involving mechanical, electrical, and electromechanical problems, can be treated accurately by using the Lagrangian method. The most important feature of the application of this method is the choice of reference frame and coordinates to be used. In most cases the inertial reference frame is generally chosen for systems where the reference frame is stationary. It also follows that when dealing with velocity specification, the velocity is expressed relative to the inertial frame. However, if a moving reference frame is selected whereby some coordinates are non-inertial, the velocity will not be expressed in the moving frame but rather the equations for velocity will be expressed relative to the inertial axes, which are in fact expressed in the moving coordinates [85]. It is very important

to note that when the *helicopter coordinates* of the system provide different equations of motion when considered in *earth coordinates*, then the system is in a non-inertial frame. Hence, any rotating frame is said to be non-inertial.

Additionally, when one consideres that since the entire flight needs to take 5 minutes, and this includes flying to the pylon location taking the images and then moving on to the next pylons. This limitation comes as a results of the 110cc engine capacity, and this works out to approximately 15 second in hover motion for the camera to take accurate images. For such a small duration, the rotation of the earth has a niglegible impact on the gimbal motion.

The process involved in the development and derivation of the Lagrangian equations [76] is as follows: first use Newton's laws of motion and from them derive D'Alembert's equations and then lastly derive Lagrange's equations.

3.3.1 Mechanical Structure

When developing a dynamic model, the links of a robot manipulator are generally taken to be rigid. However, one needs to remember that the robot is not practically a rigid structure. Much like most physical structures, it deflects under applied loads, such as its own weight and the weight of the payload. The more force that is needed to cause a deflection in the link the more the robot manipulator moves like a connected set of rigid bodies. Rigid robots have links which are designed to be stiff so that the deflections under load are less than the positioning accuracy required for their range of tasks. This is why the design of the dynamic model and the associated control algorithm can disregard the link deflection.

If proven to be necessary, one can improve the positioning accuracy of a rigid robot by widening the control algorithm that includes a model of the link deflection which results from gravity loading. One can even go as far as using strain sensors to measure loads and deflections, which in turn can be fed back to the control algorithm for more accurate improved positioning.

When flexible robots are designed, their dynamic model must include the deflection of its various links under gravity loading and under forces associated with link acceleration (also known as *inertia loading*). This impels the control algorithm to perform two major tasks: control the vibration of the system and control its gross motion. Even when dealing with rigid robot manipulators, vibration management is still required for achieving high speed and manipulating large payloads. *Figure 3.2* depicts a 2-DOF structure of a gimbal platform.

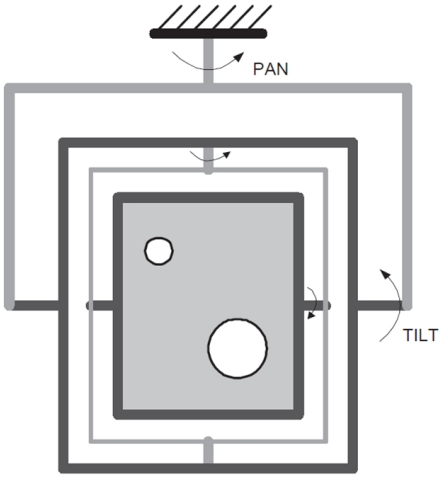

Figure 3.2: Two DOF gimbal mechanical structure.

3.3.2 Links

The biggest concern for industrial robots is the link stiffness in bending and in torsion. In order to provide this stiffness, during design, robot links are modelled as beams or shell (monocoque) structure. The thing to note about monocoque structures is that they have lower weight of higher strength-to-weight ratios and, unfortunately, as a result are more expensive and more difficult to manufacture. The alternative, machined beam-based links are more cost effective.

Another important practical consideration is whether the link structure includes bolted, welded, or adhesive bonded assemblies of cast, machined, and fabricated elements. The screw and bolted connections may initially appear straightforward, inexpensive and easily maintained, but the inevitable deflection of a link even in the manufacturing process may introduce creep into these multiple element assemblies, which changes the dimension and performance of a robot manipulator. On the contrary, the welded and cast structures are much less susceptible to creep and the associated hysteresis deformation, even though they sometimes require secondary manufacturing operations such as thermal stress relieving and finish machining.

3.3.3 Representation of Position and Orientation

This phenomenon is summarised by the term *pose*, which is the position and orientation of a robot manipulator body. This also includes the translation and rotation of the rigid body, which can also be thought of as displacements. In general, representations of spatial pose utilise sets with superabundant coordinates, and it is important to extract the independent auxiliary relationship, which is the difference between the number of derived coordinates and six. The *six* comes from the minimum required number of coordinates to locate a body in Euclidean space,

which is six [84].

Its important to define the coordinate reference frame when working with a robot manipulator, which, in general, is a frame i which consists of an origin denoted by O_i and a triad of mutually orthogonal basis vectors $(\hat{\mathbf{x}}_i, \hat{\mathbf{y}}_i, \hat{\mathbf{z}}_i)$ that are fixed within a particular body. The pose of a body will always be expressed as a pose of one coordinate frame relative to another coordinate frame. The same can be said about the displacement of rigid bodies, which is just displacement between two coordinate frames. The position of the origin of coordinate frame i relative to coordinate frame j can be expressed by the 3×1 vector in equation (3.1). *Figure 3.3* depicts the generalised coordinate frame of the helicopter UAV to aid the reader in following the various reference frames.

$$ {}^{j}p_i = \begin{bmatrix} {}^{j}p_i^x \\ {}^{j}p_i^y \\ {}^{j}p_i^z \end{bmatrix} \tag{3.1} $$

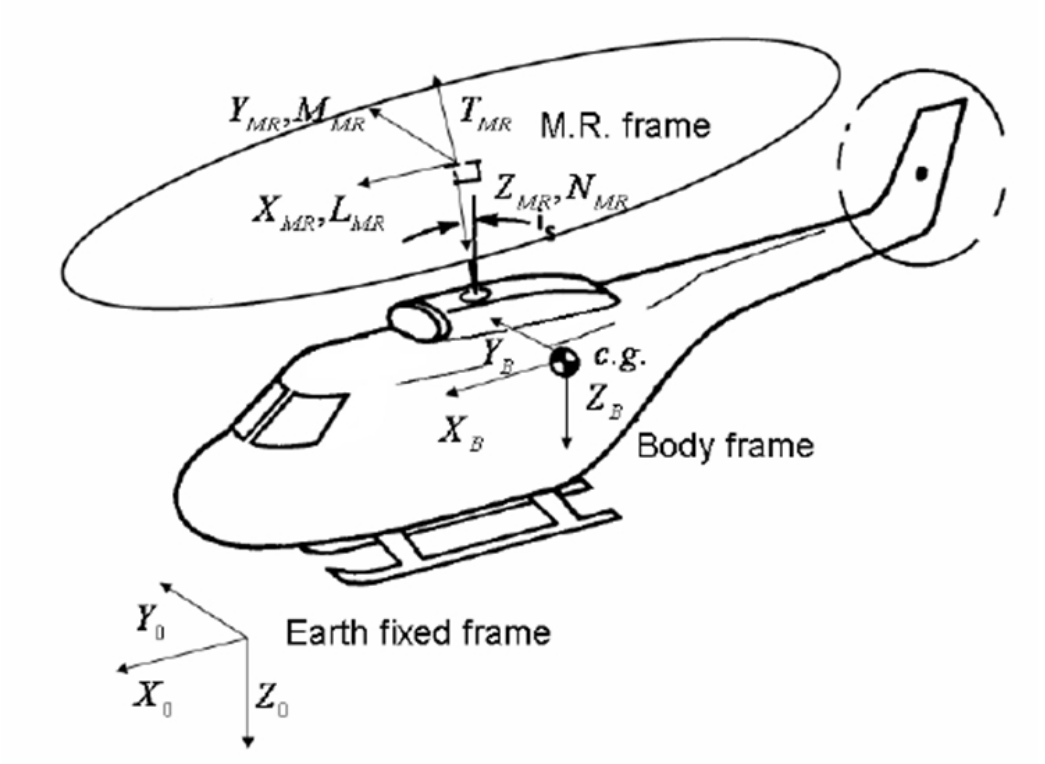

Figure 3.3: Coordinate frame for the system

To clarify this further, the component entry of this vector is the Cartesian coordinate of O_i in the j frame, which are the projections of the vector ${}^{j}\mathbf{p}_i$ onto the corresponding axes. Spherical or cylindrical coordinates can also be used and they have advantages when it comes to the analysis of robotic mechanisms, which include spherical and cylindrical joints.

The definition of translation in the theory of robotics is that it is a displacement in which no point in the rigid body remains in its initial position and that all of the straight lines in the rigid body remain parallel to their initial orientation. On the other hand, the definition of rotation in robot theory is that it is a displacement in which at least one point of the rigid body remains in its initial position and also that not all lines in the body remain parallel to their orientation [84].

By making use of coordinate frames, the orientation of coordinate frame i relative to coordinate frame j can be expressed by writing the basis vector $(\hat{\mathbf{x}}_i, \hat{\mathbf{y}}_i, \hat{\mathbf{z}}_i)$ in terms of the basis vector $(\hat{\mathbf{x}}_j, \hat{\mathbf{y}}_j, \hat{\mathbf{z}}_j)$, which produces $({}^j\hat{\mathbf{x}}_i, {}^j\hat{\mathbf{y}}_i, {}^j\hat{\mathbf{z}}_i)$. When writing together as a 3×3 matrix it is referred to as the rotation matrix, and its components are the dot products of the basis vectors of the two coordinate frames [84].

$$ {}^j\mathbf{R}_i = \begin{bmatrix} \hat{x}_i.\hat{x}_j & \hat{y}_i.\hat{x}_j & \hat{z}_i.\hat{x}_j \\ \hat{x}_i.\hat{y}_j & \hat{y}_i.\hat{y}_j & \hat{z}_i.\hat{y}_j \\ \hat{x}_i.\hat{z}_j & \hat{y}_i.\hat{z}_j & \hat{z}_i.\hat{z}_j \end{bmatrix} \tag{3.2} $$

Since the basis vectors are unit vectors and we know from mathematics that the dot product of any two unit vectors is the cosine of the angle between them, the following information can be extracted from this hypothesis: the elementary rotation of frame i about the $\hat{z}_j$ axis through an angle θ is:

$$ \mathbf{R}_z(\theta) = \begin{bmatrix} \cos(\theta) & -\sin(\theta) & 0 \\ \sin(\theta) & \cos(\theta) & 0 \\ 0 & 0 & 1 \end{bmatrix} \tag{3.3} $$

While the same rotation about the $\hat{y}_j$ is:

$$ \mathbf{R}_y(\theta) = \begin{bmatrix} \cos(\theta) & 0 & \sin(\theta) \\ 0 & 1 & 0 \\ -\sin(\theta) & 0 & \cos(\theta) \end{bmatrix} \tag{3.4} $$

And about the $\hat{x}_j$ axis is:

$$ \mathbf{R}_x(\theta) = \begin{bmatrix} 1 & 0 & 0 \\ 0 & \cos(\theta) & -\sin(\theta) \\ 0 & \sin(\theta) & \cos(\theta) \end{bmatrix} \tag{3.5} $$

The rotation matrix, ${}^{j}\mathbf{R}_{i}$, that transforms a vector expressed in coordinate frame i to a vector expressed in coordinate frame j can be interpreted as the orientation of frame i relative to j and can also be viewed as the rotation of frame i to frame j.

The methods that have been discussed allow for the representation of position and orientation separately; however, there is an advantage sometimes in representing position vectors and rotation vectors in a combined form, which annotates it in a compact notation. This is known as the homogeneous transformation, which can be represented in the following form [84]

$$ {}^{j}\mathbf{r} = {}^{j}\mathbf{R}_{i}^{i}\mathbf{r} + {}^{j}\mathbf{p}_{i} \tag{3.6} $$

This can be expanded in the following manner, as shown in equation (3.7) [84]:

$$ \begin{bmatrix} {}^{j}\mathbf{r} \\ \mathbf{1} \end{bmatrix} = \begin{bmatrix} {}^{j}\mathbf{R}_{i} & {}^{j}\mathbf{p}_{i} \\ \mathbf{0^{T}} & \mathbf{1} \end{bmatrix} \begin{bmatrix} {}^{i}\mathbf{r} \\ \mathbf{1} \end{bmatrix} \tag{3.7} $$

Whereby:

$$ {}^{j}\mathbf{T}_{i} = \begin{bmatrix} {}^{j}\mathbf{R}_{i} & {}^{j}\mathbf{p}_{i} \\ \mathbf{0^{T}} & \mathbf{1} \end{bmatrix} \tag{3.8} $$

Equation (3.8) [84] transforms vectors from coordinate frame i to coordinate frame j, and its inverse does the opposite. As an example, the homogeneous transformation of a simple rotation about an axis is sometimes expressed as **Rot** such that a rotation of θ about an axis $\hat{z}$ is:

$$ \mathbf{Rot}(\hat{z}, \theta) = \begin{bmatrix} \cos(\theta) & -\sin(\theta) & 0 & 0 \\ \sin(\theta) & \cos(\theta) & 0 & 0 \\ 0 & 0 & 1 & 0 \\ 0 & 0 & 0 & 1 \end{bmatrix} \tag{3.9} $$

Similarly, the homogeneous transformation of a simple translation along an axis is sometimes denoted **Trans** such that a translation of d along an axis $\hat{x}$ as shown in Equation (3.10) [84]:

$$ \mathbf{Trans}(\hat{x}, d) = \begin{bmatrix} 1 & 0 & 0 & d \\ 0 & 1 & 0 & 0 \\ 0 & 0 & 1 & 0 \\ 0 & 0 & 0 & 1 \end{bmatrix} \tag{3.10} $$

This type of notation is particularly attractive when compact notation is desired and actually helps with ease of programming. However, the downside is that it is computationally inefficient since it introduces a large number of additional multiplications by ones and zeros.

3.3.4 Joint Kinematics

The generic structure for most robots allows either rotary or linear movement, which is officially denoted as revolute and prismatic joints. There are other practical joints available, such as the ball-in-socket or spherical joint and the Hooke-type universal joint. When integrating the mechanical structure of the robot with its joint mechanism, which for all operational purposes includes the actuator and joint motion sensor, it basically becomes a source of structural flexibility. The deformation in the joint at the bearing housings can reduce shaft and gear pre-loads, which in turn will allow backlash or free-play, which reduces the resultant precision.

The four major components which make up the joint mechanism are: the joint axis structure, an actuator, transmission, and state sensor (this is usually for position feedback; however, velocity and force sensors are also very common in practice). When it comes to low pressure robot manipulators that accelerate the payload at less than a peak of 0.5 g (with g being the gravitational acceleration of 9.81 m/s^2), then the system inertia becomes less important that gravity forces and torques [84]. This then permits the placing of the actuators near the joint, and the compensation of the suspended weight using counter-balancing masses, springs, or even a gas pressure.

On the other hand, when dealing with high-performance robot manipulators where peak payload acceleration can reach 3 g to 10 g or more, minimising the system inertia is very important. In this case, the actuator is placed near the first joint axis of a serial link manipulator in order to minimise its inertial contribution and drive links, belts/cable/gear transmission are used to drive the joints. The design of the actuator placement and transmission for each joint is a trade-off between weight, inertia, stiffness and complexity. This choice dictates the major physical characteristics of a manipulator design.

Generally, when describing the kinematic behaviour of a robot mechanism, an idealised approach is assumed. The physical links that make up the robot mechanism are assumed to be perfectly rigid bodies and their surfaces are geometrically perfect in both their position and shape. These rigid bodies are then connected together at joints by which their idealised surfaces are in ideal contact without any clearance space between them. The freedom of motion between the two connected links is then determined by the geometries of these respective surfaces in direct contact. A more globally accepted definition of the joint kinematics is that it is a connection between two bodies that constrains their relative motion [84].

There are many classes of kinematic joint: revolute, prismatic, cylindrical, helical, spherical and planar.

3.3.5 Revolute Joint

This joint is informally known as the hinge or pin joint, and it is formally accepted in the scientific community as a lower pair composed of two congruent surfaces of revolution [84]. Generally, the surfaces are assumed to be of the same kind, except that one surface is an external (convex in any plane normal to axis of rotation) and the other is an internal surface (concave in any plane normal to the axis). The interpretation is that a revolute joint only allows rotational motion of one of the bodies relative to the other body [84].

Rotary motion joints are designed to perform pure rotation while minimising other displacements and motion that may not be desired. The most important measure of the quality of a revolute joint is its stiffness or resistance to all undesired motion behaviours. The key factors to be considered in design for stiffness are shaft diameter, clearance and tolerances, mounting configuration of the bearings, and the implementation of proper bearing pre-loading.

3.3.6 Prismatic Joint

This is informally labelled the sliding joint, and it is formally known as a lower pair formed from two congruent general cylindrical surfaces. Once again, one of the surfaces is internal while the other is external. The joint allows only sliding motion of one of the members (links) joined relative to the other along the direction of extrusion [84].

There are two basic types of linear motion joints: single-stage and telescoping joints. Single-stage joints are made up of a moving surface that slides along a fixed surface. Telescoping joints are essentially sets of nested or stacked single-stage joints. The properties of single-stage joints are its simplicity and high stiffness, whereas the primary advantage of telescoping joints is their retracted-state compactness and large extension ratio. The telescoping joints may have a lower effective joint inertia for some motions because part of the joint may remain stationary or move with reduced acceleration. The function performed by bearings in prismatic joints is to facilitate motion in a single direction and to prevent motion in all other directions.

The primary criterion for evaluating higher number (in or near the wrist or end-effector) linear motion joints or axes is the stiffness-to-weight ratio. These types of joints are not discussed in greater detail in this study.

3.3.7 Helical Joint

This joint is informally known as a screw joint, and formally defined as a lower pair formed from two helical surfaces formed by extruding any curve along a helical path. The simple and most common example is the screw and nut scenario [84].

3.3.8 Cylindrical Joint

This is defined as a lower pair formed by contact of two congruent right circular cylinders, where one is an internal surface and the other an external surface. The versatility of this joint is that it allows the rotation about the cylinder axis and sliding parallel to it [84].

3.3.9 Spherical Joint

This joint is defined as a lower pair formed by contact of two congruent spherical surfaces. This too is composed of one internal surface and one external surface. This type of joint permits rotation about any line through the centre of the sphere, which means it allows for independent rotation about axes in up to three different directions and thus has three degrees of freedom [84].

3.3.10 Planar Joint

Like the name suggests, this joint is formed by planar contacting surfaces. Much like the spherical joint, it is a lower pair joint with three degrees of freedom [84].

3.3.11 Geometric Representation

When defining the geometry of a robotic manipulator, it is generally more convenient to attach reference frames to each link that makes up the body. The main challenge to be faced is in the selection of a suitable method to locate these frames in *space coordinates*, but the objective is to achieve consistency and computational efficiency. Many conventions exist for the location of the frame on the links. The Denavit and Hartenberg (D-H) is one of the most commonly used in the industry, and its form requires only four rather than six parameters to locate a single reference frame relative to another [84].

From *Figure 3.4*, the four parameters are the link length a_i, the link twist α_i, the joint offset d_i, and the joint angle θ_i. The reference parameters are assigned in such a way that the origins and axes allow for the $\hat{\mathbf{x}}$ axis of one frame both to intersect and be perpendicular to the $\hat{\mathbf{z}}$

axis of the preceding reference frame. This convention can be applied to robot manipulators that comprise revolute and prismatic joints, so that even if multiple degree of freedom joint are present, they can be dealt with as a combination of revolute and prismatic joints. In this study, this convention is only applied to serial-chain manipulators, and it is applied in the following manner:

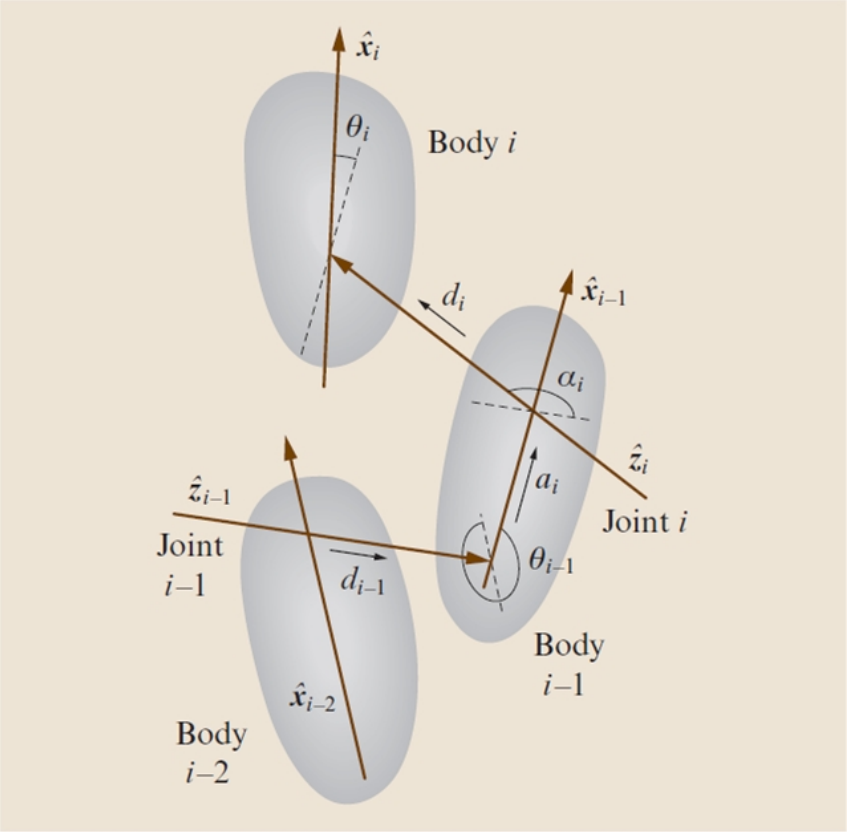

Figure 3.4: Schematic of the numbering of bodies and joints in a robotic manipulator.

- The N moving bodies of the robotic mechanism are numbered from 1 to N.
- The number of the base is 0.
- The N joints of the robotic mechanism are numbered from 1 to N, with joint i located between members (links) $i-1$ and i.

When this numbering convention is used, the attachment of reference frames follows the following convention:

- The $\hat{\mathbf{z}}$ axis is located along the axis of joint i.
- The $\hat{\mathbf{x}}_{i-1}$ axis is placed along the common normal between the $\hat{\mathbf{z}}_{i-1}$ and $\hat{\mathbf{z}}_i$ axes.

By making use of the attached frame, the four parameters that are used to locate one frame relative to another are defined as per in the D-H section below.

3.3.12 Workspace

A good sufficient general definition of a workspace of a robot manipulator is that it is the total volume that is swept out by the end-effector as the robot manipulator executes all possible manoeuvring. The workspace can be used during modelling of the manipulator in order to simulate its motions. However, the workspace is determined by having full knowledge of the geometry of the manipulator and the limitations of its joint motion capabilities [84]. The workspace could be determined from a thorough consideration of *Figure 3.4* and made relevant to the application at hand.

3.3.13 Forward Kinematics

When working with a serial-chain manipulator, the problem becomes about determining the position and orientation of the end-effector relative to the base on which it is mounted when the positions of all of the joints and the values of all of the geometric link parameters are provided. When the goal is to develop the manipulator coordination algorithm then the forward kinematic problem becomes critical simply because joint positions are typically measured by sensors which are mounted on the joints and it is necessary to calculate the positions of the joint axes relative to the fixed reference frames [84].

3.3.14 Inverse Kinematics

The task involved in this problem is to determine the values of the joint position when provided with the position and orientation of the end-effector relative to the base and the values of all of the geometric link parameters [84]. The problem of solving inverse kinematics for serial-chain manipulators requires that a solution for nonlinear sets of equations be found. For example, in the case of a six-degree-of-freedom manipulator, the three equations relate to the position vector within the homogeneous transformation and the other three relate to the rotation matrix. In the rotation matrix case, the three equations cannot be yielded from the same row or column because of the dependency within the rotation matrix.

Therefore, with these nonlinear equations, it is possible that no solution exists or multiple solutions exist. Strictly speaking, in order for a solution to be present, the desired position and orientation of the end-effector must lie in the workspace of the manipulator. Also, in cases where

solutions do exist, often they cannot be represented fully in closed form and hence numerical methods are employed to find the solution.

3.3.15 Forward Instantaneous Kinematics

This problem is stated as follows for a serial-chain manipulator: when provided with all the positions of all the links of the chains and the rates of motion about all the joints, we are required to determine the total velocity of the end-effector. The rate of motion is understood to be the angular velocity of rotation about a revolute joint or the translational velocity of sliding along a prismatic joint. Generally, the forward or inverse position kinematics problem must be solved before the forward instantaneous kinematics problem can be solved, and the same applies to the inverse instantaneous kinematics problem. The importance of the forward instantaneous kinematics becomes evident when dealing with acceleration analysis for the purpose of tackling a dynamic study of the robotic manipulator [84].

3.3.16 Analytical Jacobian

The differentiation of the forward position kinematics equations with respect to time yields a set of equations of the following form:

$$\mathbf{v}_N = \mathbf{J}(\mathbf{q})\dot{\mathbf{q}} \tag{3.11}$$

Where $\mathbf{v}_N$ is the spatial velocity of the end-effector, $\dot{\mathbf{q}}$ is an N-dimensional vector composed of the joint rates, and $\mathbf{J}(\mathbf{q})$ is a $6 \times N$ matrix (if there is rotation and translation), whose elements are, in general, nonlinear functions of $\mathbf{q}_1, ..., \mathbf{q}_N$. $\mathbf{J}(\mathbf{q})$ is called the Jacobian matrix of this algebraic system and is expressed relative to the same reference frame as the spatial velocity $\mathbf{v}_N$.

3.3.17 Denavit-Hartenberg (D-H) Conversion

When implementing this approach, it is best to commence by populating the D-H table with the geometric parameters of the serial-chain manipulator, which are defined as follows, referring back to *Figure 3.4*:

- a_i is the distance from $\hat{z}_{i-1}$ to $\hat{z}_i$ along $\hat{x}_{i-1}$.
- α_i is the angle from $\hat{z}_{i-1}$ to $\hat{z}_i$ about $\hat{x}_{i-1}$.

- d_i is the distance from $\hat{x}_{i-1}$ to $\hat{x}_i$ along $\hat{z}_i$.
- θ_i is the angle from $\hat{x}_{i-1}$ to $\hat{x}_i$ about $\hat{z}_i$.

The homogeneous transformation matrix is then used to determine the matrix for the different links at the corresponding joint coordinate frames. The general equation for the transformation equation is as follows:

$$^{i-1}T_i = Rot(\hat{x}_{i-1}, \alpha_i)Trans(\hat{x}_{i-1}, a_i)Rot(\hat{z}_i, \theta_i)Trans(\hat{z}_i, d_i) \tag{3.12}$$

$$^{i-1}T_i = \begin{bmatrix} \cos(\theta_i) & -\sin(\theta_i) & 0 & a_i \\ \sin(\theta_i)\cos(\alpha_i) & \cos(\theta_i)\cos(\alpha_i) & -\sin(\alpha_i) & \sin(\alpha_i)d_i \\ \sin(\theta_i)\sin(\alpha_i) & \cos(\theta_i)\sin(\alpha_i) & \cos(\alpha_i) & \cos(\alpha_i)d_i \\ 0 & 0 & 0 & 1 \end{bmatrix} \tag{3.13}$$

The general Lagrange equation in canonical form is as follows:

$$\mathbf{H}(\mathbf{q})\ddot{\mathbf{q}} + \mathbf{C}(\mathbf{q}, \dot{\mathbf{q}})\dot{\mathbf{q}} + \tau_g(q) = \tau_a \tag{3.14}$$

Where, in equation (3.14):

- The first term is an $n \times n$ symmetric positive definite matrix called the Joint-Space Inertia Matrix (JSIM).
- The second term is an $n \times n$ matrix such that $\mathbf{C}\dot{\mathbf{q}}$ is a vector of coriolis and centrifugal terms, which are collectively known velocity product terms.
- The third term describes the gravitational conservative forces acting on the system (they usually fall-away).
- q represents the chosen coordinates of a point in the mechanical configuration space.

Recall the Lagrange function:

$$\mathbf{L = T - V} \tag{3.15}$$

The kinetic energy can generalised in a compact form as follows:

$$T = \frac{1}{2}\dot{\mathbf{q}}^T \mathbf{H}\dot{\mathbf{q}} \tag{3.16}$$

In general the canonical formula takes the following form:

$$\sum_{j=1}^{n} H_{ij}\ddot{q}_j + \sum_{j=1}^{n}\sum_{k=1}^{n} C_{ijk}\dot{q}_j\dot{q}_k + \tau_{g_i} = \tau_i \tag{3.17}$$

Where the Christoffel symbols [91] of the first type are as follows:

$$C_{ijk} = \frac{1}{2}\left(\frac{\partial H_{ij}}{\partial q_k} + \frac{\partial H_{ik}}{\partial q_j} + \frac{\partial H_{jk}}{\partial q_i}\right) \tag{3.18}$$

and:

$$C_{ij} = \sum_{k=1}^{n} C_{ijk}\dot{q}_k \tag{3.19}$$

3.4 Gimbal Motion Control

The focus here is on controlling the motion of rigid body robotic manipulators, and not mobile robots, flexible manipulators, and manipulators with elastic joints. The main challenge is the complexities of the rigid manipulator dynamics and the uncertainties. The former challenge actually results from non-linearities and coupling in the configuration of the robot manipulators. The latter challenge is divided into two types: which is structured and unstructured uncertainties. The formal definition of structured uncertainty means imprecise knowledge of the dynamic parameters. On the other hand, unstructured uncertainty result from joint and link flexibility, actuator dynamics, friction, sensor noise and unknown environmental dynamics.

3.4.1 Robot Performance

Industrial robot performance is often specified in terms of functional operations and cycle times. Examples of performance measures on very common industry robot manipulators are as follows:

- For assembly robots, the specification is often the number of typical pick-and-place cycles per minute.

- Arc-welding robots are specified with a slow weld pattern and weave speed as well as by a fast repositioning speed.
- Painting robots use the deposition or coverage rate and spray pattern speed.

The peak robot velocity and acceleration catalogue data is generally just calculated numbers and will vary due to dynamic (inertia) and static (gravity) coupling between robot joints due to configuration changes as a robot moves.

3.4.2 Robot Speed

The maximum joint velocity (angular or linear) is not an independent value. For much longer motions it is often limited by the servomotor bus voltage or maximum allowable motor speed. For manipulators with high accelerations, even short point-to-point motions may be velocity limited. Conversely, for low-acceleration robots, only gross motions will be velocity limited. Typical peak end-effector speeds can range up to 20 m/s for large robot manipulators [92].

3.4.3 Robot Acceleration

In most modern robot manipulators, because the payload mass is small when compared to the manipulator mass, more of the power is exhausted by accelerating the manipulator than the load. The acceleration affects gross motion time as well as cycle time (gross motion time plus settling time). Manipulators which are capable of greater acceleration tend to be stiffer manipulators. In high-performance robot manipulators, acceleration and settling time are more important design parameters than velocity or load capacity. Maximum acceleration for some assembly and material handling robots is in excess of 10 g (where g is the gravitational acceleration of 9.81 m/s^2) with light payloads [92].

3.4.4 Repeatability

This specification is very important as it represents the ability of the manipulator to return repeatedly to the same location. Depending on the method of teaching or programming the manipulator, most manufacturers intend this figure to indicate the radius of a sphere that encloses the set of locations to which the arm returns when sent from the same origin by the same program with the same load and set-up conditions. This sphere may not include the target point because calculation round-off errors, simplified calibration, precision limitation, differences during the teaching and execution modes can cause significantly larger errors than those just

caused by friction, unresolved joint and drive backlash, servo system gain, and structural and mechanical assembly clearance and play.

Repeatability becomes very important when performing repetitive tasks such as blind assembly or machine loading. Typical repeatability specifications range from 1 mm to 2 mm for large spot-welding robots to 0.005 mm for precise micro-positioning manipulators [92].

3.4.5 Resolution

In simpler terms, this specification represents the smallest incremental motion that can be produced by the manipulator. The concept of resolution becomes very important when dealing with sensor-controlled robot motion and with fine positioning. Although most manufacturers calculate the system resolution from the resolution of the joint position encoders, or from servomotor and drive step size, this calculation is misleading because the system friction, windup, backlash, and kinematic configuration affect the system resolution. Typical encoder or resolver resolution is $10^{14} - 10^{25}$, which counts for full-axis or joint travel, but actual physical resolution may be in the range 0.001 mm to 0.5 mm [92].

3.4.6 Accuracy

This specification covers the ability of a robot to position its end-effector at a pre-programmed location in space. Robot manipulator accuracy is important in the performance of non-repetitive types of tasks programmed from a database, or for taught tasks that have been remapped or offset owing to measured changes in the installation.

Accuracy is a function of the precision of the arm kinematics model (joint type, link lengths, angles between joint, any accounting for link or joint deflections under load, etc.); the precision of the world, tool, and fixture models; and the completeness and accuracy of the arm solution routine [92].

Typical accuracies for industrial manipulators range from ± 10 mm for uncalibrated manipulators that have a poor computer model to ± 0.01 mm for machine-tool-like manipulators that have controllers with accurate kinematic models and solution and precisely manufactured and measured kinematic elements [92].

3.4.7 Component Life and Duty Cycle

The three sub-assemblies in an electrically powered robot manipulator with the greatest failure problems are the actuators (servomotors), transmission, and power or signal cables. Mean time between failures (MTBF) should be a minimum or 2000 h on-line and ideally at least 5000 operating hours should pass between each major component preventative maintenance replacement schedule [92].

Short-term peak performance is frequently limited by maximum drive loading, whereas long-term, continuous, performance is limited by the motor heating. Instead of designing for equal levels of short-term and long-term performance, cost savings and performance improvement can result from designing for an anticipated duty cycle. This then permits the use of smaller, low-inertia, lighter motors [92].

Industrial robots usually become obsolete and are replaced before they reach their design cycle life.

3.4.8 Collisions

In the course of operation, unforeseen or unexpected situations may occasionally result in a collision that involves the manipulator, its tools, the workspace, or other objects in the workspace. These accidents may result in no, little or extensive, damage depending in large part on the design of the manipulator. Crash-resistant design options should be considered early in the design process if the time lost or cost of such accidents could be significant [92].

Typical damages due to accidents include fracture or shear failures of gear teeth or shaft, dented or bent link structures, slipping of gears or pulleys on shafts, cut or severely abraded or deformed wires, cables or hoses, and broken connectors, fittings, limit stops or switches.

Compliant elements such as overload (slip) clutches, elastic members, and padded surfaces can be incorporated to reduce shock loads and help decouple or isolate the actuators and drive components in the event of such collisions [92].

3.4.9 Dynamic Model

The dynamic model of rigid robot manipulators is best described by Lagrange dynamics. If we allow the $(n \times 1)$-vector $\mathbf{q}$ of joint variables to be $\mathbf{q} = [q_1, ..., q_n]^T$, then

$$\mathbf{H}(\mathbf{q})\ddot{\mathbf{q}} + \mathbf{C}(\mathbf{q}, \dot{\mathbf{q}})\dot{\mathbf{q}} + \tau_g(\mathbf{q}) = \tau \tag{3.20}$$

Where from (3.20), $\mathbf{H}(\mathbf{q})$ is the $(n \times n)$ inertia matrix, $\mathbf{C}(\mathbf{q}, \dot{\mathbf{q}})\dot{\mathbf{q}}$ is the $(n \times 1)$-vector Coriolis and centrifugal forces, $\tau_g(\mathbf{q})$ is the $(n \times 1)$-vector of gravity forces, and τ is the $(n \times 1)$-vector of joint control inputs to be designed. Note that this is a generic and general representation, which neglects the friction and disturbance inputs.

It is important to bear in mind that other contributions to the dynamic description of the robot manipulators may include the dynamics of the actuators, joint and link flexibilities, friction, noise, and disturbances. Some properties of the dynamic model in equation (3.20) are as follows:

Property 1

The inertia matrix is a symmetric positive-definite matrix, expressed as follows:

$$\lambda_h \mathbf{I}_n \leq \mathbf{H}(\mathbf{q}) \leq \lambda_H \mathbf{I}_n \tag{3.21}$$

Where λ_h and λ_H denote positive constants.

Property 2

The matrix $N(q, \dot{q}) = \dot{H}(q) - 2C(q, \dot{q})$ is skew-symmetric for a particular choice of $C(q, \dot{q})$, which is always positive; i.e.:

$$Z^T \mathbf{N}(\mathbf{q}, \dot{\mathbf{q}})Z = 0 \tag{3.22}$$

For any $(n \times 1)$ vector Z

Property 3

The $(n \times n)$-matrix $\mathbf{C}(\mathbf{q}, \dot{\mathbf{q}})$ satisfies

$$\|\mathbf{C}(\mathbf{q}, \dot{\mathbf{q}})\| \leq c_0 \|\dot{\mathbf{q}}\| \tag{3.23}$$

For some bounded constant c_0.

Property 4

The gravity force/torque vector satisfies

$$\|\tau_g(\mathbf{q})\| \leq g_0 \tag{3.24}$$

For some bounded constant g_0.

Property 5

The equation of motion is linear in the inertia parameters, which simply means that there is a $(r \times 1)$ constant vector $\mathbf{a}$ and an $(n \times r)$ regressor matrix $\mathbf{Y}(\mathbf{q}, \dot{\mathbf{q}}, \ddot{\mathbf{q}})$ such that:

$$\mathbf{H}(\mathbf{q})\dot{\mathbf{q}} + \mathbf{C}(\mathbf{q}, \dot{\mathbf{q}})\dot{\mathbf{q}} + \tau_g(\mathbf{q}) = \mathbf{Y}(\mathbf{q}, \dot{\mathbf{q}}, \ddot{\mathbf{q}})\mathbf{a} \tag{3.25}$$

The vector $\mathbf{a}$ comprises link masses, moments of inertia, and various combinations.

Property 6

The mapping $\tau \rightarrow \dot{q}$ is passive; i.e., there exists $\alpha \geq 0$ such that

$$\int_0^t \dot{q}^T(\beta)\tau(\beta)d\beta \geq -\alpha, \forall_t < \infty, \tag{3.26}$$

Remarks:

- Property 3 and property 4 are vital to the establishment of upper bounds on the non-linear terms in the dynamic robot manipulator model.
- For property 5, the parameter vector $\mathbf{a}$ constitutes a combination of various variables. Another important factor is that the dimensionality of the parameter space is not unique and the search over the parameter space is a crucial task.
- An assumption has to be made concerning the configuration of the robot manipulator, which is that it is fully actuated - which means that there is an independent control input for each degree-of-freedom (DOF).

3.4.10 Generic Control Methods

In general, the approach is to classify the control objectives in the following classes.

Trajectory Tracking

This method is aimed at following a time-varying joint reference trajectory specified within the robot manipulator workspace. In general, this desired trajectory is assumed to comply with the actuator's capacity. This means that the joint velocity and acceleration associated with the desired trajectory should not violate, respectively, the velocity and acceleration limit of the robot manipulator. In practice, the capacity of actuators is set by torque limits, which results in bounds on the acceleration that are complex and state dependent.

Regulator

This method is sometimes referred to as *point-to-point control*. A fixed configuration in the joint space is specified; the objective is to bring to and keep the joint variable at the desired position in spite of torque disturbances and independently of the initial conditions. The behaviour of transients and overshooting are, in general, not guaranteed.

When it comes to selection of the type of controller, it will depend on the type of task to be tackled. As an example, the tasks which only require the robot manipulator to move from one position to another without requiring significant precision during the motion between these two points can be solved by regulators. In contrast tasks such as welding, painting and so on require tracking controllers.

It is important to note that the regulator problem may be seen as a special case of the tracking problem (for which the desired joint velocity and acceleration are zero).

Two schemes of controls employed in robot manipulators: joint space control and operational space control.

Joint Space Control

The main goal of the joint space control scheme is to design a feedback controller so that the joint coordinates $\mathbf{q}(t) \in R^n$ track the desired motion $\mathbf{q}_d(t)$ as closely as possible. Paying particular attention to equation (3.20), this equation of motion of an n-DOF manipulator is expressed in the joint space. In this case, the control of the robot manipulator is naturally achieved in the

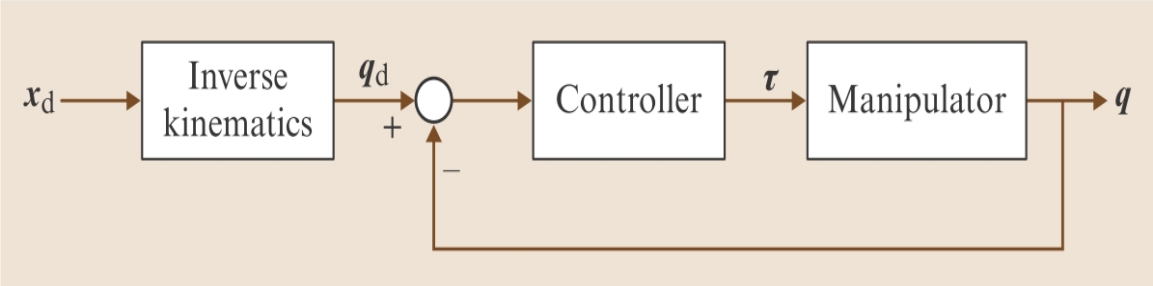

Figure 3.5: The joint-space control scheme

joint space, since the control inputs are the joint torques. Nevertheless, the user must specify a motion in terms of end-effector coordinates; this is why the following strategy is important.

Figure 3.5 shows the basic outline of the joint space control scheme and its operation is elaborated as follows. Firstly, the desired motion, which is described in terms of end-effector coordinates, is converted to a corresponding joint trajectory using the inverse kinematics of the manipulator. Then the feedback controller determines the joint torque that is necessary to move the manipulator along the desired trajectory specified in the joint coordinates, starting from measurements of the current joint states. The joint space control includes, as part of the feedback control, a simple PD control, PID control, inverse dynamics control, etc.

Operational Space Control

When it comes to more complicated and less certain environments, end-effector motion may be subject to on-line modification to accommodate unexpected events or to respond to sensor inputs. This is crucial when controlling the interaction between the manipulator and environment is of concern. This requires precise control of the end-effector motion.

Independent-joint Control

In independent-joint control the control inputs of each joint only depend on the measurement of the corresponding joint displacement and velocity. There are many advantages offered arise from its simple structure. For example, by using independent-joint control, communication among different joints is saved. Moreover, since the computational load of controllers may be reduced, only low-cost hardware is required in actual implementations. Finally, it has the additional feature of scalability, since the controllers on all the joints have the same formulation.

Controller Design Based on the Single-joint Model

The most simple independent-joint control strategy is to control each joint axis as a single-input single-output (SISO) system. The coupling effects among joints due to varying configuration during motion are treated as disturbance inputs. Without the loss of generality, the actuator is taken as a rotary electric direct-current (DC) motor.

Controller Design Based on the Multi-joint Model

In recent years, independent-joint control schemes based on the complete dynamic model of the robot manipulators (i.e., a multi-joint model) have been proposed. Since the overall dynamic model is considered, the effects of coupling among joints are handled.

3.5 PID Control Method

PID control technique is the earliest and still most used control strategy in industrial applications. The earliest application of PID control was in pneumatic devices, and this was then followed by vacuum and solid state analogue electronics. In today's world, PID is largely digitally implemented in microprocessors. The main reason for its use is its simple control structure, which can be understood by non-technical plant operators and is relatively easy to tune. According to a 1989 survey conducted for process control systems, more than 90% of the control loops were of PID type. The subject of PID control has been an active research topic for many years and interest has been to determine methods for setting satisfactory controller parameters to improve performance. Interestingly enough, 98% of control loop in the pulp and paper industries is controlled by PI controllers and in more general applications of process control, 95% of the controllers are of PID type [84].

The mathematical description of a PID controller has the following form as presented by equation (3.27). Most PID tuning rules are based on first-order plus time delay (FOPTD) or first-order plus dead time (FOPDT) assumptions of the plant and this is the reason that those tuning rules struggle to ensure optimum control performance [84]. Modern optimisation techniques tune a PID controller based on the actual transfer function of the plant to optimise the closed-loop performance.

To prevent the control performance optimisation search algorithm from being trapped in a local minimum, the initial controller parameters are set using those determined by an existing tuning rule. In this particular case the Ziegler-Nichols tuning rule is used to determine the initial parameters.

$$u(t) = k_p[e(t) + \frac{1}{T_i}\int_0^t d\tau + T_d\frac{de(t)}{dt}] \tag{3.27}$$

The next subsections explore various techniques for automatically tuning the PID controller. Researchers in [19–27] detail various techniques for the auto-tuning of PID parameters using methods such as genetic algorithms and neural networks.

3.5.1 Ziegler-Nichols Tuning

This is an empirical tuning formula which was proposed by Ziegler and Nichols in early 1942. The tuning formula is obtained when the plant model is given a FOPDT which can be expressed using the following equation:

$$G(s) = \frac{k}{1 + sT}e^{-sL} \tag{3.28}$$

In real-time process control systems in the industry, equation (3.28) can be used to approximate a model in a large variety of plants. By measuring the step response of the plant model through an experiment, the output signal can be sketched, from which the parameters of k, L, and T can be extracted. The *Table 3.1* can be used to determined the PID parameters for the control system.

Table 3.1: Ziegler-Nichols setting rule

Controller Type	K_p	T_i	T_D
P	$k_u/2$	-	-
PI	$k_u/2.2$	$p_u/1.2$	-
PID	$k_u/1.7$	$p_u/2$	$p_u/8$

3.5.2 Integral Performance Criteria

There are two generic performance standards according to which PID control performance is measured. The first standard measures performances based on the step response of the plant and these include the maximum dynamic derivation, adjusting the time and the settling ratio. The second approach evaluates the performance exhibited by the function of the system response error and the time from when it started to when it reaches stability [93].

The conventional method for optimising the search for the best PID parameters is the use of the brute force approach. However, modern techniques use cost functions for optimisation or

objective functions to guide the algorithm to search the optimised controller parameters. The performance indices are presented in the subsections below. The main objective is to minimise the disturbance response. The following parameters are used in the equations below:

- t - time (seconds)
- e(t) - error signal
- r(t) - reference signal
- y(t) - output signal

It is important to remember that the performance indexes are used to find the optimal values for k_p, k_i and k_d from the search space that minimises the objective function in order to tune the controller. The search space is a three-dimensional one and when/if the search does not converge with an optimal parameter value, then the search range can be increased. A unity reference signal is generally selected for most of the process model.

A function of **Matlab Optimization Toolbox**, the **fminsearch**, is used to calculate the minimum of the objection function. The standard syntax for the *fminsearch* function is as follows:

$$x = fminsearch(fun, x0) \tag{3.29}$$

Where:

- x - is the local minimum being searched for.
- fun - is the described function to be searched.
- x0 - is the initial estimate where the search algorithm begins.

3.5.3 Integral Absolute Error

This method takes the absolute value of the error signal to remove the negative error components. General observation of the results from scholars suggests that this algorithm is good for simulation purposes.

$$J_{IAE} = \int_0^T |e(t)|\, dt = \int_0^T |r(t) - y(t)|\, dt \tag{3.30}$$

3.5.4 Integral Square Error

This algorithm simply squares the error signal to get rid of the negative error components. A noticeable aspect of this method is that it discriminates between over-damped and under-damped systems, and hence a compromise needs to be made to minimise the ISE.

$$J_{ISE} = \int_0^T [e(t)]^2 dt = \int_0^T [r(t) - y(t)]^2 dt \tag{3.31}$$

3.5.5 Integral Time Absolute Error

The performance index was proposed by Graham and Lathrop in (1953) [18], through the derivation of a set of normalised transfer function coefficients from 2^{nd}-order to 8^{th}-order in order to minimise the ITAE criterion for a step response type input. The objective function is chosen in a manner which allows the minimisation of the ITAE performance index. Equation (3.32) represents the parameters required to evaluate this performance index and is able to provide the controllers with a high load disturbance rejection and minimise the system overshoot while maintaining the robustness of the system under consideration [94, 95].

This algorithm measures the error signal with time and this emphasises the magnitude of the error values later on in the response rather than the initial large errors.

$$J_{ITAE} = \int_0^T t \times |e(t)|\, dt = \int_0^T t \times |r(t) - y(t)|\, dt \tag{3.32}$$

3.5.6 Integral Time Square Error

With this algorithm, the evaluation is conducted by taking the square error with time. This results in a larger amplification of the error values than with the ITAE performance criteria.

$$J_{ITSE} = \int_0^T t \times [e(t)]^2 dt = \int_0^T t \times [r(t) - y(t)]^2 dt \tag{3.33}$$

3.5.7 Robust H_∞ Controller

One of the most important properties in control design is feedback, as it allows correction of the measured output to match the reference input accurately. In the early 1960s many researchers (including the prominent control pioneers HW Bode and IM Horowitz) began to scrutinise the

usefulness of the property of feedback in control. The result of this initiative was the birth of modern control, and it was then that the design of optimal control dominated research. One of the greatest highlights was the solution to the Linear Quadratic Gaussian (LQG) [96] method. Later on, as research began to advance, it became apparent that LQG control failed to perform satisfactorily in real environments as:

- The controller became more unstable as more realism was introduced to the plant model; and
- Too much emphasis was paid on the optimality and not enough to the model uncertainty to capture plant variations.

It was then that researchers started to realise that more attention needed to be given to feedback and frequency-domain techniques to address the limitations of LQG control.

The main objective of control system design is to design a system capable of operating in real environments. It should be noted that the real environment experiences variations with time (aging components or temperature variations); also the load or disturbances may change, but the control system must be able to resist all variations.

The issue of model uncertainty arises as a result of simplifying assumptions made on the mathematical model representation, and nonlinearities which are either unknown and not included in the model, or modelled but later ignored to simplify the analysis. This requirement that the controller needs to perform satisfactorily in realistic situations is formally referred to as *robustness* [97]. This term can be split into two definitions:

- **Robust stability** - stabilise a system for a family of plant; and
- **Robust performance** - satisfying specifications such as steady state tracking, disturbance rejection and response time for a family of plants.

Some definitions of the skeleton structure of a feedback system are necessary:

- *r(s)* - reference signal: this is the command the designer wishes the gimbal to follow (track).
- *d(s)* - disturbance signal: this could be wind gust disturbing aircraft or disturbances coming from actuators which the system must reject.
- *n(s)* - measurement noise: this is introduced to the system via sensors (such as inertial sensors), which usually occur at high frequencies.

In general, the goal of robust control is to design a controller that ensures that a system can follow a command input with only a fairly small error and reject all disturbances and noise.

The general structure is presented in *Figure 3.6*.

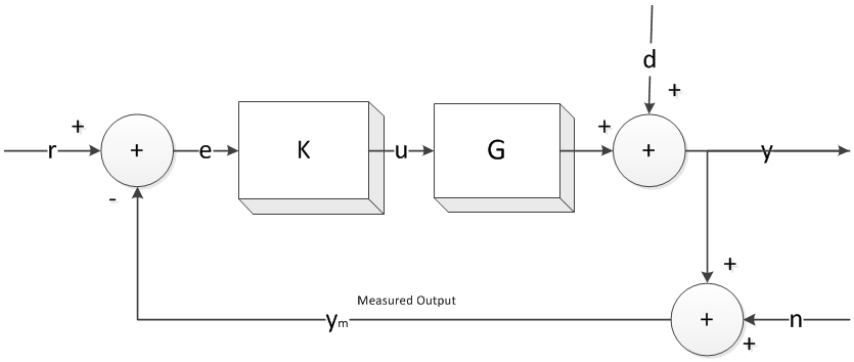

Figure 3.6: General feedback system model with controller

The following can be deduced from *Figure 3.6*:

- $L(s) = G(s)K(s)$ - Loop transfer function;
- $S(s) = \frac{1}{1+G(s)K(s)}$ - Sensitivity transfer function; and
- $T(s) = \frac{G(s)K(s)}{1+G(s)K(s)}$ - Complementary transfer function.

It must be noted that for all frequencies, the following statement holds for a SISO system, expressed in equation (3.34). When dealing with a Multi-Input Multi-Output (MIMO) system, the functions are vectors and the "1" is replaced by an identity (I) matrix.

$$S(s) + T(s) = 1 \tag{3.34}$$

The following statements can be made:

Command response: $y(s) \approx r(s)$, when $d(s) = n(s) = 0$ is set for a given range of frequencies. This requires $S(s)$ to be small or $L(s)$ to be large.

Disturbance rejection: Once again, in order to minimise the effect of disturbances, $S(s)$ must be small. Usually disturbances occur at low frequencies.

Noise suppression: We require $T(s)$ to be kept small in order to mitigate sensor noise on the output and, for this to be met, $L(s)$ must be small.

In summary, the loop transfer function is desired to have high gain at low frequencies (command following, and disturbance rejection) and low gain at high frequencies (for noise suppression) in order to satisfy S(s) and T(s) simultaneously.

When analysis is performed on MIMO systems, the singular value is computed and then related to the condition for loop gain for good command following performance, disturbance and noise suppression.

In order to obtain satisfactory nominal performance and robustness, bounds need to be imposed on the sensitivity function and complementary function. This process is formerly recognised as the loop shaping problem, and it is realised by introducing compensator or weighting function. This is depicted in *Figure 3.7*.

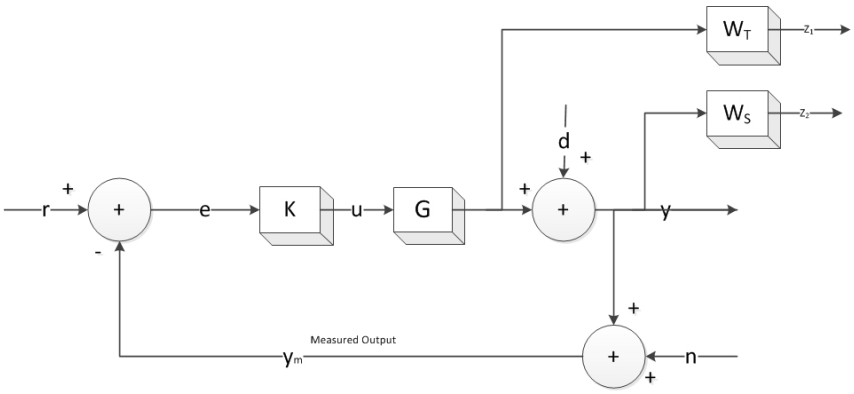

Figure 3.7: General system model with weighting functions

This then results in the generalised solution constraints, which needs to be satisfied:

$$|SW_s| \leq 1 \tag{3.35}$$

And:

$$|TW_T| \leq 1 \tag{3.36}$$

This holds for all frequencies, and it is commonly known as the *mixed-sensitivity* problem.

3.5.8 Model Uncertainty

The concept of model uncertainty is classified into two categories, *structured* and *unstructured* uncertainty. When dealing with structured uncertainty, the uncertainty is modelled and the

range and bounds of the uncertain parameters (such as *tolerances* of components) are actually known and can be modelled. The problem of unstructured uncertainty is outlined through insufficient knowledge of the system being modelled: the assumption made is that two bounds exist on the frequency response of the system [98, 99]. The modelling can be presented in two forms, additive and multiplicative uncertainty as follows:

$$\tilde{G}(s) = G(s) + \Delta_a(s) \tag{3.37}$$

For additive uncertainty, and

$$\tilde{G}(s) = (1 + \Delta_m(s))G(s) \tag{3.38}$$

For multiplicative uncertainty, where $\tilde{G}(s)$ represents the true model of the plant and $G(s)$ represents the mathematically derived model of the system, while $\Delta_a(s)$ and $\Delta_m(s)$ are the model errors [99]. It should be noted that the additive uncertainty structure is best for dealing with unmodelled dynamics or model reduction and multiplicative uncertainty structure is better suited for dealing with sensor/actuator noise dynamics.

A performance measure that can be used to verify the robust stability of the system can be carried out with the application of the small gain theorem, which requires that the loop gain be less than 1. For this study, only unstructured uncertainty is considered.

3.5.9 H_∞ Control Design

While success has been achieved when it comes to control solutions for SISO systems, as an extension initially it remained difficult to analyse and design controllers for MIMO systems. The difficulty was that the transfer function of a MIMO system is a vector (*matrix*). As the limitations of LQG methods became more apparent, researchers began to dedicate more time to investigating ways to extend classical control concepts. This gave birth to H_∞ [100–102] control paradigm in the 1980s. The formulation for this control technique was first realised by G. Zames [89].

The technique has been widely applied to many problems such as those defined in the article by Nawash [103]. By definition, H_∞ denotes the space of stable and proper transfer function. This means that, firstly, by *stable* - it is desired that the poles be strictly in the Left Hand Plane (LHP), and secondly, by *proper* - the degree of the denominator $\geq$ the degree of the numerator [104].

Since H_∞ is an optimisation technique, its primary concern is with the transfer functions describing the performance characteristics of the system. The optimisation procedure presupposes a cost function, which it uses to compare the various transfer functions and choose the best one in space according to the ∞-norm. The ∞-norm of a transfer function is defined by:

$$\|G\| = \underbrace{sup}_{\omega} |G(j\omega)| \tag{3.39}$$

where *sup* stands for the supremum.

Graphically, this is the peak in the bode magnitude plot of the transfer function. So, in summary, the aim is to minimise the ∞-norm of some transfer function, and this will increase the robust stability of the margin of the system. The general solution to the H_∞ control problem contains very cumbersome Riccati equations, and this is why robust control toolboxes have been developed to deal with the multiple differential equations. The general two-port block diagram that is used for the formulation of an H_∞ control problem is as presented in *Figure 3.8*.

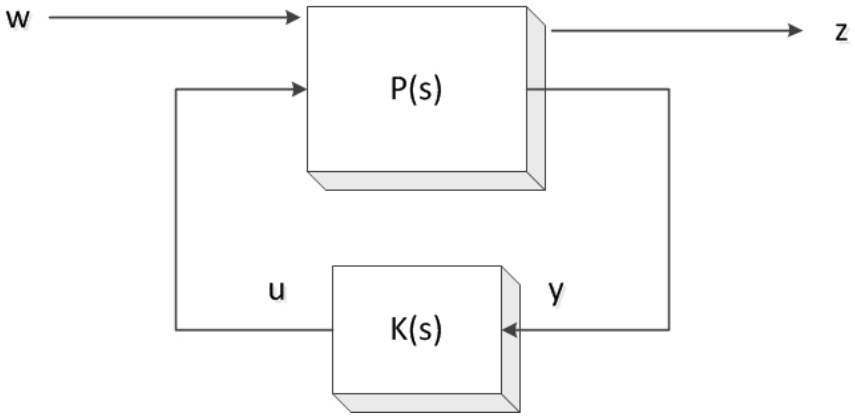

Figure 3.8: Two-port block diagram structure of H_∞

Where w is a vector which contains the exogenous inputs such as command input, noise and disturbance signals, and z is another vector which contains regulated outputs such as error signals, states and control signals. Lastly, y contains the measured output signal and u is the controlled input signal to the plant.

After applying all the inputs and outputs, the resulting system is of a MIMO type and its states space representation results in a transfer function matrix from w to z called the linear fractional transformation (LFT). The plant can also be represented in a packed-matrix notation. The elements A to D in equation equations (3.40) are vector entries derived from the state-space notation.

$$P(s) = \begin{bmatrix} A & B_1 & B_2 \\ C_1 & D_{11} & D_{12} \\ C_2 & D_{21} & D_{22} \end{bmatrix} \tag{3.40}$$

The designer must be aware that the solution to the H_∞ control problem contains very cumbersome Riccati equations that can be complex to solve analytically by hand; hence, it was preferred to use the Robust Control Toolbox.

3.5.10 Weights in H_∞ Control Problem

It is well understood that when working with practical control problems, it makes a lot more sense to apply weights on the input and outputs. In general, constant weights are used for unit conversion; however, transfer function weights are used to shape the robust performance characteristics in the frequency domain. To be more specific, in H_∞ control problems, the weights are used to satisfy the rank conditions which are specified on the generic form of the H_∞ problem.

The weights are still selected on the basis of the requirements on the loop transfer function for good tracking, disturbance rejection and noise suppression. This requires solving the mixed sensitivity problem, as discussed earlier. The most common notation discussed in the article by [105–107] for the weighting function required for loop shaping satisfaction is presented as follows:

$$W_s = \frac{s/M + \omega_B}{s + \omega_B A} \tag{3.41}$$

$$W_t = \frac{s + \omega_B/M}{As + \omega_B} \tag{3.42}$$

Where A (< 1) is the maximum allowed steady state offset, M is the sensitivity peak and ω_B is the desired bandwidth.

3.6 Quantitative Feedback Theory

When the objective is to attain robust performance from a dynamic system, then the QFT [1, 108, 109] technique in control provides a more direct, frequency-domain-based design approach for dealing with feedback control problems. The approach involves specifying plant dynamics

by the frequency response data or by a transfer function containing (parametric and non-parametric) uncertainty models. Its ability to deal directly with uncertainty models and the robust stability and performance criteria is what distinguishes QFT from other frequency-domain methods. The way it achieves this is by translating the robust performance specifications and uncertainty models into QFT bounds. The bounds are then displayed on a Nichols chart plot, and serve as a guide for shaping the nominal loop transfer function (which involves the manipulation of gain, poles and zeros). Note that the design process is executed using CAD software such as the QFT control design *Matlab Toolbox* [110].

QFT, first proposed in 1959, is an amalgamated theoretical concept which deals with the design and implementation of a robust control system for a model system that has structured parametric uncertainty to satisfy the desired performance specification, even when subjected to the presence of disturbances, noise amplification or resonance [90]. This very rigorous robust control approach was developed by Professor IM Horowitz. This control approach works on $T(s)$ from equation (3.34) in the design on the controller. It also requires that the designer have upfront knowledge of the plant variations (structured parametric uncertainty). It should be stated that this control approach is a strictly frequency domain design technique.

QFT control engineering designers who do not produce satisfactory solutions are usually challenged by the lack of gain-phase loop-shaping experience and could benefit from algorithms which present automatic procedures [111–114] for the loop-shaping problem.

The general idea behind the design is to maintain a low loop gain ($L(s) = G(s)K(s)$) because, as stated before, $T(s)$ requires low $L(s)$ at high frequencies. Ultimately, the QFT main control objective is to synthesise (loop-shape) a simple, low-order controller with minimum bandwidth, which satisfies the desired specifications and handles feedback control problems with robust stability and performance objectives.

The block diagram for a generalised structure of a QFT system is presented in *Figure 3.9*.

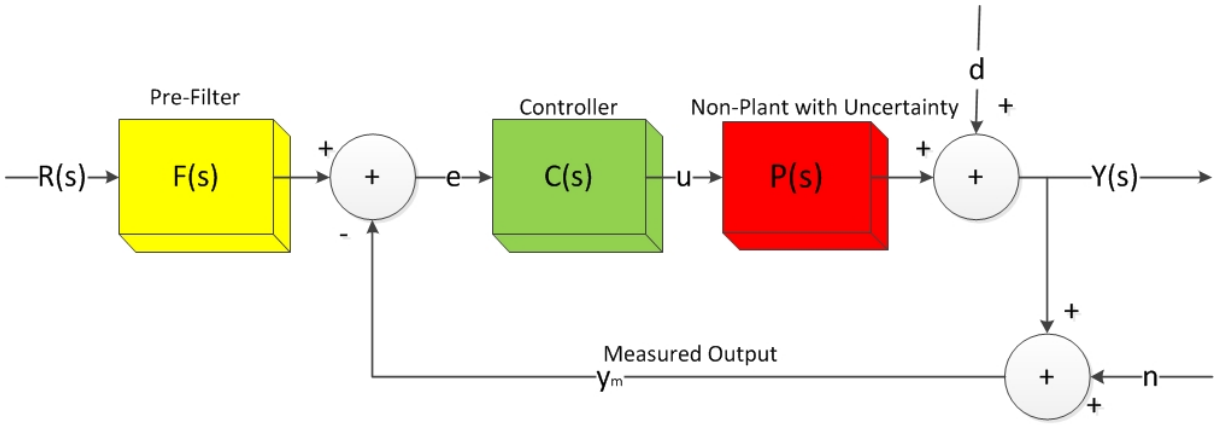

Figure 3.9: QFT generalised block diagram

The equation for the complementary sensitivity function is as follows:

$$T(s) = \frac{F(s)C(s)P(s)}{1 + C(s)P(s)} \tag{3.43}$$

The design steps are summarised in *Figure 3.10*.

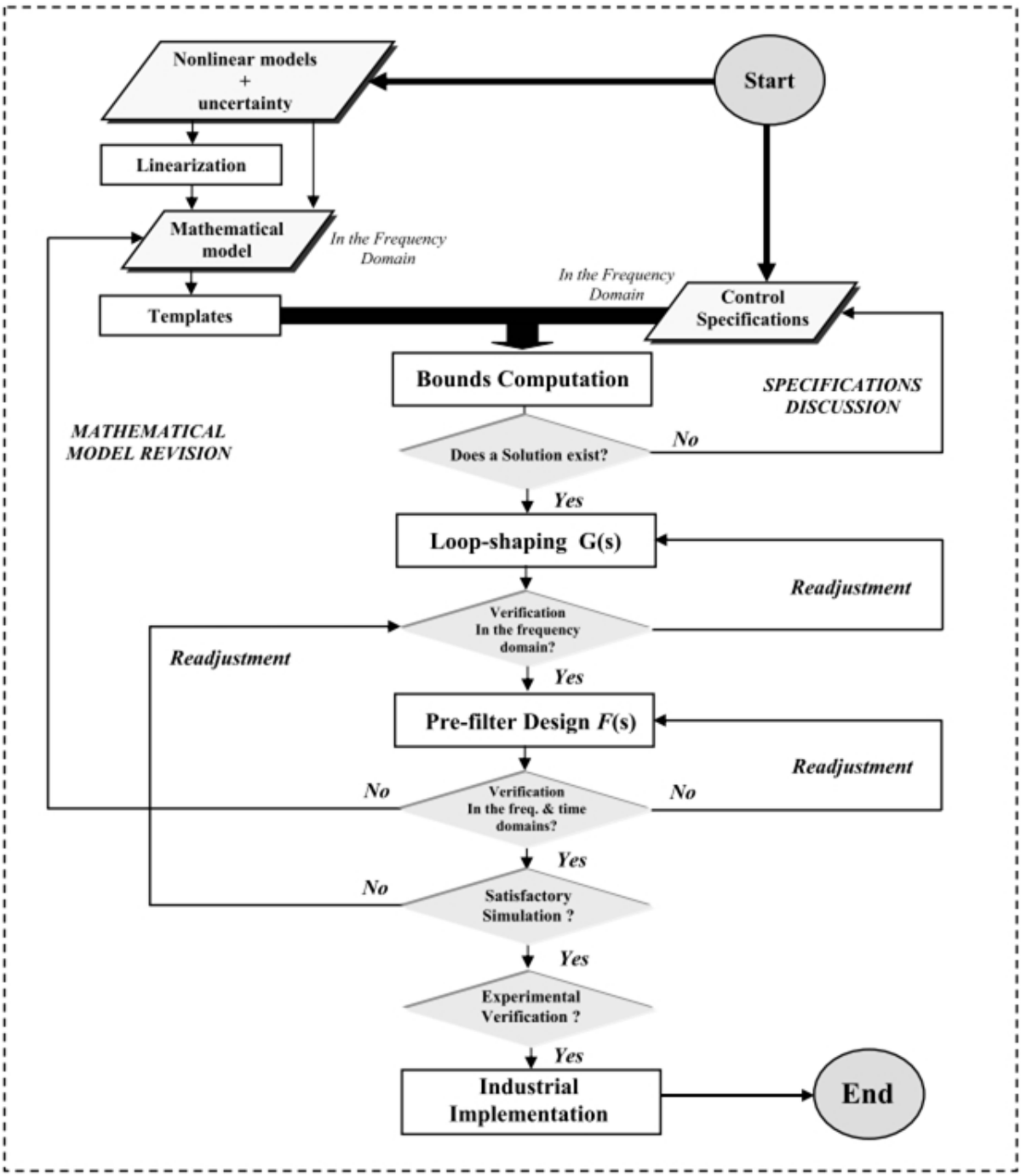

Figure 3.10: QFT design and implementation flowchart methodology for a multi-input single-output (MISO) system, figure courtesy of "Adapted from M. Garcia-Sanz [1]".

The researchers in [115–123] present some of the practical problems, which range from industrial furnace and large wind turbines to waste water treatment plants, to which the QFT control technique has been applied with plausible success. The benefits of using the QFT control design approach can be summarised as follows:

- The obtained result is a robust design which is insensitive to model plant variations.
- Any design limitations in the system are apparent up front.
- There is one design for the full envelope (which means that there is no need to verify plants inside templates).
- The engineer can determine what specifications are achievable early on in the design process.
- It is possible to redesign for changes in the specifications quickly and with ease.
- In comparison to other multi-variable design techniques there is less development time for a full envelope design.
- The structure of the compensator (controller) is determined up front.

3.7 Robust Adaptive Control

Research in adaptive control commenced in the early 1950s. It was motivated by the problem of designing autopilots for high-performance aircrafts operating at a wide range of speeds and altitudes. The basic idea was to design a good fixed-gain controller which is insensitive to these (large) parameter variations; however, general observation became that a single constant gain controller is not sufficient. Initially, adaptive control was proposed as a way of automatically adjusting the control parameters while subject to changing aircraft dynamics [124]. However, the strong interest diminished as a result of insufficient knowledge and the crash of the test flight. It was only in the years 1980 to 1990 that coherent theory on the subject matured using a number of tools from nonlinear control theory. The advancement in the theory and availability of cheap computation opened up a wide spectrum of practical applications in areas such as aircraft and rocket control, chemical processes, power systems, ship steering, bioengineering and robot manipulation.

Robust control has some desirable features which adaptive control does not have, such as the ability to deal with disturbances, quickly varying parameters and unmodelled dynamics. In more advanced cases, such features can be *combined* with adaptive control, to lead to *robust adaptive controllers*. This results in the uncertainties on constant or slowly varying parameters

being reduced by parameter adaptation and other sources of uncertainty are taken care of by using *robustification* techniques. Robustification is another form of optimisation technique and it is applied to make a system less sesnititve to the effects of random variability [124].

Another very important point is that the existing adaptive techniques for nonlinear systems generally require a linear parametrisation of the plant dynamics.

Control problems where model uncertainty is a primary issue generally fall under the nonlinear class of model plants, and thus require non-linear controllers to deal with them. Two types of non-linear controllers are prescribed to deal with model uncertainty: robust and adaptive control. Robust control has already been discussed and the application of adaptive control on the gimbal platform is elaborated below.

Adaptive control can be a specific type of control where the process is controlled in closed-loop, and where knowledge about the system characteristics is obtained on-line while the system is operating. On the basis of refreshed information obtained during normal operation, specific interventions in the control loop are made in order to satisfy the control objective [124]. Interventions can be various but mainly they can be categorised as interventions obtained by changing:

- Signal - signal adaption
- Parameters - parameter adaption
- Structure - structure adaptation

The basic idea in adaptive control is to estimate the uncertain plant parameters (or, equivalently, the corresponding controller parameters) *on-line*, based on the measured system signals, and then use the estimated parameters in the control input computation [124]. Thus, an adaptive control system can be regarded as a control system with on-line parameter estimation. As mentioned before, adaptive control systems are inherently nonlinear, irrespective of whether they are designed for linear or nonlinear plants.

In principle, adaptive control is superior to robust control in dealing with uncertainties in constant or slowly varying parameters. The reason for this is that an adaptive controller improves its performance as adaptation goes on, while a robust controller simply attempts to keep consistent performance [124].

3.7.1 Adaptive Control Design Steps

The following are the sequential steps required when designing an adaptive controller for a generic system:

1. Establish the differential equation or transfer function for the generic/nominal plant model;
2. Choose a control law containing uncertain variable parameters;
3. Choose an adaptation law for adjusting those parameters; and
4. Analyse the convergence properties of the resulting control system.

There are two main generic techniques for implementing adaptive controllers. One is referred to as the *model-reference adaptive control* method and the other is called the *self-tuning* method [124]. A brief description is be provided of the two generic techniques, as an attempt to provide context for the chosen application.

3.7.2 Model-Reference Adaptive Control

A model-reference adaptive control (MRAC) system consists of four main components: a *plant* containing unknown parameters, a *reference model* which is used to specify the desired output of the control system, a feedback *control law* which consist of the adjustable parameters, and an *adaptation mechanism* to be used to update the adjustable parameters [124].

Figure 3.11 shows all the main components.

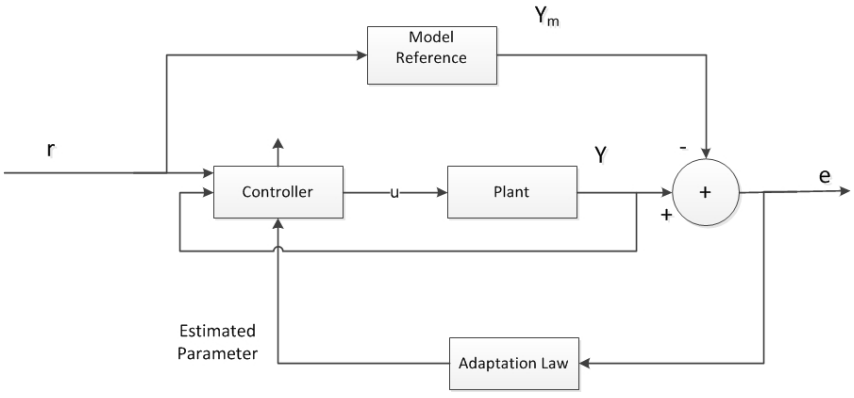

Figure 3.11: Model reference adaptive control generic structure

Generally, the structure of the plant is assumed to be known, even though the embedded parameters are unknown. The main purpose of the introduction of a reference model is to

specify the ideal response of the adaptive control system to the external command. This serves the purpose of providing the ideal plant response for which the adaptation mechanism should look in adjusting the parameters. The choice of the reference model is crucial because it needs to satisfy the required performance specifications in the control task, such as rise time, settling time, overshoot, steady state error or the frequency domain characteristics. It should be noted that this choice for the ideal behaviour should also be achievable for the adaptive control system [124].

The controller is not specified by a fixed gain or a transfer function with fixed parameters; instead, it is usually parameterised by a number of adjustable parameters. Another strict requirement is that the controller should have perfect tracking capacity in order to allow the possibility of tracking convergence. This implies that when the plant parameters are exactly known, the corresponding controller parameters should make the plant output identical to that of the reference model, but when the plant parameters are not known, then the adaptation mechanism must adjust the controller parameters so that perfect tracking is asymptotically achieved [124].

In more simpler terms, the adaptation mechanism is utilised to adjust the parameters in the control law. More specifically, in MRAC systems, the adaptation law searches for parameters so that the plant response under adaptation control becomes the same as that of the reference model. This is achieved by making the tracking error converge to zero.

The biggest challenge in designing this adaptation mechanism is to ensure stability and that the tracking error converges to zero as the parameters are varied. The Lyapunov theory is used to verify stability.

3.7.3 Self-tuning Adaptive Controller

In a more formal definition, a controller that results from coupling a controller with an on-line (*recursive*) parameter estimator is called a self-tuning controller. The unknown plant parameters are estimated through the implementation of a particular *identification* algorithm, such as the least square method and its extension. In layman terms, parameter estimation through an identification algorithm can be understood as the process of finding a set of parameters that fits the available measured input-output data from an unknown plant [124].

There are two generic structures in self-tuning adaptation control systems: *indirect* adaptive control and *direct* adaptive control. The former involves the estimation of plant parameters and the computation of the controller parameters. The latter requires the parameterisation of the plant model using controller parameters, and then using standard estimation techniques for the update.

In self-tuning control systems the estimator design is separate from the controller design. This means that the estimator law is independent of the choice of the control law. However, the drawback of self-tuning controllers is the difficulty in performing analysis of the convergence and stability performance.

Figure 3.12 illustrates all the main components.

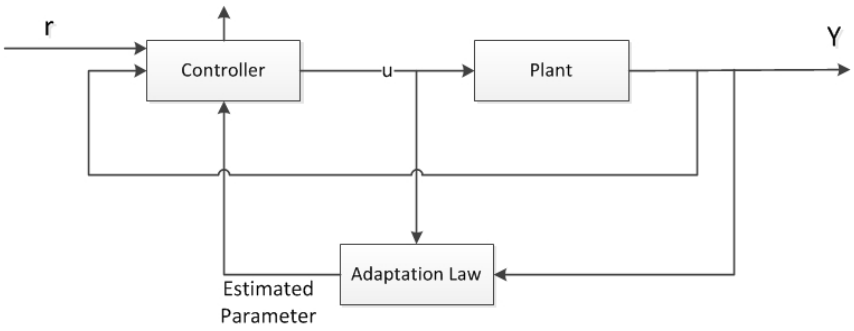

Figure 3.12: Self-tuning adaptive control generic structure

3.7.4 Adaptive Control Design Steps

The following sequential steps are required when designing an adaptive controller for a generic system:

1. Establish the differential equation or transfer function for the plant model;
2. Choose a control law containing uncertain variable parameters;
3. Choose an adaptation law for adjusting those parameters; and
4. Analyse the tracking convergence properties of the resulting control system.

When one compares the self-tuning adaptive control method to the MRAC method, it is apparent that self-tuning controllers are more flexible because of the possibility of coupling various estimator algorithms to the controller. On the other hand, the stability and convergence of self-tuning controllers are more difficult to guarantee [124].

Sometimes the estimated parameters will not converge to the ideal controller parameters unless the reference signal, denoted by $r(t)$, satisfies certain conditions. If the reference signal is too simple, such as zero or a constant, convergence might never be achieved; however, if the reference signal is more complex, such as a sinusoidal function, then convergence is more likely to be achieved.

3.7.5 On-line Parameter Estimation

One way of reducing parameter uncertainty in a dynamic system (it can be linear or nonlinear) is to use parameter estimation. Note that parameter estimation can be carried out on-line or off-line. When dealing with constant parameters and there is enough time for estimation before control, off-line estimation may be preferable. However, if one is presented with slowly varying parameters while the system is in operation, then on-line parameter estimation is a preferred route to keep track of the parameter values [124].

It must be stated that in off-line estimation, the designer collects the input-output data for a period of time and solves the equation used to estimate parameters. In on-line estimation, the equation is solved recursively, meaning that the estimated parameter value is updated every time a new set of data is available. The quality of the estimation (how well and how fast the parameters are estimated) depends on two general aspects: the estimation method used and the information content (persistent excitation).

One of the most common estimator methods is the least-square estimator algorithm [124].

3.8 Research Instruments

The instruments that were used in the study listed below:

- Host Computer (Microsoft OS)
- Matlab
- Simulink
- Control Systems Toolbox
- QFT Toolbox
- SimMechanics Toolbox
- Arduino Starter Kit (with microcontroller and breadboard)
- Two-axis camera tripod gimbal
- Hi-tec Servos (2 off)
- Incremental Optical Encoder
- 9 V Battery

3.8.1 Rotational Position Measurement

When precise information about the rotational movement of the gimbal is required, two types of feedback units can be installed, analogue or digital units. Analogue rotational movement detectors are referred to as *potentiometers* and digital detectors are *encoders*. The disadvantage of potentiometers is that they may cause drift and they have rotational limits which can hinder certain required motions for some applications, such as the continuous pan axis. Rotational encoders, on the other hand, do not have rotation limits and drift because the output signal is a digital one. Note that rotational encoder output can be either absolute or incremental, where absolute has a unique binary code for every position and thus the number of contact wires increases in conjunction with the resolution. On the other hand, incremental encoders usually have two channels and two signal wires, which give out readings pertaining to the direction and increments of rotational position, although the main contributor is the main rotor, which rotates at about 1500 rpm to 2000 rpm [53].

A detailed discussion on the available sensors and estimation mechanism is presented in Appendix A, Sections A.3 and A.4.

3.9 Data

The data required will be generated through simulation using the host computer and associated software, Matlab, Simulink and associated toolboxes, and Arduino software. An incremental optical encoder is used to obtain feedback angular position data for the control system.

3.10 Analysis

The analysis was performed by plotting graphs and presenting tables to compare the performance from the various controllers. A tripod gimbal hardware was also used to verify the performance of the controller, where it received commands from the controller and its response could be visually observed. From the results obtained a critical analysis was performed for the performance comparison of the different controllers.

3.11 Limitations

The notable limitation stemmed from the inability to integrate the gimbal platform with the helicopter UAV and verify compatibility and joint performance. This would require an autopilot

to be installed on the UAV which provides motion command and control to the helicopter and gimbal. This crucial hardware was unfortunately not purchased due to circumstances beyond the control of the researcher. Hence, all results presented here relate to the performance of the gimbal alone.

Another test which would have allowed the gimbal assembly to be subjected to varying-frequency mechanical vibrations from a shaker table (vibration table) was never carried out. The test was supposed to be performed at *Denel Dynamics*. The initial test (2 day duration) was going to be the **modal test** to be carried out on the aircraft as follows:

1. Measure the R-UAV platform frequency spectrum response, and
2. And then provide a detailed report on the results obtained.

The seconds test (1 day duration) was going to be the aircraft and gimbal assembly **vibration test** to be performed as follows:

1. Attach multiple (over 20) accelerometers on the aircraft, at critical resonance location, to measure its vibration spectra;
2. Use the results obtained (frequency spectra) to inject vibrations on the *shaker-table* holding the gimbal platform and observe/measure how the gimbal performs under various disturbances;
3. Provide a detailed report on the results obtained (giving a vibration spectrum for all three axes).

The reason the test was never performed is because there were too many draw-backs on the aircraft's operation, and it required too many repairs which delayed the time. A cost breakdown on how much the test would have cost is provided in Appendix D, section D.3.

The projected time-line for the critical milestones to be conducted on the project is summarised in a Gantt chat in Appendix C, Section C.1 and figure C.1, and this comes from the reality that the University has explicit rules governing how long the study is allowed to continue (which is 2 years for full-time registered students).

3.12 Ethical Considerations

A major ethical consideration was that every time the UAV was tested a certified pilot had to fly it. None of uncertified researchers where allowed to fly the UAV aircraft. This was because,

even though there is no direct or specific law governing the usage of UAVs in SA, the CSIR as a respected institution is required to set certain standards. Some of these standards will hopefully be incorporated by the Aviation Authority of SA. The other ethical consideration was in the usage of properly licensed software for the development of the control algorithms.

3.13 Conclusion

The methodology that was used to complete this project successfully was presented in this chapter. A detailed theoretical background was also presented for the modelling and control aspects of the projects. The tools that were used to implement the control algorithm were described and the data, limitations and the ethical considerations were highlighted.

Chapter 4

Modelling Implementation

4.1 Introduction

The model implementation of the actuators and gimbal platform is presented in this chapter. The technical analytical procedures undertaken to derive the dynamic equations used to describe the behaviors of the system are also provided in detail.

4.2 DC Motor

The chosen motor for providing the required torque to the gimbal platform is a brushed DC motor. A detailed discussion on the selection method, taking into consideration the power requirements and torque requirements for the gimbal system is presented in Appendix A. *Figure 4.1* presents the simplified electro-mechanical model of the DC motor. Appendix B, section B.1 presents the derivation of of the equations governing the motion of the motor.

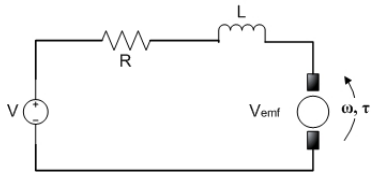

Figure 4.1: Electromechanical model of brushed DC motor

Following the derivation in Appendix B, from Kirchof's Voltage Law, the following electrical equations are presented:

$$V = Ri + L\frac{di}{dt} + V_{emf} = Ri + L\frac{di}{dt} + K_m\omega \tag{4.1}$$

$$\begin{bmatrix} \ddot{\theta} \\ \dot{i} \end{bmatrix} = \begin{bmatrix} \frac{-B_m}{J_m} & \frac{K_t}{J_m} \\ \frac{-K_m}{L_a} & \frac{-R_a}{L_a} \end{bmatrix} \begin{bmatrix} \dot{\theta} \\ i \end{bmatrix} + \begin{bmatrix} 0 \\ \frac{1}{L_a} \end{bmatrix} V \tag{4.2}$$

$$\dot{\theta} = \begin{bmatrix} 1 & 0 \end{bmatrix} \begin{bmatrix} \dot{\theta} \\ i \end{bmatrix} \tag{4.3}$$

In an ideal PM DC motor, the motor constant K_m and torque constant K_t are assumed to be equal in the modelling and the damping coefficient is neglected.

4.2.1 Dynamic Analysis

It should be noted that robot dynamics provide the relationship between actuation and contact forces, and the acceleration of motion trajectories that result. It is crucial to obtain the dynamic equations of motion for the system since they form the basis for a number of computational algorithms that are useful in electro-mechanical design, control realisation and simulation.

In the industry and academia, their application has grown, especially in computer animation of mobile systems through the use of human and humanoid models. The commonly used low-order algorithms are summarised as follows:

- Inverse dynamics, in which the required joint actuator torque/forces are computed from a specification of the robot's trajectory (position, velocity and acceleration);
- Forward dynamics, in which the applied joint actuator torques/forces are specified and the joint acceleration is to be determined;
- The joint-space inertia matrix, which maps the joint acceleration to the joint torques/forces; and
- The operational-space inertia matrix, which maps task accelerations to task forces in operational or Cartesian space.

Once the dynamic equations of motion are derived, they can be represented in two basic forms: the joint-space formulation and the operational-space formulation. The derivation process followed when deriving the joint-space formula is the Lagrangian formulation. In brief, the Lagrangian formulation forms a link between the joint actuator forces and the motion of the mechanism, and it fundamentally operates on the kinetic and potential energy in the system. The equation can be represented in a compact form, which is scientifically known as the canonical form.

A basic rigid-body model of a robot mechanism has four components: a connectivity graph (not elaborated on in this study), link and joint geometry parameters, link inertia parameters, and a set of joint models. To the same model, one can add various force-producing elements, such as springs, dampers, joint friction, actuators, and drives. The actuators and drives may in fact have their own detailed elaborate dynamic models. It is also possible to add extra motion freedoms to model other imperfections such as elasticity in the joint bearings or links.

D-H convention is applied to the 2-DOF gimbal platform.

Table 4.1: Denavit-Hartenberg convention table

Gimbal Joint i	α_i	a_i	d_i	θ_i
1	0	0	0	θ_1
2	$-\pi/2$	0	0	θ_2

The transformation matrix is as follows:

$$ {}^{0}T_1 = \begin{bmatrix} \cos(\theta_1) & -\sin(\theta_1) & 0 & 0 \\ \sin(\theta_1) & \cos(\theta_1) & 0 & 0 \\ 0 & 0 & 1 & 0 \\ 0 & 0 & 0 & 1 \end{bmatrix} \tag{4.4} $$

And

$$ {}^{1}T_2 = \begin{bmatrix} \cos(\theta_2) & -\sin(\theta_2) & 0 & 0 \\ 0 & 0 & -1 & 0 \\ \sin(\theta_2) & \cos(\theta_2) & 0 & 0 \\ 0 & 0 & 0 & 1 \end{bmatrix} \tag{4.5} $$

And it follows that:

$$ {}^{2}\mathbf{T}_0 = {}^{1}\ \mathbf{T}_0^2\mathbf{T}_1 \tag{4.6} $$

Calculating the Jacobian matrix:

$$ J_{o1}^{(\ell_1)} = \begin{bmatrix} 0 \\ 0 \\ 1 \end{bmatrix} \tag{4.7} $$

To find the kinetic energy for the gimbal, the following equation is used:

$$T_i = \frac{1}{2}\dot{\theta}_i^T J_i^{(\ell_i)T} R_i I_{\ell_i}^i R_i^T J_i^{(\ell_i)} \dot{\theta}_i \tag{4.8}$$

First the inertia matrix is calculated:

$$R_1 I_{\ell_1}^0 R_1^T = \begin{bmatrix} \cos(\theta_1) & -\sin(\theta_1) & 0 \\ \sin(\theta_1) & \cos(\theta_1) & 0 \\ 0 & 0 & 1 \end{bmatrix} \begin{bmatrix} I_1 & 0 & 0 \\ 0 & I_1 & 0 \\ 0 & 0 & I_1 \end{bmatrix} \begin{bmatrix} \cos(\theta_1) & \sin(\theta_1) & 0 \\ -\sin(\theta_1) & \cos(\theta_1) & 0 \\ 0 & 0 & 1 \end{bmatrix} = \begin{bmatrix} I_1 & 0 & 0 \\ 0 & I_1 & 0 \\ 0 & 0 & I_1 \end{bmatrix} \tag{4.9}$$

Therefore:

$$T_1 = \begin{bmatrix} 0 & 0 & \theta_1 \end{bmatrix} \begin{bmatrix} 0 & 0 & 1 \end{bmatrix} \begin{bmatrix} I_1 & 0 & 0 \\ 0 & I_1 & 0 \\ 0 & 0 & I_1 \end{bmatrix} \begin{bmatrix} 0 \\ 0 \\ 1 \end{bmatrix} \begin{bmatrix} 0 \\ 0 \\ \theta_1 \end{bmatrix} = \frac{1}{2} I_1 \dot{\theta_1}^2 \tag{4.10}$$

Applying the Lagrangian equation:

$$\frac{\partial T_1}{\partial \dot{\theta_1}} = I_1 \dot{\theta_1} \tag{4.11}$$

And

$$\frac{d}{dt}\frac{\partial T_1}{\partial \dot{\theta_1}} = I_1 \ddot{\theta_1} \tag{4.12}$$

and also

$$\frac{\partial T_1}{\partial \theta_1} = 0 \tag{4.13}$$

Therefore:

$$\frac{d}{dt}\frac{\partial T_1}{\partial \dot{\theta_1}} - \frac{\partial T_1}{\partial \theta_1} = I_1 \ddot{\theta_1} = \tau_1 \tag{4.14}$$

Following the same approach for the second degree of freedom (with $i = 2$), the Jacobian matrix is as follows:

$$J_1^{(\ell_2)} = \begin{bmatrix} 0 \\ 1 \\ 0 \end{bmatrix} \tag{4.15}$$

The transformation matrix follows:

$${}^1T_2 = \begin{bmatrix} \cos(\theta_2) & -\sin(\theta_2) & 0 & 0 \\ 0 & 0 & -1 & 0 \\ \sin(\theta_2) & \cos(\theta_2) & 0 & 0 \\ 0 & 0 & 0 & 1 \end{bmatrix} \tag{4.16}$$

Once again, the kinetic energy is calculated using equation (4.8) and substituting ($i = 2$) the following equation is obtained:

$$T_i = \frac{1}{2}\dot{\theta}_2^T J_1^{(\ell_2)T} R_2 I_{\ell_2}^1 R_2^T J_1^{(\ell_2)} \dot{\theta}_2 \tag{4.17}$$

And the kinetic energy after solving equation (4.17):

$$T_2 = \frac{1}{2} I_2 \dot{\theta_2}^2 \tag{4.18}$$

After applying the Lagrangian formulation, the resulting equation is:

$$\frac{d}{dt}\frac{\partial T_2}{\partial \dot{\theta_2}} - \frac{\partial T_2}{\partial \theta_2} = I_2 \ddot{\theta_2} = \tau_2 \tag{4.19}$$

From the mathematical derivation, it can be clearly observed that the equations are not coupled at all. When all the gimbal assembly parameter are considered such as the damping coefficient, B, and the stiffness coefficient, K, the generalised equation takes the following form as per equation (4.20):

$$\tau = I\ddot{\theta} + B\dot{\theta} + K\theta \tag{4.20}$$

4.3 Conclusion

A thorough and rigorous approach for deriving the equations of motions necessary for the accurate dynamic modelling of the actuator dynamics and the gimbal dynamics was presented. The

two-DOF gimbal assembly is modelled following the standard robotic manipulator techniques integrated with the Lagrangian method. Its amazing to notice how the gimbal model simplifies to this basic LTI system after considering the mechanical construction of the assembly.

Chapter 5

Control Implementation

5.1 Introduction

The implementation procedures of the control algorithms applied on the two-axis gimbal platform which is mounted to a multi-sensor camera are discussed in this chapter. These are the PID control with associated auto-tuning algorithms, robust H_∞ control, QFT.

5.2 PID Control

Traditionally, control design in robot manipulators can be understood as the simple fact of tuning a PD or PID compensator at the level of each motor driving the manipulator joints. Fundamentally, a PD controller is a position and velocity feedback that has good closed-loop properties when applied to a double integrator system. In actuality, the strong point of PID control lies in its simplicity and clear physical meaning. When it comes to the industry, simple control is preferable to complex control if the performance enhancement obtained by using complex control is not significant enough. The physical meaning of PID control is noted as follows:

- P-control means the present effort of making a present state into a desired state;
- I-control means the accumulated effort of using the experience information of previous states; and
- D-control means the predictive effort of reflecting the information about trends in future states.

5.2.1 PD Control for Regulation

A simple design method for manipulator control is to utilise a linear control scheme based on the linearisation of the system about a operating point. An example of this technique is a PD control with a gravity compensation scheme. Gravity compensation acts as a bias correction, which compensates only for the amount of force that creates overshooting and an asymmetric transient behaviour. Formally, it has the following form:

$$\tau = \mathbf{K}_P(\mathbf{q}_d - \mathbf{q}) - \mathbf{K}_V\dot{\mathbf{q}} + \tau_g(\mathbf{q}) \tag{5.1}$$

Where $\mathbf{K}_p$ and $\mathbf{K}_v \in R^{n\times n}$ are positive-definite gain matrices [84]. This controller is very useful for set-point regulation, i.e., $q_d = constant$. When this controller is applied to equation (3.20), the closed-loop equation becomes:

$$\mathbf{H}(\mathbf{q})\ddot{\mathbf{q}} + \mathbf{C}(\mathbf{q},\dot{\mathbf{q}})\dot{\mathbf{q}} + \mathbf{K}_V\dot{\mathbf{q}} - \mathbf{K}_P\mathbf{e}_q = \mathbf{0}, \tag{5.2}$$

Where $\mathbf{e}_q = \mathbf{q}_d - \mathbf{q}$, and the equilibrium point is $\mathbf{y} = [\mathbf{e}_q^T, \dot{\mathbf{q}}^T] = \mathbf{0}$.

5.2.2 PID Control for Regulation

An integral action may be added to the previous PD control to deal with gravity forces, which to some extent can be considered as a constant disturbance (from the local point of view). The PID regulation controller can be written in the following general form:

$$\tau = \mathbf{K}_P(\mathbf{q}_d - \mathbf{q}) + \mathbf{K}_I\int f(\mathbf{q}_d - \mathbf{q})dt - \mathbf{K}_V\dot{\mathbf{q}} \tag{5.3}$$

Where $K_I \in R^{n\times n}$ is a positive-definite gain matrix, and if:

- $f(\mathbf{q}_d - \mathbf{q}) = \mathbf{q}_d - \mathbf{q}$, we have PID control
- $K_I\int(-\dot{\mathbf{q}})dt$ is added, we have PI^2D [84]control
- $f(\cdot) = \tanh(\cdot)$, we have PD plus nonlinear integral control

5.2.3 PID Gain Tuning

The PID control can be utilised for trajectory tracking as well as set-point regulation. The general PID controller can be written in the following general form:

$$\tau = \mathbf{K}_V \dot{\mathbf{e}}_q + \mathbf{K}_P \mathbf{e}_q + \mathbf{K}_I \int \mathbf{e}_q dt \tag{5.4}$$

Or, in another form:

$$\tau = (K + \frac{1}{\gamma} I)(\dot{\mathbf{e}}_q + \mathbf{K}_P \mathbf{e}_q + \mathbf{K}_I \int \mathbf{e}_q dt) \tag{5.5}$$

Actually, if a PID controller is repeatedly applied to the same set-point or desired trajectory, then the maximum error will be proportional to the gains in the following form:

$$0 \leq \overset{max}{t} \leq t_f \ \|\mathbf{e}_q(t)\| \, \alpha \frac{\gamma^2}{\sqrt{2k\gamma^2 + 1}}, \tag{5.6}$$

Where t_f denotes the final execution time of a given task and $\mathbf{K} = k\mathbf{I}$. This relation can be utilised to tune the gain of a PID controller and is referred to as the *compound tuning rule* [84]. The compound tuning rule implicitly includes simple tuning rules as follows:

- Square tuning: $max \, \|\mathbf{e}_q\| \, \alpha\gamma^2$, for small k
- Linear tuning: $max \, \|\mathbf{e}_q\| \, \alpha\gamma$, for large k

5.3 Optimal and Robust Control

Given a nonlinear system, such as robotic manipulators, one can develop many stabilising controls. In other words, the stability of the control system cannot determine a unique controller. It is natural that one seeks an optimal controller among the many stable ones. However, the design of an optimal controller is possible provided that rather exact information on the target system is available, such as an exact system model. In the presence of discrepancy between the real system and its mathematical model, a designed optimal controller is no longer optimal, and may even end up being unstable in the actual system. Generally speaking, the optimal control design framework is not the best framework to deal with system uncertainty. To handle system uncertainty from the control design stage, a robust control design framework is necessary. One

of the main objectives of robust control is to keep the controlled system stabilized even in the presence of uncertainties in the mathematical model, unmodelled dynamics, and so forth.

Consider an affine non-linear system described by non-linear time-varying differential equation in the state $\mathbf{x} = (x_1, x_2, ..., x_n)^T \in R^n$:

$$\dot{\mathbf{x}} = \mathbf{f}(\mathbf{x}, t) + \mathbf{G}(\mathbf{x}, t)\mathbf{u} + \mathbf{P}(\mathbf{x}, t)\mathbf{w}, \tag{5.7}$$

Where $\mathbf{u} \in R^m$ is the control input, and $\mathbf{w} \in R^w$ is the disturbance. Without disturbance and unmodelled dynamics, the system simplifies to:

$$\dot{\mathbf{x}} = \mathbf{f}(\mathbf{x}, t) + \mathbf{G}(\mathbf{x}, t)\mathbf{u}. \tag{5.8}$$

5.4 PID Tuning

5.4.1 Ziegler-Nichols and Integral Performance Indices Tuning

The implementation of the integral absolute error, integral square error, integral time absolute error and integral time square error algorithm is simplified by adapting the code that has already been developed specifically for the purpose of comparison to the Ziegler-Nichols tuning method. The code is borrowed courtesy of the *Mathworks development team* [88]. The search algorithm is implemented and performed using the *fminunc* Matlab optimization algorithm which works similarly to the *fminsearch*, except that it is unconstrained.

5.5 Robust H_∞ Control Algorithms

The implementation procedure for the H_∞ controller is demonstrated in this section, and some of the required toolboxes are mentioned in the implementation subsection.

5.5.1 Matlab Implementation of H_∞ Controller

The mathematical computation required to solve the H_∞ problem is very cumbersome; in fact, for every γ optimised value, two Riccati equations need to be solved and the math can get very tedious quickly. However, Matlab has very useful toolboxes designed specifically for this kind of problem. The Control Systems Toolbox (CST) and the Robust Control Toolbox (RCS)

are used extensively during the implementation stage. The procedure followed to obtain the required system simulated on Matlab is as follows:

1. Obtain the system plant either in transfer function form or in state-space form; the Matlab commands ***ss*** and ***tf*** are useful here. Preferably with the final model in state space form.
2. Because the structure of the mixed-sensitivity problem is MIMO, the system must be represented in a packed-matrix notation by using the command ***pck***.
3. The next step is to create the generalised plant, which includes all inputs and outputs such as u, W_s and W_t. The command ***sysic*** is used.
4. Finally, the controller is synthesised by making use of the command ***hinfsyn***, which yields the optimised controller, closed-loop plant and final minimised value for γ.
5. Once the controller has been synthesised, the analysis of the results can be performed through the commands ***step*** for step response, ***bode*** for bode frequency plots and ***sigma*** for singular value plot [100] on the stability transfer functions S, T and GK. The singular values are used on transfer matrices, and they are a used to evaluate the largest singular value of a transfer function.

5.6 Quantitative Feedback Theory

The implementation of the QFT controller using the CAD-based Matlab toolbox is discussed here. The reader is reminded that the modelling of the gimbal started off as a non-linear system when you consider that the gimbal structure can be modelled as a flexible structure, the system can be subjected to static friction, and the viscous friction could be non-linear. To linearise the system the following steps were taken: the gimbal platform structure is assumed to be rigid, not flexible, this comes from the consideration of the material that is used to construct it which is steel. The joint axes are assumed to be orthogonal, this allows one to decouple the equations of motion so that one can focus on one degree of motion at a time in designing the controller. The static friction is neglected and the viscous friction is assumed to be linear.

5.6.1 QFT Main Design Steps

1. First, design $C(s)$, the controller, so that uncertainties and noise on the closed-loop system are reduced to an acceptable level, which is determined by the closed-loop robust stability and performance specification.
2. Secondly, design $F(s)$, the pre-filter, to achieve the desired frequency response.

5.6.2 QFT Main Design Specifications

1. Robust Stability Margin
$$\left|\frac{L(j\omega)}{1+L(j\omega)}\right| \leq \gamma \tag{5.9}$$
for all P(s) $\in$ **P** $\omega \in [0, \infty]$

2. Tracking Performance
$$|a(\omega)| \leq \left|\frac{F(j\omega)L(j\omega)}{1+L(j\omega)}\right| \leq |b(j\omega)| \tag{5.10}$$
for all P(s) $\in$ **P** $\omega \in [0, \infty]$

3. Disturbance Attenuation Performance
$$\left|\frac{P(j\omega)}{1+L(j\omega)}\right| \leq |d(j\omega)| \tag{5.11}$$
for all P(s) $\in$ **P** $\omega \in [0, \infty]$

Where P is the uncertainty family of plants and γ, $a(j\omega)$, $b(j\omega)$ and $d(j\omega)$ are the stability performance specifications, robust stability margin, the low and upper tracking performance bounds, and the disturbance performance bounds, respectively.

One of the powerful incentives for this control technique is that QFT design for non-minimum phase and stable/unstable plants results in a stable minimum phase closed-loop system.

Important notes on the design:

- The plant transfer function must be Linear Time-Invariant (LTI).
- The controller and pre-filter must be rational functions.
- The pre-filter is only required if the problem at hand requires reference tracking.
- Loop-shaping for $L(j\omega)$ is performed on the Nichols chart and a graphical CAD environment for controller design on Matlab.
- The stability criterion is based on the Nyquist theorem and has been extended to Nichols chart.

5.6.3 Stability Analysis

In the QFT design technique, its main attractive feature is that robust stability is guaranteed by ensuring that the nominal case is stable and also by making sure that the equality holds $1 + L(jw) \neq 0$ for any allowable uncertainty in the system plant [125]. The reader is reminded

that $L(jw)$ is referred to as the *open-loop transmission* or *open-loop gain plant.* To ensure that good robust stability has been achieved during the loop-shaping design process, the design engineer must ensure the following are satisfied:

1. For the closed-loop system to be stable, the open-loop transmission plant must never cross the 0 dB horizontal line outside of the $-180°$ vertical line (i.e, from $-180°$ to negative infinity, going left) on the Nichols chart.
2. The feedback system is stable if and only if the Nichols plot will intersect the magnitude $0dB$ line within the phase range $(-180°, 180°)$.

5.6.4 CAD Interface Implementation

This section briefly provides an overview of the process that is involved in designing a QFT controller with a pre-filter using the CAD-based QFT control Matlab toolbox.

Plant Definition

The definition of the plant model structure, its parameters, the uncertainty and the frequencies of interest are taken care of here, *Figure 5.1.* Note the different forms that the plant can be defined in, and the uncertainties are represented or defined as shown in *Figure 5.2.*

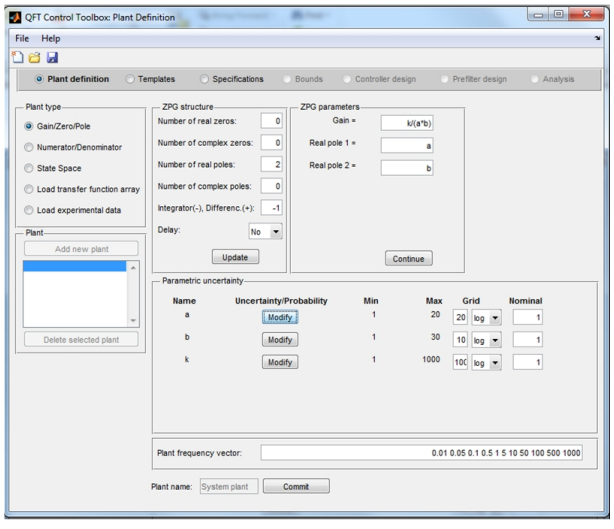

Figure 5.1: Plant Definition Window

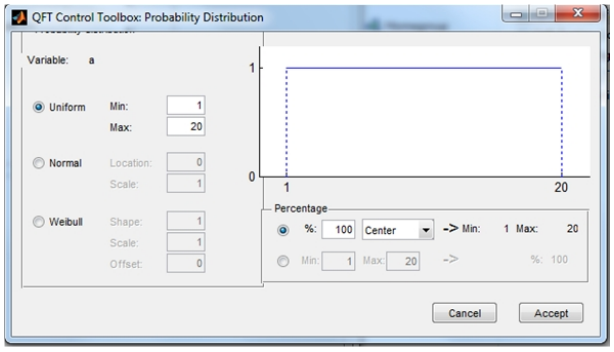

Figure 5.2: Uncertainty probability distribution window

Templates

The full representation of the frequency response of the plants, including the uncertainty, is provided in the Nichols Chart at a particular frequency, as depicted in *Figure 5.3*.

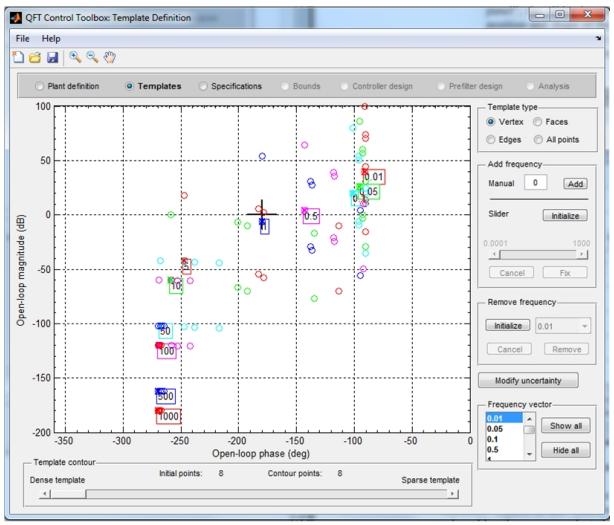

Figure 5.3: Template definition window

Specifications

It is here that the design engineer introduces the robust stability and performance control specifications, as shown in *Figure 5.4*.

Bounds

Given the defined plant templates and the control specifications, QFT then converts the closed-loop magnitude specification $[T_1(jw)$ to $T_6(jw)]$ into magnitude and phase constraints for the

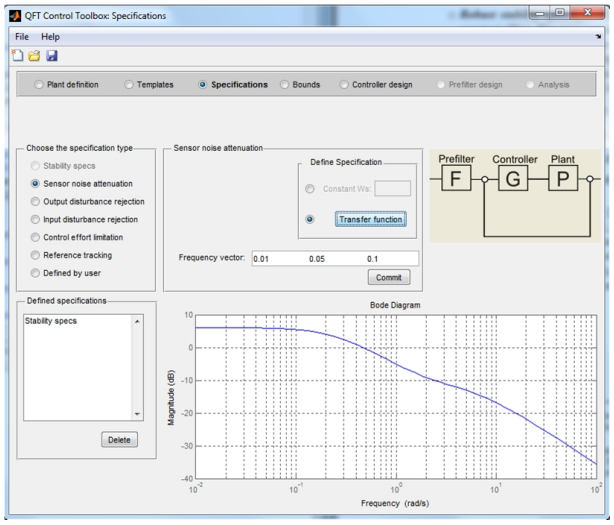

Figure 5.4: Robust stability and performance specification definition window

nominal open-loop function $L_0(jw)$, *Figure 5.5*.

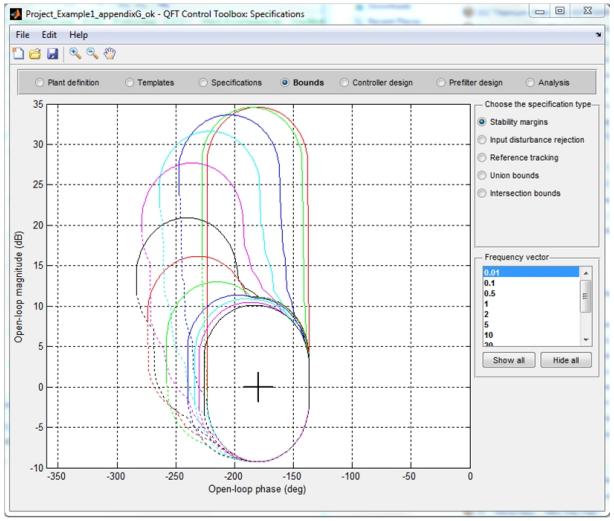

Figure 5.5: Bounds definition window

Controller Design

The design (loop-shaping) of the controller, *Figure 5.6*, can now be tackled since sufficient information about the plant, control specifications, and the templates and bounds has been calculated. Generally, the loop-shaping design involves changing the gain and adding poles and zeros (real or complex), until the nominal loop $L_0(jw)$ lies near its bounds (above the solid line and below the dashed-line bounds at each frequency of interest).

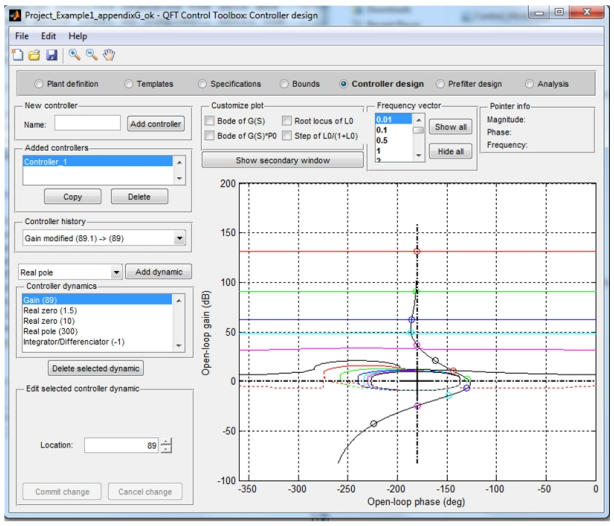

Figure 5.6: Robust controller design window

Pre-filter

Only in conditions where the control problem requires reference tracking and the accompanying specifications have been provided can then the Pre-filter design window, illustrated in *Figure 5.7*, become activated immediately after the design of the controller. The design proceeds similarly to the controller design. The only difference is the objective, which in this case is to obtain the worst upper and lower closed-loop response cases of $L_0(jw)F(jw)/[1 + L_0(jw)]$ over the plant uncertainty.

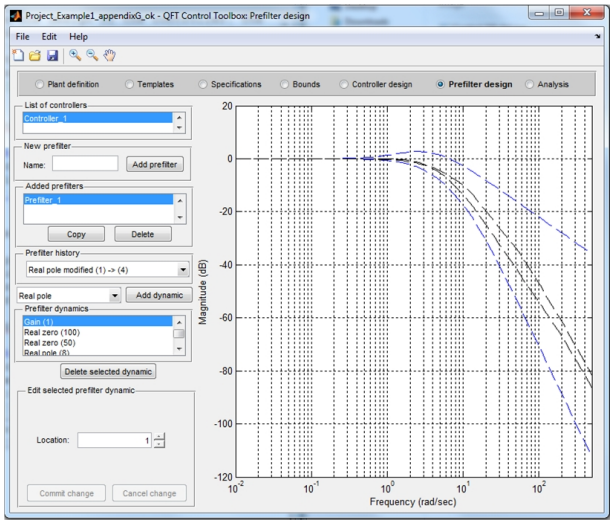

Figure 5.7: Pre-filter design window

Analysis

The analysis, shown in *Figure 5.8*, is performed in both the frequency domain and the time domain. The objective here is to analyse the controller and pre-filter in the worst case scenario over the plant uncertainty.

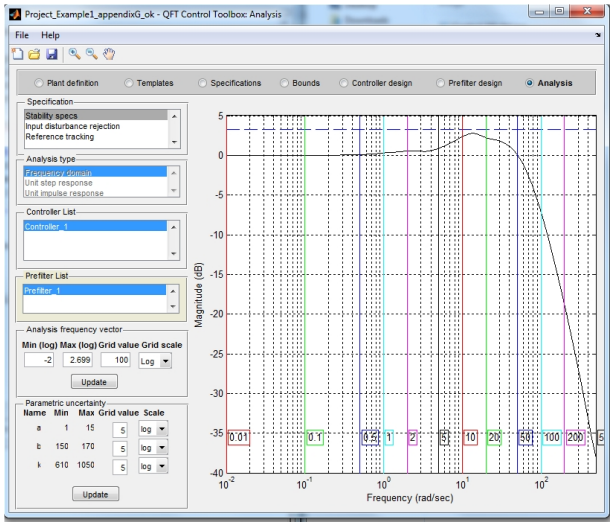

Figure 5.8: Frequency domain and time domain analysis window

5.7 Adaptive Control

The transfer function of the gimbal model is presented as follows in equation (5.12), and the Model Reference Adaptive Controller (MRAC) is implemented as follows.

$$\frac{\theta}{\tau(s)} = \frac{1}{Js^2 + Bs + K} \tag{5.12}$$

The MIT rule [126] will be used to form the update rules for the adaptive parameters in the controller. This is conducted by deriving the equation for the error signal and the cost function as follows:

$$e = y_{plant} - y_{model} \tag{5.13}$$

$$J(\theta) = \frac{1}{2}e^2(\theta) \tag{5.14}$$

$$\frac{d\theta}{dt} = -\gamma \frac{\delta e}{\delta \theta} \tag{5.15}$$

Equation (5.15) shows how the θ parameter is updated by using the sensitivity derivative. From here it is then assumed that the controller has both an adaptive feedforward (θ_1) and an adaptive feedback (θ_2) gain. The sensitivity derivatives associated with the parameters must be re-defined to include θ_1 and θ_2. The equation for the error signal is first rewritten as the transfer function of the plant and model multiplied by their respective inputs. It is important to note that the input u_c is not a function of either of the adaptive parameters, and therefore can be ignored for now. However, the input u can be rewritten using the feedforward and feedback gains. The equation for y_{plant} is derived as follows:

$$u = \theta_1 u_c - \theta_2 y_{plant} \tag{5.16}$$

$$e = y_{plant} - y_{model} = G_p u - G_m u_c \tag{5.17}$$

$$y_{plant} = G_p u = \left(\frac{1}{Js^2 + Bs + K} \right) (\theta_1 u_c - \theta_2 y_{plant}) \tag{5.18}$$

$$y_{plant} = \frac{\theta_1}{Js^2 + Bs + K + \theta_2} u_c \tag{5.19}$$

We are now in a position to write the error signal with the adaptive terms included, and taking the partial derivatives of the error with respect to θ_1 and θ_2 yield the sensitivity derivatives.

$$e = \left(\frac{\theta_1}{Js^2 + Bs + K + \theta_2} \right) u_c - G_m u_c \tag{5.20}$$

$$\frac{\partial e}{\partial \theta_1} = \frac{1}{Js^2 + Bs + K + \theta_2} u_c \tag{5.21}$$

$$\frac{\partial e}{\partial \theta_2} = \frac{\theta_1}{(Js^2 + Bs + K + \theta_2)^2} u_c \tag{5.22}$$

$$\frac{\partial e}{\partial \theta_2} = -\frac{\theta_1}{Js^2 + Bs + K + \theta_2} y_{plant} \tag{5.23}$$

Note that the sensitivity derivatives obtained contain the parameters from the plant, and recall that the premise of design with MRAC assumes that the plant characteristics are not absolutely known. This seemingly places the design process at an almost dead-end. However, the goal is to make the plant approach the model. If the model is close to the actual plant, the model characteristics can be substituted for the plant characteristics using the following protocol:

$$Js^2 + Bs + K + \theta_2 \approx J_m s^2 + B_m s + K_m \tag{5.24}$$

$$\frac{\partial e}{\partial \theta_1} = \frac{B_m s + K_m}{J_m s^2 + B_m s + K_m} u_c \tag{5.25}$$

$$\frac{\partial e}{\partial \theta_1} = -\frac{B_m s + K_m}{J_m s^2 + B_m s + K_m} y_{plant} \tag{5.26}$$

After applying the MIT rule, the update rules for each θ can be written, and the Simulink model for the entire system with the derived controller is shown in *Figure 5.9*. Note how the plant input and output measurements are filtered before being multiplied by the error and γ.

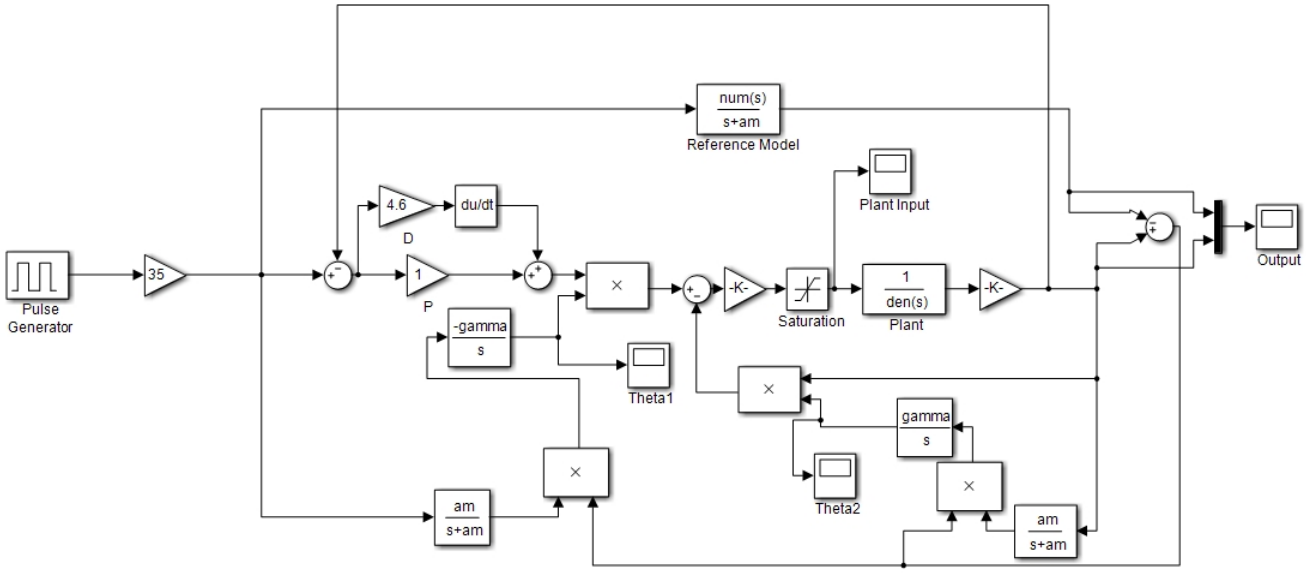

Figure 5.9: MRAC Simulink model with controller implementation

5.8 Conclusion

The implementation of the robust controller in the gimbal model to ensure it follows the commanded signals and responds as quickly as possible has been discussed and implemented.

A procedural method of implementing the QFT controller is presented with the aid of screen shots from the Matlab toolbox CAD environment. Methods for evaluating the stability of the system are also reviewed in the context of the specific robust controller being implemented. The chosen adaptive controller is the MRAC-type, using the MIT rule, and its implementation has been discussed.

Chapter 6

Results Discussion

6.1 Outline

The results obtained from the modelling and control implementation on the two-axis gimbal assembly are presented in the following subsection. The analytical modelling for the gimbal and actuator is compared to the physical system-based model. The robust performance and stability of the control actions are also compared to establish which controller performs better and thus can be chosen for final implementation.

The presentation of the results is organised in the following manner: Section 6.2 discusses the modelling of the actuator and gimbal assembly results and Section 6.3 presents the PID control action results. Section 6.4 focuses on the robust control action of the H_∞ controller results, Section 6.5 demonstrated how the QFT controller performs and Section 6.6 indicates the final robust controller performance from the adaptive controller. Section 6.7 examines the aforementioned results with the focus on robust stability and robust performance. Finally Section 6.8 provides recommendations for future work and draws conclusions on the presented results.

6.2 Modelling Results

The results obtained from the simulations of the models that have been derived is presented in this section. The results indicate that there is definitely a need for some control action.

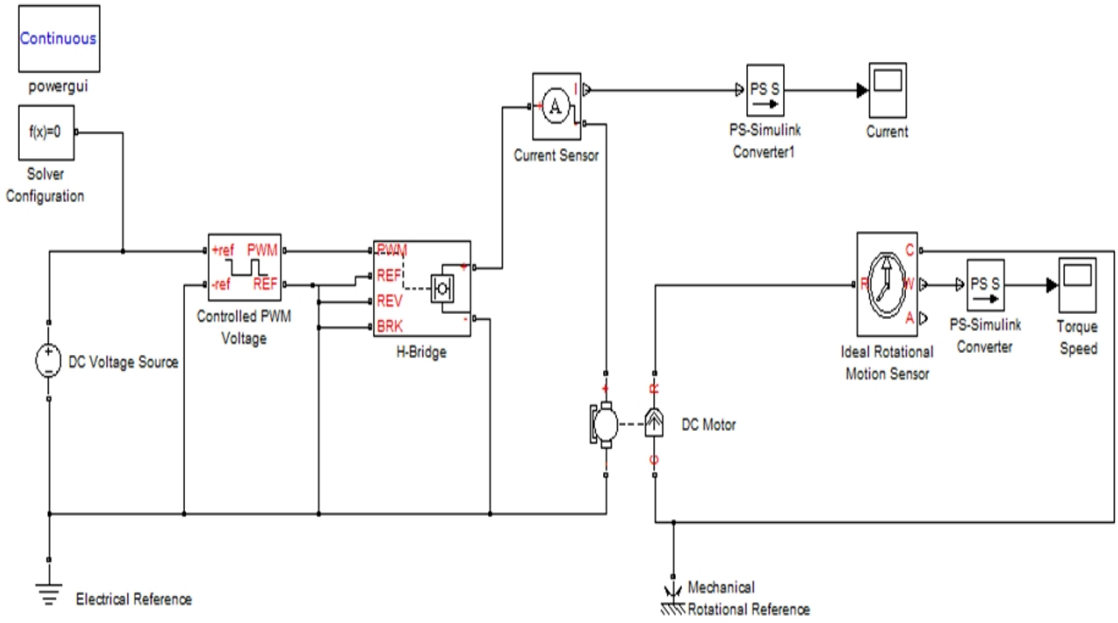

Figure 6.1: Physical modelling of PM DC motor

6.2.1 DC Motor Modelling Results

The DC motor is simulated and also compared to the more practical equivalent motor, which utilises Simulink (*SimElectronics*) physical blocks. The model for the practical PM DC motor is illustrated in *Figure 6.1*.

The motor parameters are presented as follows, *Table 6.1*, and they are not too far from the *Maxon RE 35* motor parameters.

Table 6.1: PM DC motor final modelling parameters

Parameter symbol	**Parameter value**
R_a	2.07 Ω
L_a	0.62 mH
K_m	0.052 $\mathrm{N}m^{-1}A^{-1}$
K_t	0.000048 $\mathrm{Nms}rad^{-1}$
B_m	0.052 $\mathrm{Vs}rad^{-1}$
J	$7.2\times10^{-6}\mathrm{kg}m^2$

6.2.2 Gimbal without Controller Performance

The Lagrangian model of the gimbal without the controller present is shown in *Figure 6.2*, and the performance is illustrated in *Figure 6.3*. The step response of the system shows a rise time of about four seconds with a percentage overshoot of 18%; the settling time is about 15 seconds with a very minumum steady state error.

The reason we are able to obtain these results is because the gimbal damping coefficients and inertial coefficients were investigated through trial and error. The same was applied for the motor actuator. To improve the results, one would have to keep on trying different combinations of the damping coefficient, stiffness coefficient, and inertial coefficients.

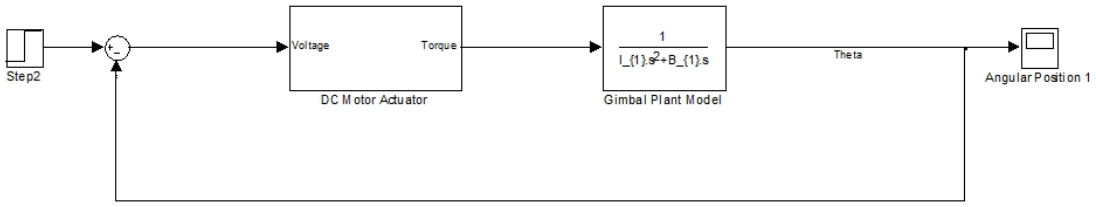

Figure 6.2: Gimbal model without the presence of a controller

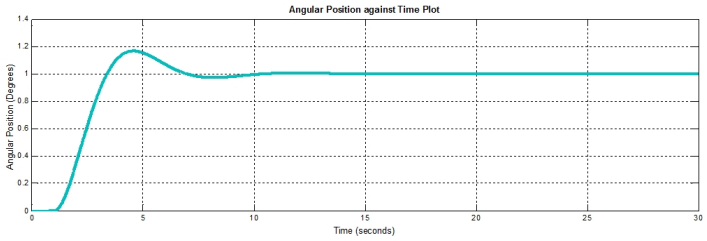

Figure 6.3: Gimbal angular position performance without the presence of a controller

6.2.3 Physical Gimbal Model without Controller Model

Following the import of the CAD model of the double gimbal platform from *SolidWorks* to *Simulink* using the *SimMechanics* toolbox for mechanical models, the initial simulation of the model was completely unsuccessful. The only observable result was some incomprehensible vibrations of the equivalent Simulink mechanical model. After some thought, it was realised that the reason for this behaviour was that the mechanical model in SolidWorks did not have the degrees of freedom properly defined and the material type definition (such as steel, aluminium or copper) was also missing. As a result, it was impossible to activate motion either in the pan

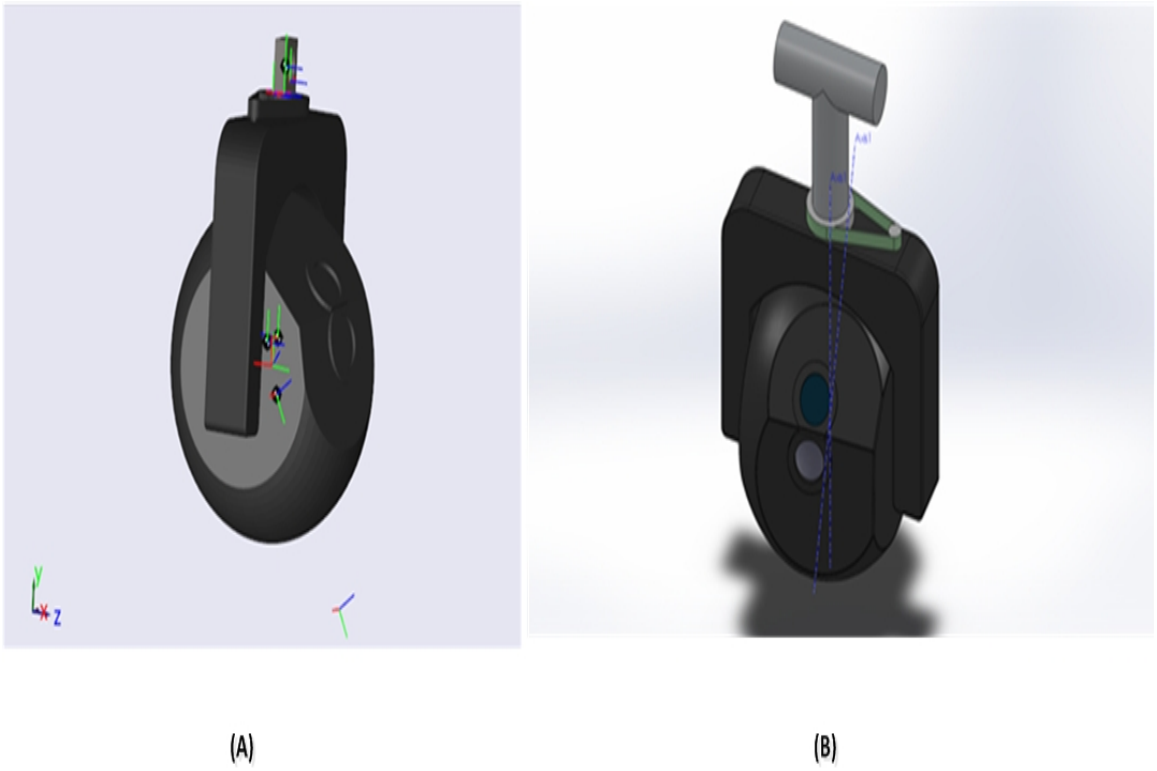

Figure 6.4: (A) Simulink model of gimbal, (B) CAD model of gimbal platform

gimbal axis or the tilt axis via force actuators. To solve this problem the mechanical CAD model in SolidWorks was then separated into specific parts which represent the various gimbal axes for motion. The material definition was also updated to carbon steel sheet (SS) for the initial simulations with the characteristics shown in *Table 6.2*.

After the CAD mechanical model had been reassembled it was then imported again into Simulink. Using the SimMechanics toolbox, force actuators were added to the model and a constant torque was then applied to a single degree of freedom while the other degree of freedom was actuated with zero torque. The revolute joints were successfully actuated and rotational motion was observed. The immediate observable issues were the instabilities and vibrations. The other present, and expected, issue was the cross-coupling effect between the pan and tilt gimbal axis. The vibrations from the gimbal axis were induced to the gimbal axis, which in turn introduced unwanted rotational motion. However, this was expected because the simulation was an open-loop simulation of the system.

The model that was exported from *SolidWorks* to *SimMechanics* is presented in *Figure 6.4*, and the compelling resemblance is clearly shown. The equivalent SimMechanics blocks, which represent the physical modelling of the gimbal, are presented in *Figure 6.5*. The two inputs and two outputs can clearly be seen on this model.

The introduction of a closed feedback loop PID controller solved most of the instabilities, cross-coupling effect and vibrations. The system is a MIMO system, which means each input-output configuration requires its own dedicated feedback controller to provide stabilisation and reduce vibrations. The performance of the PID controller can be improved by tuning the PID controller, and the PID Simulink block has been devises with a linearised manual tuning bar.

Table 6.2: CAD Gimbal platform material specifications from SolidWorks

Gimbal Material Specifications	
Property Description	**Specification**
Elastic modulus	$2.05 \times 10^{11} N/m^2$
Poisson's ratio	0.29 N/A
Shear modulus	$7.99 \times 10^{10}\ N/m^2$
Mass density	7858 $kg.m^3$
Tensile strength	425000003.2 N/m^2
Yield strength	282685049 N/m^2
Thermal expansion coefficient	$1.2e^{-005}\ /K$
Thermal conductivity	52 $W/(m.K)$
Specific heat	486 $J/(kg.K)$

6.3 PID Control Results

The gimbal Lagrangian model shown in *Figure 6.6* depicts the following performance when the plain PID controller is applied, with a proportional gain of 40, integral gain of 1 and a derivative gain of 10 depicted in *Figure 6.7*. As can be seen the overshoot has been minimised to almost zero, the rise time is still roughly five seconds while the settling time has been improved to about 5.5 seconds. The steady state error performance is much smoother than before.

This improvement is accomplished by tuning the PID gains through trial and error, and a further improvement, if at all possible, could be accomplished by trying different combinations of the PID gains.

When a frequently occurring vibration disturbance torque, which could be as a result of the helicopter vibrations being introduced to the gimbal assembly, is added to the system, the lack of robustness is evident in the way the disturbances become part of the output signal. The PID controller is unable to reject the disturbance signal with the set gains; hence, it now needs to be tuned to get better gains that are able to reject the disturbance signal. However, this also means

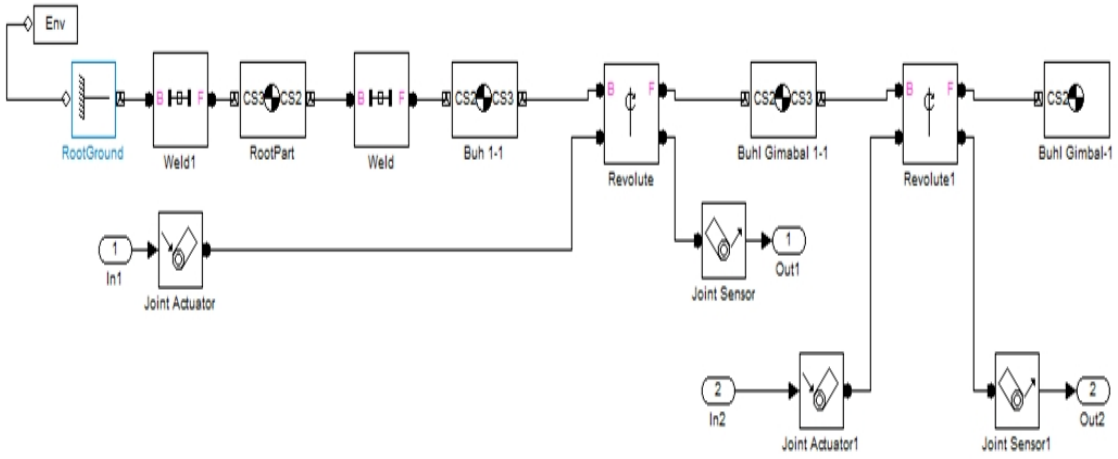

Figure 6.5: Physical modelling of gimbal platform using SimMechanics

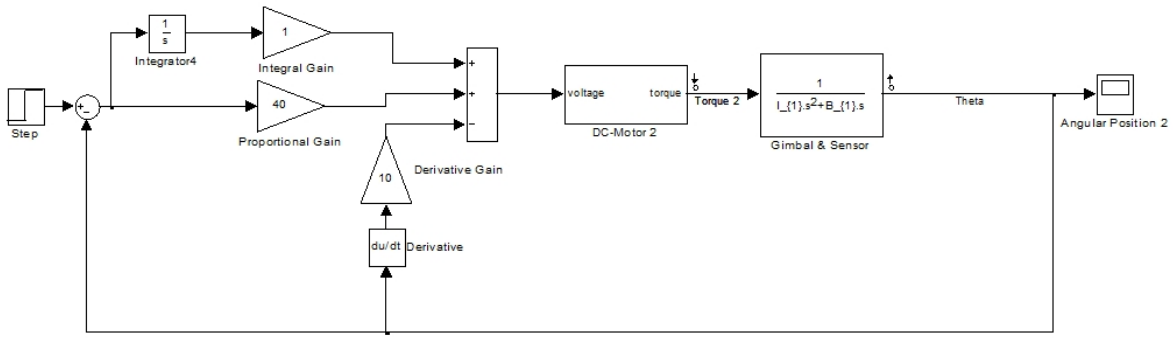

Figure 6.6: Gimbal Lagrangian model with PID controller

that for every different form of disturbance, new controller gains would have to be determined. This is the other drawback presented by PID controllers.

The output signal when the disturbance is applied, is presented in *Figure 6.8*. A white noise was applied to disturb the signal, and a different type of noise signal can be added to obtain different results.

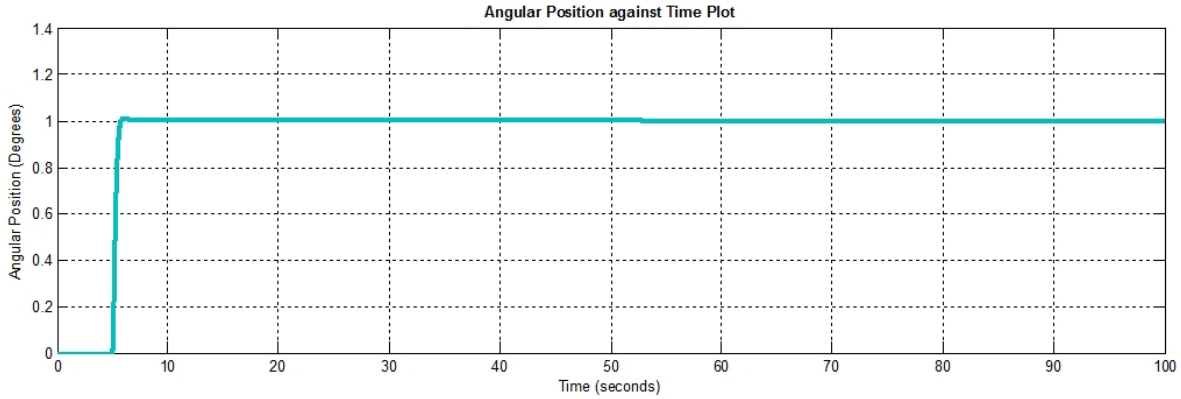

Figure 6.7: Gimbal angular position performance response with PID

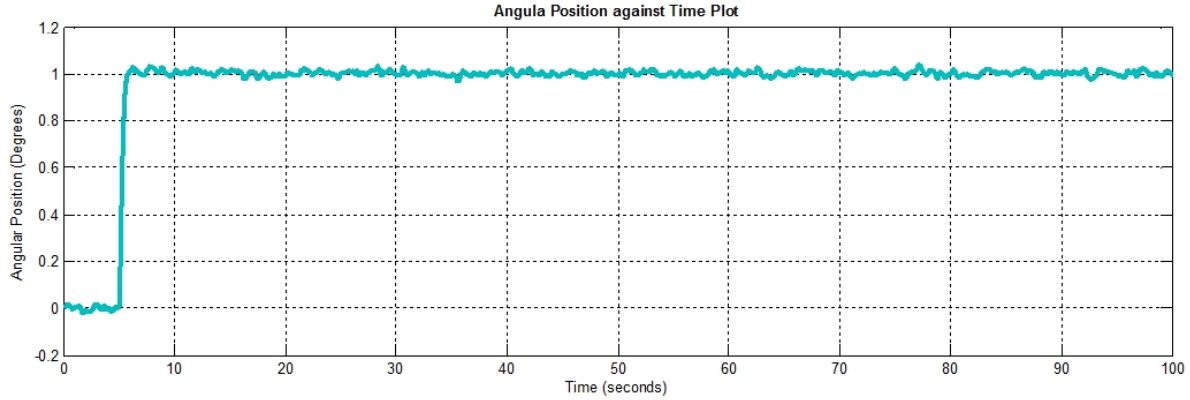

Figure 6.8: Gimbal angular position output response with PID controller when disturbance is applied

6.3.1 PID and Auto-tuning

After failed several attempts to improve the performance of the system, the plant had to be modified to a higher order-type by introducing a second order low-pass filter of the form as represented in equation (6.1). This then made the plant into a fourth order system, and the integral tuning techniques worked successfully.

$$W(s) = \frac{1}{(s+1)^2} \tag{6.1}$$

The application of the Ziegler-Nichols (Z-N) tuning algorithms with the integral performance indexes tuning algorithms is presented in *Figure 6.9*, which shows the closed-loop step response of the controlled signal. The Z-N tuning computed control gains according to *Table 3.1* (Chapter 3, section 3.6.1), are $K_p = 7.9797$, $T_i = 1.2079$ & $T_d = 0.3020$. The controller obtained using the Integral Square Error (ISE) algorithm is presented in equation (6.2), and the minimised cost function is $\gamma = 0.2655$. The controller obtain by implementing the Integral Absolute Error

(IAE) is shown in equation (6.3) and the cost function is minimised to $\gamma = 0.5154$. The controller obtained by implementing the Integral Time Square Error (ITSE) is shown in equation (6.4) and the associated cost function is $\gamma = 0.0605$. The controller obtained by implementing the Integral Time Absolute Error (ITAE) is shown in equation (6.5) and the associated cost function is $\gamma = 0.2654$.

$$C_1(s) = \frac{12.52s^2 + 7.845s + 8.595}{s} \tag{6.2}$$

$$C_2(s) = \frac{6.47s^2 + 8.687s + 4.168}{s} \tag{6.3}$$

$$C_3(s) = \frac{7.566s^2 + 8.738s + 5.1}{s} \tag{6.4}$$

$$C_4(s) = \frac{3.93s^2 + 6.815s + 3.228}{s} \tag{6.5}$$

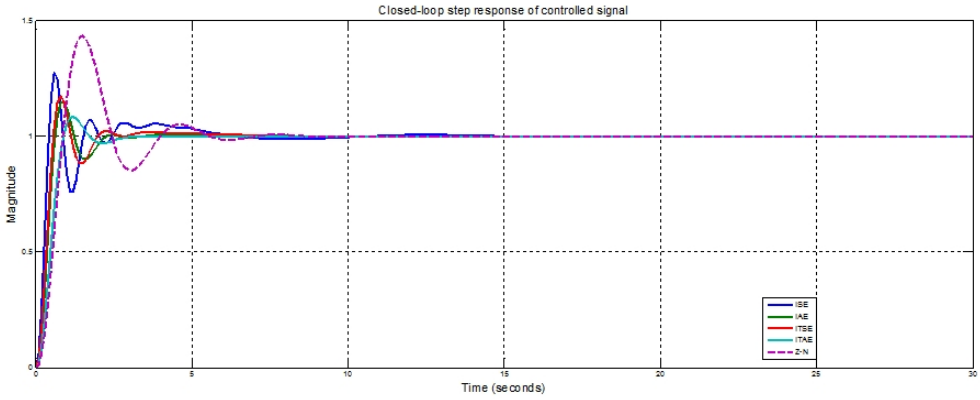

Figure 6.9: PID control with Z-N, IAE, ISE, ITAE, ITSE auto-tuning algorithms

As can be observed from *Figure 6.9*, the Z-N tuning method performs the worst out of all of them with a large percentage overshoot of 43.2% and an undesirable settling time of just above 10 seconds even though it has the second fastest rise-time, the fastest one out of all of them is the ISE protocol with a peak-time of 0.6 seconds. The ITAE has the slowest response out of all of them of 1.2 seconds peak-time, but it has the best overall response with a low overshoot percentage of 8.3% and a low settling time of about 3.2 seconds. The seconds best tuning technique is the IAE, even though it has the second slowest response.

The reason the auto-tuning work is because of the nature of the *fminsearch* algorithm and the initial estimate of the search. To improve the results, one can increase the order of the plant

(gimbal model). A little trial and error can help in terms of attempting different initial estimates for the algorithm and the order of the plant, even though the tuning of the gain is automated.

6.4 H_∞ Control Results

The results obtained by applying the H_∞ control algorithm are presented in this section, and it is revealed that the robust stability and robust performance is much better than the one presented from PID control.

The step response for the improved system is presented in *Figure 6.10*. From the figure it can be seen that the system does not necessarily have the best response; however, it can be improved by moving poles, adding integrators and adjusting the bandwidth until a desirable response is achieved. This can be done via trial and error until a better response is obtained.

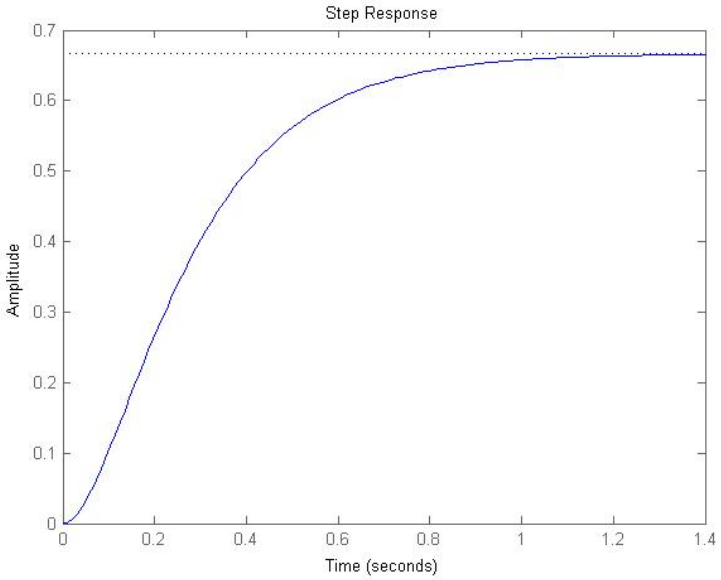

Figure 6.10: Improved step response

The controller is presented in equation (6.6) or (6.7) which explicitly demonstrates the poles and zeros on the controller. This is achieved at a minimized cost function of $\gamma = 2.6066$.

$$K(s) = \frac{2.421 \times 10^{004} s^2 + 3.631 \times 10^{005} s + 1.21 \times 10^{006}}{s^3 + 9625 s^2 + 1.721 \times 10^{005} s + 172.1} \tag{6.6}$$

Or:

$$K(s) = \frac{24208.6409(s+10)(s+5)}{(s+9607)(s+17.91)(s+0.001)} \tag{6.7}$$

When dealing with a MIMO system, its singularity points are examined to measure its robustness. *Figure 6.11* shows the singularity plot of the desired sensitivity function (*doted line*) and achieved sensitivity function (*solid line*), and it can be clearly seen that they are very close to each other with a marginal error. Also, it can be seen that they both satisfy the robust stability conditions set out by equation (3.35).

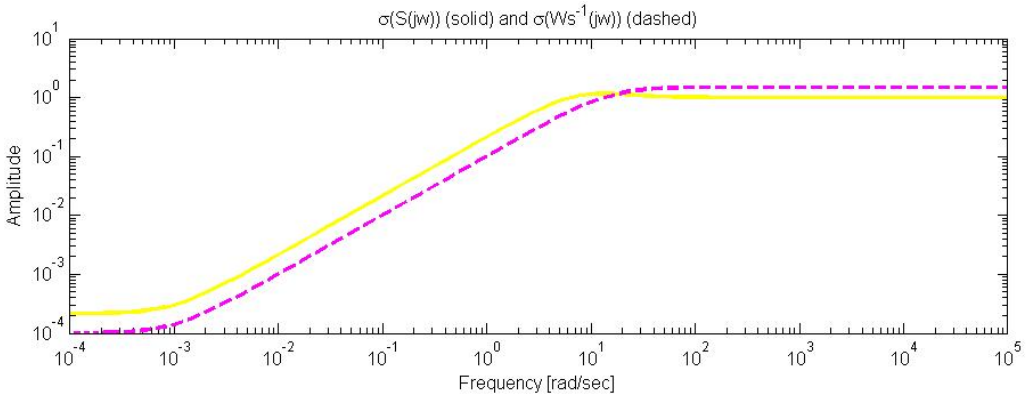

Figure 6.11: Comparison between desired and actual singularity sensitivity function

Figure 6.12 illustrates the singularity plot of the comparison between the sensitivity, loop-gain and complementary sensitivity function. An important observation is that because this is a mixed sensitivity problem as stated before, during low frequency regions the sensitivity function takes preference while the complementary sensitivity function is compromised. This is expected because both depend on the loop-gain function, which has two simultaneous conditions to satisfy; that is, very small gain for the sensitivity function and very large gain for the complementary function.

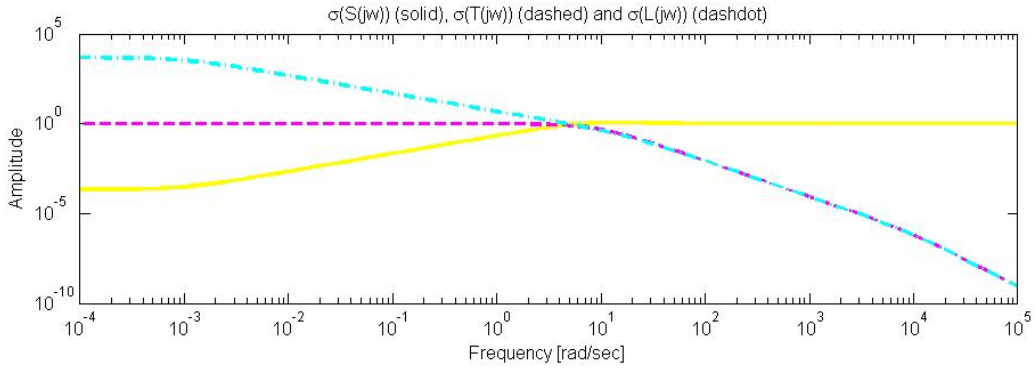

Figure 6.12: Comparison between sensitivity, complementary and loop-gain singularity function

The step response of the controlled system is presented in *Figure 6.13* illustrating the robust stability and performance of the designed controller. It can be immediately observed that the performance is better than the one obtained from PID control implementation. The rise time is much shoter at 0.5 seconds, there is no overshoot, and the steady state error is much smoother.

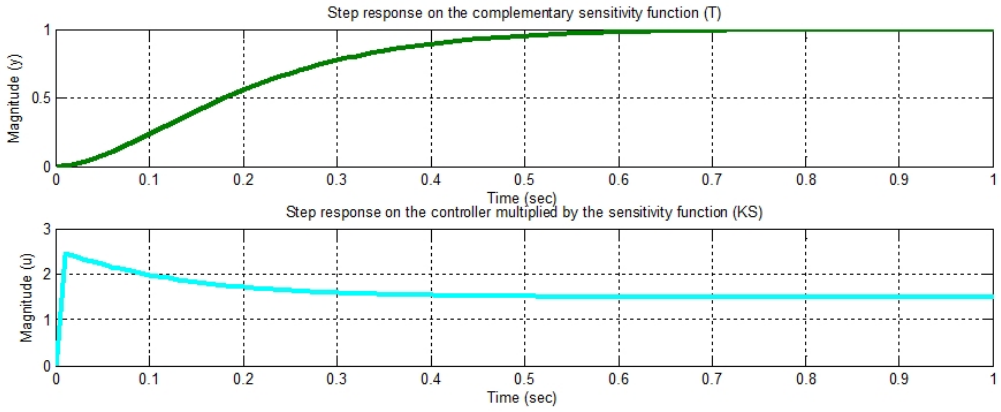

Figure 6.13: Step response of the closed-loop system

6.5 QFT Control Results

This section presents the controller performance results when applying the QFT control methodology.

6.5.1 Model Uncertainties Results

The model uncertainties are presented in *Figure 6.14*, which illustrates the templates for the parametric plant variations for various frequencies.

6.5.2 Performance Results

The controller transfer function can be presented in the following form, as shown in equations (6.8) and (6.9). This is obtained after a rigorous loop-shaping design of the loop transmission for the desired specifications.

$$C(s) = \frac{7.862 \times 10^{-005} s^2 + 0.03993s + 0.2442}{7.461 \times 10^{-009} s^3 + 1.147 \times 10^{-005} s^2 + 0.005871s + 1} \tag{6.8}$$

Or.

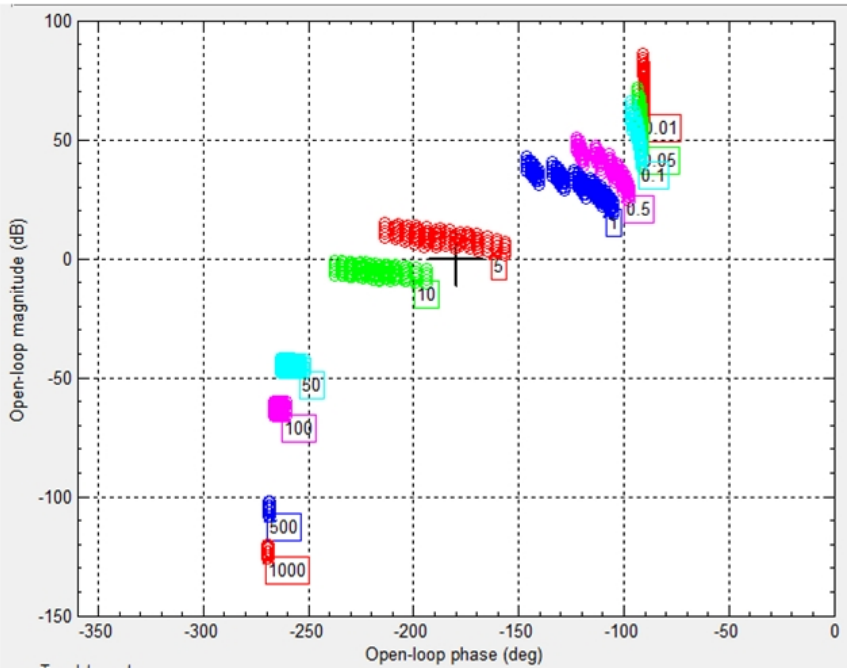

Figure 6.14: Model uncertainty plot of the open-loop plant

$$C(s) = \frac{10537.3373(s + 501.7)(s + 6.19)}{(s + 551.8)(s + 504.3)(s + 481.6)} \tag{6.9}$$

And the pre-filter transfer function is shown in equation (6.10):

$$F(s) = \frac{2.0068(s + 13.78)(s + 1.525)}{(s + 17.22)(s + 2.408)} \tag{6.10}$$

Figure 6.15 shows a very much improved step response compared to the response obtained with the PID controller. The improved rise time is 0.65 seconds, with a settling time of 1.03 seconds and a percentage overshoot of 0.73% at a peak time of 1.47 seconds. To improve the results, one could expand the template for more parametric uncertainty, however it must be noted that this could reduce the response time as it might require more computaional time.

Figure 6.16 shows the stability performance of the controller and loop-gain of the system. The loop-gain roots are minimum-phase, which is what is required.

Figure 6.17 shows the bode magnitude plot of the results obtained after a successful pre-filter design.

Figure 6.18 and *Figure 6.19* show the stability bode magnitude plot of the system. This indicates how well the system rejects disturbances.

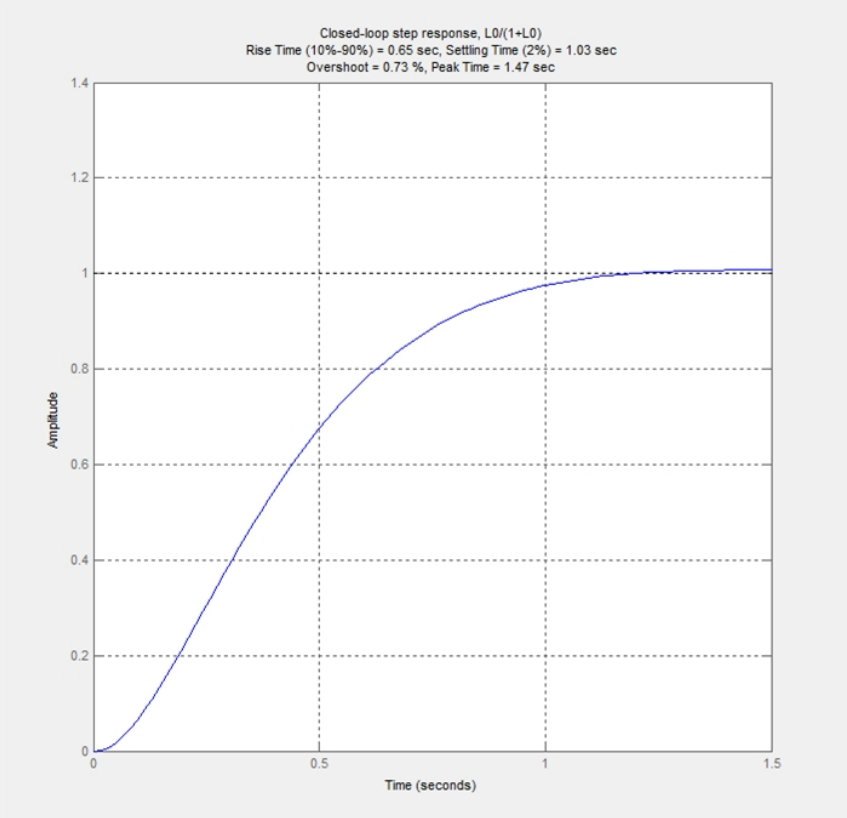

Figure 6.15: Step response of the complementary sensitivity function

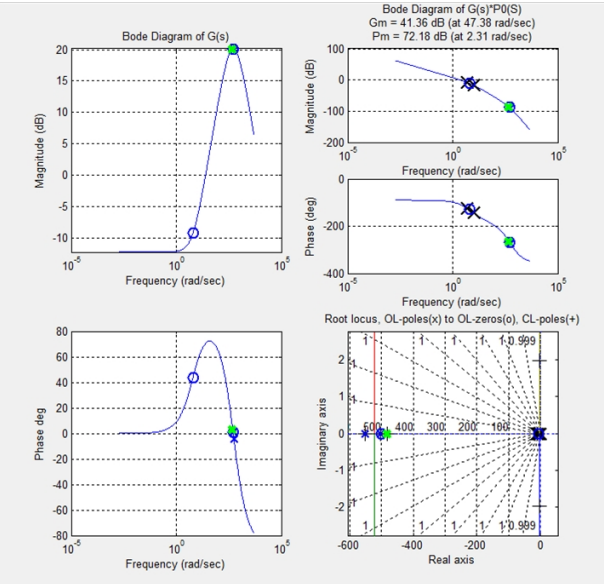

Figure 6.16: Bode plot of controller and root locus plot of loop-gain function

Figure 6.20 illustrates how well the system is able to track a reference signal; the plot indicates a step and an impulse response of the system.

Figure 6.21 presents the time responses, step and impulse of the system for the input disturbance rejection specification.

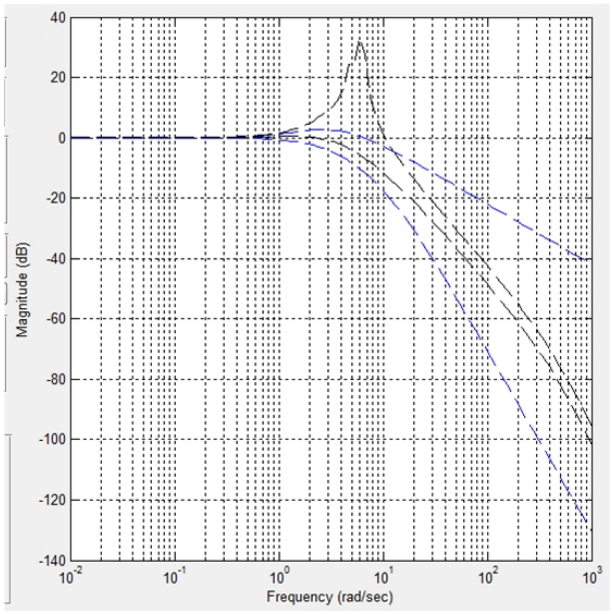

Figure 6.17: Bode magnitude plot of the pre-filter results

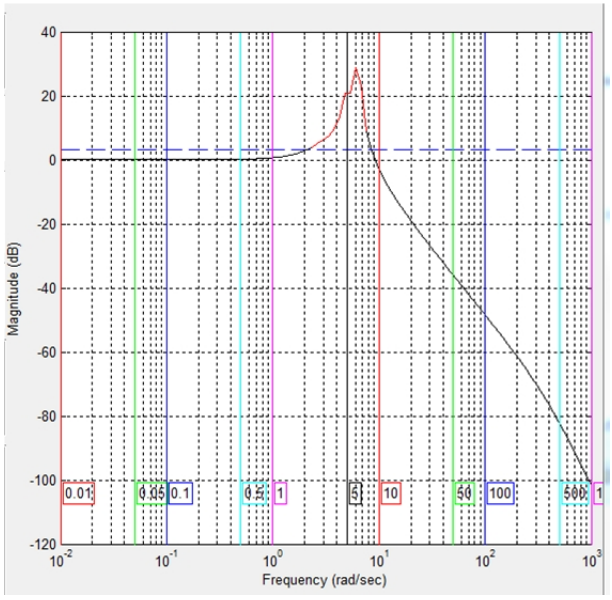

Figure 6.18: Bode magnitude plot of the stability results

6.6 Adaptive Control Results

The control action of the Model Reference Adaptive Controller (MRAC) is illustrated by showing the plant and reference model response and how they converge once the θ parameter has been updated to the correct value using the update law. The convergence of the responses is presented in *Figure 6.22*

The performance indicates that the system takes quite a while to settle to the desired response and eliminate steady state error, about 30 seconds, and this is because of the algorithm being

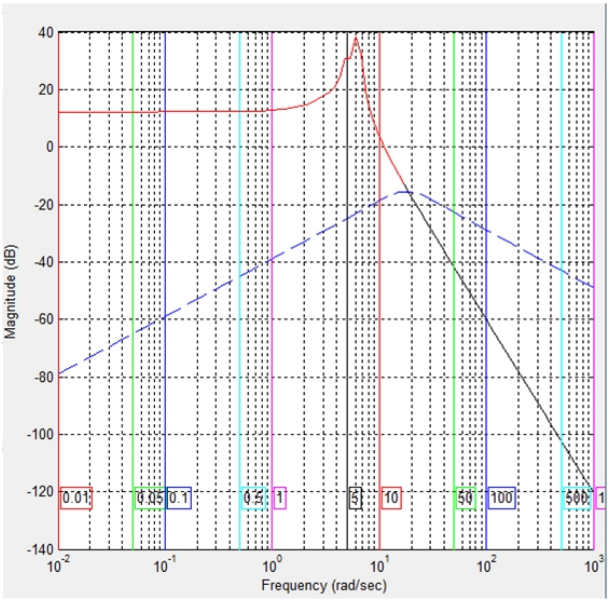

Figure 6.19: Bode magnitude plot of the input disturbance rejection results

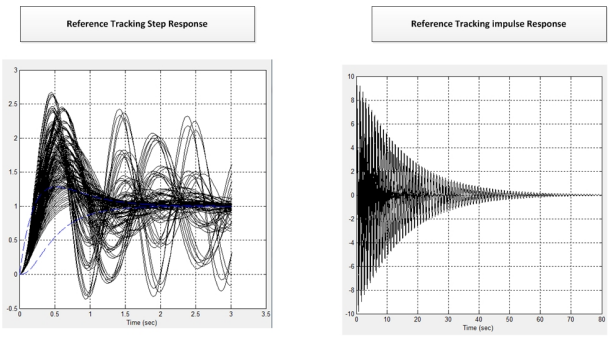

Figure 6.20: Step and Impulse response of the reference tracking results

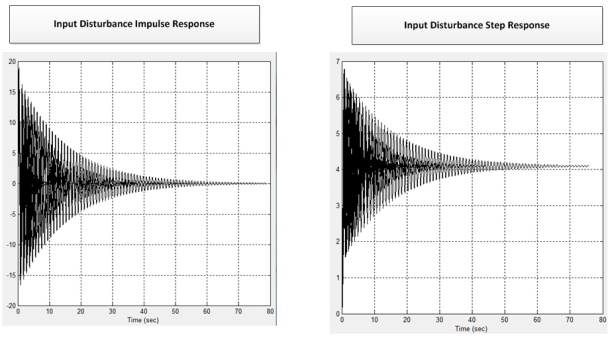

Figure 6.21: Step and impulse response of the input disturbance rejection results

used to implement the adaptive law to effectively tune the model parameters. The advantage of this result is that once the system settles to the desired response, it will stay there, because now the model accurately approximates the plant model in a robust fashion. To improve the result one could intrucude a better system identification method to better approximate the parameters.

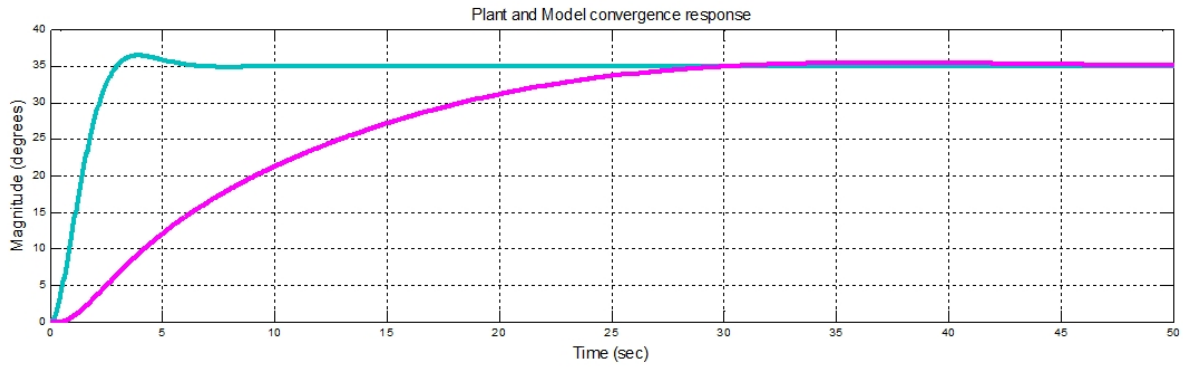

Figure 6.22: Convergence of the plant and model dynamic response

6.7 Critical Analysis

The H_∞ controller is very useful, especially for cases where the manufacturing of the gimbal platforms is improved constantly with different sizes, shapes and weights. Traditionally, the controller would have to be updated and re-tuned. The H_∞ controller stabilises the plant for a range of variations; hence, it only needs to be designed once.

The trade-off between robust stability and robust performance is noted. Conventionally H_∞ controllers are meant to prioritise the robust stability over performance, while the designer implements weighting functions to customise performance according to design specifications. The available methods for tuning these weighting functions are not satisfactory, and require extensive trial and error effort.

The researcher has investigated better methods to tune the weighting functions automatically, such as genetic optimisation algorithm and neural network. However, they were not implemented in this study and are recommended for future work.

6.8 Proposed System Verification and Validation

6.8.1 Introduction

This chapter focuses attention to the methods used to implement the verification and validation procedures. The resources used are presented and their operation is briefly described. The construction of the test prototype is also presented, and a description of the implementation method is provided.

6.8.2 Experimental Setup

To be able to verify and validate the control algorithms on the gimbal platform, the following components were used to construct a test setup:

1. Arduino micro-controller development starter kit (includes Arduino Uno board & small breadboard)
2. Hi-Tec HS-322HD servo actuator
3. Agilent optical incremental encoder
4. Two-axis servo camera tripod
5. DC power supply source (9 V battery)
6. Host computer (running Microsoft OS) for running Arduino code and Matlab/Simulink simulation
7. Breadboard wires
8. USB cable

A brief descriptive background of the core components is presented in the following subsection.

6.8.3 Servos

Servos are miniature motors that are used to control either orientation or rotational velocity of an axis, which may be a servo arm, wheel, or any other physical object that is attached to the servo. The main construction of these servos consists of:

- A printed circuit board
- A small motor
- Several reduction gears inside a housing
- A shaft for connecting to the object to be rotated

The servo has three standard wires: power (red, middle), ground (black, on the right side), and control signal (yellow, on the left side). The control signal wire requires a Pulse Width Modulation (PWM) signal in order to command the motor to rotate to a certain angle or at a certain velocity.

Servos derive from analogue radio control (RC) and have been widely used in RC for decades. There are two generic types: the standard servo, which can only reach and hold a position specified by the user, and the continuous servos, which can reach and hold a velocity specified by the user. The servos have a configuration that is typically internally closed-loop; however, they are externally open-loop. This means that the user has no way of telling if the servo was actually successful. Also, continuous servos do not contain internal encoders, so there is no ready way to tell their position. However, one can install an external encoder for this purpose.

There are now digital encoders, which operate similarly to the above, but have the addition of a micro-processor and Mosfet built into the circuitry of digital servos. They have two advantages over the other kinds of servos: they are externally programmable and the microprocessor is able to pulse the motor in order to move the servo.

Typically when the servo needs to apply torque, it sends varying-width pulses of power at 50 Hz to the motor. However, digital servos pulse at 300 Hz, with the pulse reduced to $1/6^{th}$ of the standard pulse width and this allows for a faster and more accurate response, as well as smooth operation.

The way to connect the servo to the power supply (bearing in mind that the servo comes in a three-wire configuration, with black or brown being ground, the lightest (yellow) wire is for the signal and the middle (red) wire is for power) is to use 0.254 cm three-heading connections which plug straight into most controller micro-processors.z

Most servos accept a small range of voltage inputs (typically 4.8 to 6 V DC), with a requirement for around 100 mA of available current. The Arduino micro-processor controller will provide a three pin connection with 5 V.

6.8.4 Pulse Width Modulation Signal

The majority of servos require a pulse-width modulation (PWM) signal to operate. These signals are square wave (digital) signals at CMOS level (0 to 5 V). The wave period is typically on the order 20 ms (50 Hz) and can be chosen by the user within limits, while the pulse width itself modulates between a minimum and maximum set by the servo manufacturer. The signal is shown in *Figure 6.23*. The *minimum* pulse width corresponds to the counterclockwise extreme of a standard servo or the maximum negative velocity of a continuous servo. The *neutral* corresponds to the middle position, or no velocity, while *maximum* corresponds to the clockwise extreme or maximum positive velocity for a continuous servo.

While it is entirely possible to control a single servo directly from a function generator such as an oscilloscope, using visual feedback to guide the servo, this is often not that practical because

most robotic applications require the automatic control of several servos. The most important characteristics of the pulse being generated are summarised below:

- *Period* - this is how long each complete pulse cycle takes.
- *Frequency* - this is how often the pulses are generated.
- *Duty cycle* - this refers to the amount of time in the period that the pulse is active or high.

$$Duty\ Cycle = \frac{Pulse\ Duration}{Cycle\ Period} \times 100 \tag{6.11}$$

It has been observed that when controlling motors, much greater PWM efficiency is achieved at frequencies of above 20 to 30 kHz.

Figure 6.23: The PWM signal

6.9 Implementation

6.9.1 Arduino Micro-controller Setup on Simulink

To simulate and run the models created on Simulink, specifically for the purpose of implementing them on the hardware via the Arduino Uno micro-controller, the following steps need to be performed:

- Enter '*simulink*' at the MATLAB prompt, This opens the Simulink Library Browser.
- Create a new blank model, and then navigate to **tools->run on target Hardware->Install/Update support Packages->** select '**Arduino Uno**' and install.
- The bock-sets will be installed on the Simulink library browser.
- To run the models created, navigate to **tools->run on target hardware->prepare to run->**set the target to '**Arduino Uno**' and leave the defaults->**run**.

It uses the ordinary differential equation **ODE3**(Bogacki-Shampine) solver. The gain between the analog input and standard servo write connection is set to 0.1760, which is the maximum servo motor displacement in degrees divided by analogue input digital resolution (i.e. 180/1023).

The output from the designed controller will be connected to the input block of the output Arduino Uno module to implement on the hardware, and this block can either be a PWM signal block (most used on DC motors) or a digital output block (most used on servo motors). When using the PWM Arduino block, its input (which is the controller output) controls the duty cycle of the PWM signal which is at a constant frequency of 490 Hz (i.e, a value of 0 produces 0% duty cycle, and an input value of 255 produces 100% duty cycle).

The implementation environment of the controller and how it is physically connected to the bread board and the micro-controller is presented in *Figure 6.24*. The actual system after assembling all the electrical components, such as the tripod gimbal with the two pan-tilt servos, and Arduino Uno micro-controller is illustrated in *Figure 6.25*.

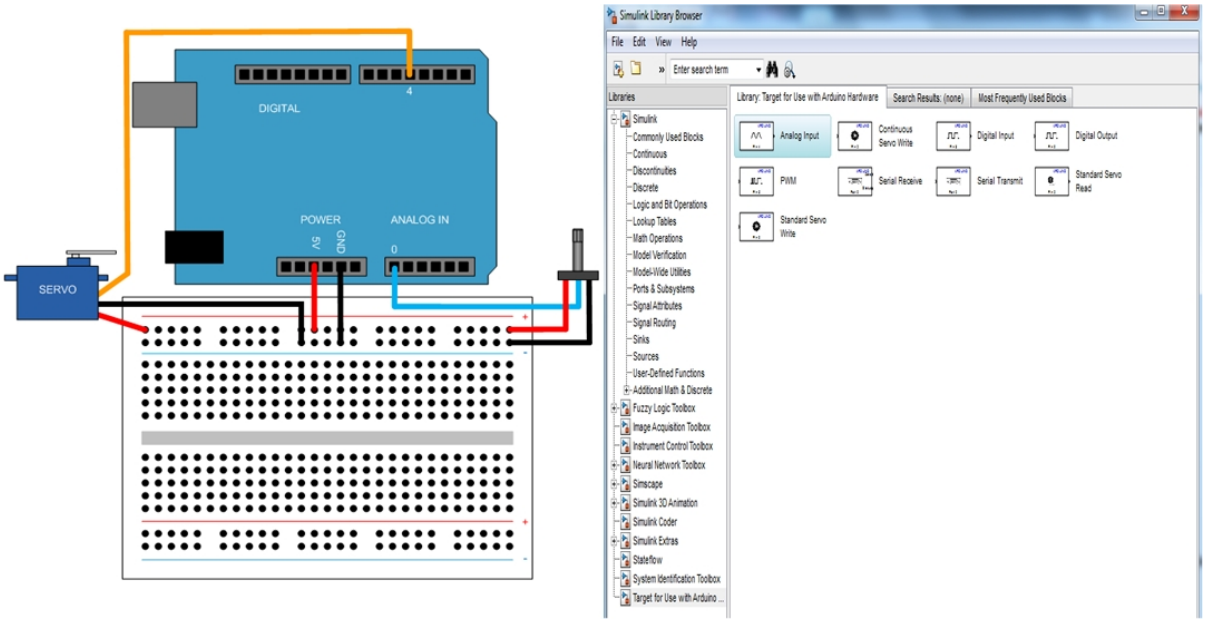

Figure 6.24: MRAC Arduino and Simulink implementation environment

It is noted that the lack of the rotational encoder restricts the test from verifying the performance of the controllers, on the external hardware, since there is no means of feedback in the system hardware. For testing purposes, this is compensated by the precision of the servo motor since it already contains an internal controller (PD-type, meaning that it has an internal feedback) which ensures that it travels to the commanded rotational position with reasonable accuracy.

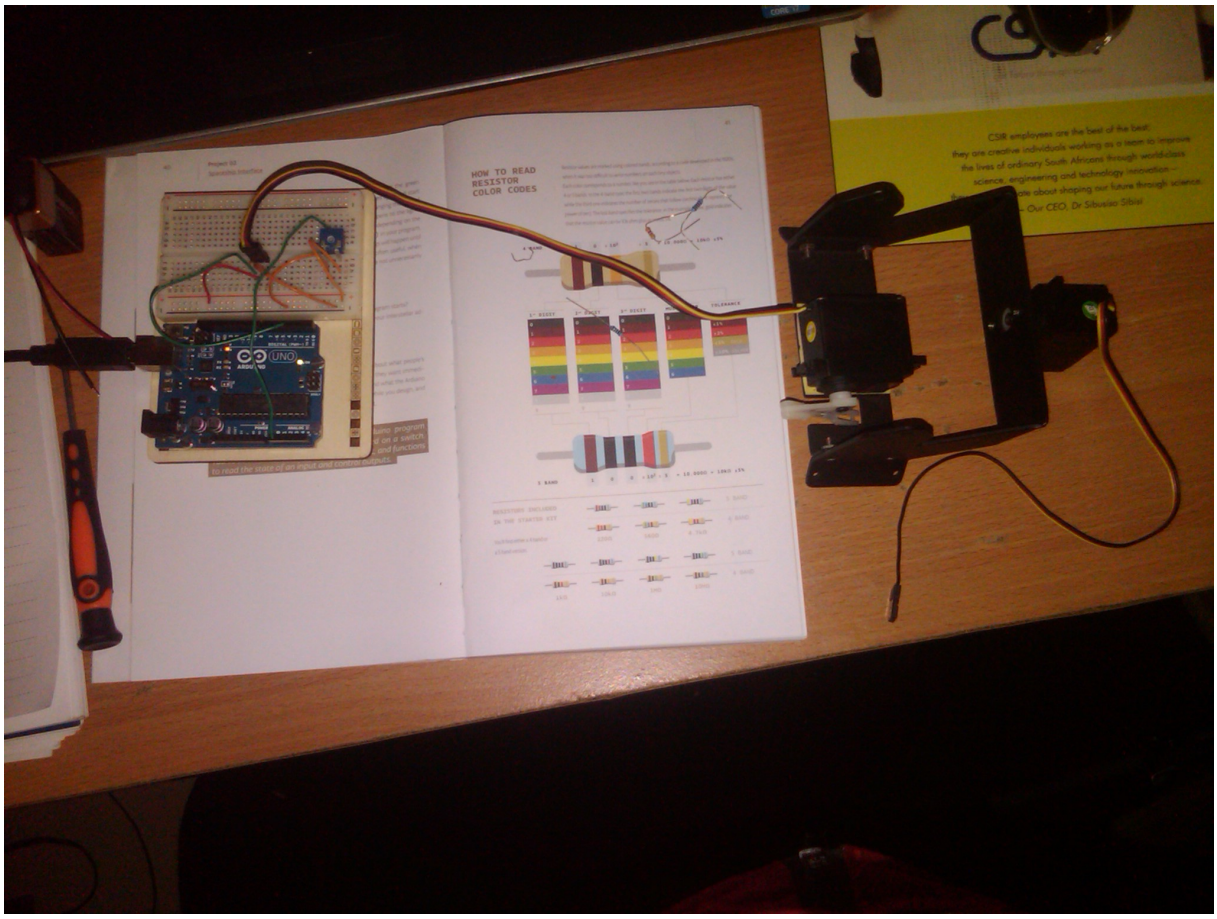

Figure 6.25: Actual system being connected for testing

6.9.2 System Rationale

Unfortunately, since the verification and validation test was not performed adequately, because of the incremental encoder hardware that could not be acquired in time. This then left the proposed setup without the ability to measure and provide feedback of the rotational position that has been travelled to the host computer running the cotroller commands. The system that is proposed here is similar to the system that has been designed and simulated in the following manner.

While the verification system is smaller, however, it presents similar functionality to what is being operated at CSIR. The csir gimbal could not be used to perform these test for the reason that it could break or get permanately damaged. Therefore, it made sense to construct a system which is similar to it and present similar functionaly to perform all the necessary tests on it to verify the designed algorithms. The important parameters to recall on the gimbal is the inertia and damping coefficient. For the system to operate, there must be some presents of a driving mechanism, and that is why a servo motor is chosen as the driver.

The tripod gimbal that is presented in this section is chosen because it present very similar

functionality to the gimbal platform that is used at CSIR. The tripod gimbal has three degrees of freedom, being the tilt, pan and roll. The roll degree of freedom will not be necessary since this is not available in the CSIR gimbal. Because it has already been established that the pan and tilt axes are independant, a single motor can be used for the testing, and it will be used to drive one degree of freedom at a time. In terms of the parameters, they can easily be scale down to represent the smaller gimbal platform and would obviously note the scaling factor which would be the factor that disnguishes the smaller gimbal from the larger gimbal. However, the same equations of motion will be used to represent both systems.

The reason that PWM is introduced in the discussion is because it is the only way that the servo motor can be driven. The PWM signal only serves that single purpose, to provide a digital signal that will drive the gimbal to move to the desired position. The PWM signal can also be used to control the speed at which the gimbal platform travels, thus allowing better capturing of the images of the power line pylons during actual an actual inspection.

During testing, this proposed system was able to receive the commands from the host computer via the Arduino microcontroller, and this then let the researcher to believe that with the incoporation of the encoder, and utilizing the Arduino Matlab blockset from the toolbox, it would be possible to verify and validate the designed controller and substantiate simulation results provided.

it is still believed that this proposed system will be able to properly verify and validate the system that has been discussed. There will be some tweaking required of the results which will mostly stem from trial and error, in order to obtain similar results. The discussion presented here attmpts to demonstrate to the reader that the verification and validation procedure was endeavoured and the only missing piece was the feedback mechanism which would have allowed for the complete close-loop test of the designed controllers. In essence, an open-loop visual verification test was conducted, and it is suggested that the closed-loop verification test be pursued.

A lot of the equipment that was required and planned for in order to fully complete the design of the model and controllers was never purchased and this limited a lot of the functional tests that were intended. It is hoped that considering the information that is presented here, the next researcher will not struggle as much and at worst the struggles will be anticipated and planned for.

6.9.3 Conclusion

The practical implementation of the gimbal control using a tripod gimbal assembly commonly used for small portable commercial photography cameras has been presented. It has been verified

that the gimbal assembly can be commanded to yield a specific desired rotational motion via the programming environment of Simulink; integrated with the Arduino-based blocks, and Arduino Uno micro-controller.

6.10 Recommendations for Future Work

1. The gimbal control system needs to be integrated with the helicopter UAV through an autopilot so that combined system performance can be tested.
2. A more realistic model of the frequently occurring vibration disturbances would help in tuning the control gains appropriately.
3. The system needs to be tested on hardware with a proper feedback sensor mechanism installed.
4. The H_∞ control weight parameters can be automatically tuned using evolutionary algorithms such Neural Network (NN) or Genetic Algorithm (GA).
5. A self-tuning adaptive controller which encompasses a system identification portion in its algorithm could produce better results if implemented properly, this is because it provides a more accurate model of the system especially when implemented on-line.
6. The verification and validation proposed system be fully tested.

Chapter 7

Conclusion

7.1 Introduction

The thesis statement for the dissertation is summarised in the section to follow and the recommendations for future work are presented.

7.2 Summary

The project being pursued at the Council for Scientific and industrial Research (CSIR); Sensor Science and Technology (SST) department, dealing with the development of an autonomous electrical power line inspection mechanism to be used by ESKOM in South Africa and eventually the world, has been briefly introduced.

The scope for this study has been narrowed to the modelling and robust control of the gimbal assembly. A Lagrange and physical system-based modelling approach has been applied to the gimbal and actuators. The investigation included the evaluation and comparison of the robust control using PID control, Ziegler-Nichols, IAE, ISE, ITAE and ITSE tuning algorithm. The H_∞ control, QFT and MRAC controllers where also synthesised and their performance compared to the PID performance. A method of practically verifying and validating the system has been proposed.

7.3 Recommendations for Future Work

1. The gimbal control system needs to be integrated with the helicopter UAV through an autopilot so that combined system performance can be tested.

2. A more realistic model of the frequently occurring vibration disturbances would help in tuning the control gains appropriately.

3. The system needs to be tested on hardware with a proper feedback sensor mechanism installed.

4. The H_∞ control weight parameters can be automatically tuned using evolutionary algorithms such Neural Network (NN) or Genetic Algorithm (GA).

5. The vibration frequency of the aircraft rotor can be included in the control effort by increasing the bandwidth of the controller. This will allow the rejection of vibration disturbances resulting from the aircraft rotor, which is the main source of vibrations in the entire system.

6. A self-tuning adaptive controller which encompasses a system identification portion in its algorithm could produce better results if implemented properly, this is because it provides a more accurate model of the system especially when implemented on-line.

7. The verification and validation proposed system be fully tested.

7.4 Conclusion

The gimbal assembly actuator has been modelled as a PM DC motor and both analytical an physical system-based models have been presented. The gimbal platform has been modelled using the dynamic Lagrangian analytical approach and physical system-based methods. The performance of the model clearly indicated the need for a controller. The PID control with the trial-and-error tuning mechanism has been presented with unacceptable performance. To improve the results the Ziegler-Nichols (Z-N), IAE, ISE, ITSE and ITAE auto-tuning techniques were applied with the Z-N tuning method showing a faster rise-time but second faster peak-time response than the other algorithms, but with the largest overshoot. The ITAE indicated the lowest acceptable overshoot with a good enough settling time, but with the slowest rise-time and peak-time. The performance of the controlled system had reached acceptable levels; however, the robustness and stability of the system required improvement. The H_∞ controller has been demonstrated with the best robust stability and robust performance. The QFT controller also indicated the best robust stability and performance results compared to PID.

The Model Reference Adaptive Controller depicted a response that showed a slow starting and peak time magnitudes, the settling time and steady state response. The superior thing about the response is evident in its robustness, because the adaptive law ensure the model is updated until it approximates the plant model.

Appendix A

Actuators, Transmission and Sensors

A.1 Actuators

In simple terms, the actuators supply the motive power for robot manipulators. The large majority of these actuators are commercially available components, which are adapted or modified accordingly to suit the application. The three most commonly used groups of actuators are hydraulic, pneumatic and electromagnetic.

A.1.1 Hydraulic Actuators

These were chosen as the power source for the earliest industrial robot manipulators and they can produce very large forces and have high power-to-weight ratios. The hydraulic system produces power mechanically from an electric motor or engine-driven high-pressure fluid pump. The properties on a hydraulic actuator are summarised as follows:

- They are most commonly linear cylinders, rotary vane (blade) actuators and hydraulic motors.
- The control is via a solenoid valve (on/off control) or a servo-valve (proportional control), which is driven electrically from a low-power electronic control circuit.
- The hydraulic power supply is bulky and the cost of the proportional, fast-response servo-valves is very high.

The main reason that hydraulic actuators have limited use in current applications is because of leaks and maintenance issues.

A.1.2 Pneumatic Actuators

When dealing with highly simple robot manipulators, pneumatic actuators are generally used. Typically they supply uncontrolled motion between mechanical limit stops and they provide very good performance in point-to-point motion. Their application properties are:

- They are low in cost and very simple to control.
- They have low energy efficiency.
- Although a few small actuators can be run with typical factory air supply, extensive use of pneumatic actuated robot manipulators requires the purchase and installation of an expensive dedicated compressed-air source.
- Proportional, closed-loop, servo-controlled pneumatic manipulators have been successfully developed and applied, especially in applications where safety concerns and environmental and application conditions discourage electric drives.

Examples of these are the widely known early version of the DeLaval international AB Tumba, and the Swedish VMS cow-milking robot manipulators.

A.1.3 Electromagnetic Actuators

These are the most common types in current applications of robot manipulators.

Other actuators that have been widely applied to robot manipulators include thermal, shape-memory alloy (SMA); bimetallic, chemical, piezoelectric, magnetostrictive, electroactive polymer (EPAM); bladder; and micro-electromechanical system (MEMS) actuators. Most of these actuators have been applied to research-based applications and used for academic purposes rather than for mass production industrial robots.

Stepper Motors

In industry applications, the small and simple robot manipulators, such as bench-top adhesive dispensing robot manipulators, use stepper or pulse motors of the PM hybrid type or sometimes the variable reluctance (VR) type. The properties for this motor are as follows:

- The robot applications are usually open-loop position and velocity control.
- They are relatively low in cost.

- They interface easily with electronic drive circuits.
- Micro-step control can produce 10 000 or more discrete robot joint positions.
- In open-loop step mode, the motors and the robot motions have significant settling time, which can be damped either mechanically or through the application of control algorithms.
- Power-to-weight ratios are lower for stepper motors than for other types of motors.
- When they are operated with closed-loop control they actually function similarly to DC or AC servomotors.

Permanent-Magnet DC Motors

The PM DC brush-commutated motor is widely available in many different types and configurations. The lowest-cost permanent-magnet motors use ceramic (ferrite) magnets. The robot toys and hobby robot manipulators often use this type of motor as their actuators. The most ideal to use when the application requires most torque and power against physical size is the Neodymium (NEO) magnet motors, because they have the highest energy-product magnets.

The other motor is the ironless rotor motor, which is often used in small robots. These motors have copper wire conductors moulded into epoxy or composite cup or disc rotor structure. The main advantages of these motors are: low inductance, low friction, and no cogging toque. The disc armature motors have several advantages, such as their short overall lengths and their production of a smooth output with low torque ripple because their rotors have many commutation segments.

The disadvantage of ironless armature motors is that they have a low thermal capacity due to low mass and limited thermal paths to their case. Thus, when driven at high power levels they have rigid duty-cycle limitation or require forced-air cooling.

Brushless Motors

These are also called AC servomotors or brushless DC motors and they are widely used in industrial robot manipulators. Their key contribution is in the substitution of magnetic or optical sensors and electronic switching circuitry for the graphite brushes and copper bar commutator. This eliminates the friction, sparking, and wear of commutating parts. Their decreased complexity allows them to provide good performance at very low cost. However, their controllers are more complex and expensive than brush-type motor controllers. The brushless motor's passive multi-pole Neodymium magnet rotor and wire-wound iron stator provide good heat dissipation and excellent reliability.

A.2 Transmission

The main purpose of a transmission or drive mechanism is to transfer mechanical power from a source to a load. Its design and selection must include the consideration of motion, load, power requirements, and the placement of the actuator with respect to the joint. The major design considerations in transmission are the stiffness, efficiency and the cost. The backlash and windup also impact the drive stiffness, especially in robot manipulator applications where motion is constantly reversing and the loading is highly variable. On the other hand, high transmission stiffness and very low or no backlash will result in increased friction losses. The majority of robotic manipulator transmission elements have good efficiencies when they are being operated at or near their rated power levels but note that this is not always the case when they are lightly loaded.

The physical size of the transmission drive is important, as larger than necessary drives add weight, inertia and friction loss to the entire system response. Also, under-designed drives have lower stiffness, and can wear rapidly in continuous or in high duty-cycle operation or simply fail due to accidental overloads.

The joint actuation in robot manipulators is generally performed by drive mechanisms which interface the actuator (also known as the mechanical work source) to the robot links through the joint in an energy-efficient approach. The transmission ratio of the drive mechanism sets the torque, speed, and inertia relationship of the actuator to the link accurate placement, and sizing. The design of the drive mechanism sets the stiffness, mass and overall operational performance of the root manipulator.

The various and most common drives in practice are discussed in the following subsections.

A.2.1 Direct Drives

When observing the kinematics of this drive, it is by far the simplest drive mechanism. In the case where pneumatic or hydraulic actuated robot manipulators are used, the actuator is directly connected between the links. The electric direct-drive robots employ high-torque, low-speed motors which are directly interfaced to the links.

One of the most important features of a direct drive mechanism is the complete elimination of free play and smooth torque transmission. However, there is often a poor dynamic (inertia ratio) match of the actuator to the link, requiring a larger, less energy-efficient actuator.

A.2.2 Band Drives

A variant of the direct drive is the band drive. The method of application is that a thin alloy steel or titanium band is fixed between the actuator shaft and the driven link to yield limited rotary or linear motion. Drive ratios in the order of up to 10:1 (which is 10 actuator revolutions for one revolution of the joint) can be obtained. In order to reduce robot inertia and gravity loading, the actuator mass is also moved away from the joint towards the base.

This is usually a much smoother and generally stiffer drive than a cable or belt drive mechanism.

A.2.3 Belt Drives

When dealing with the treatment of smaller robots and some axes of larger robots, the synchronous (toothed) belts are often employed in the drive mechanism. The belt drive functions in much the same way as the band drive; the only difference is that the belt drive posseses the capability to drive continuously. For the production of large drive ratios (up to 100:1), multiple stages (two or three) of belts are employed. The tension is usually controlled with idlers or centre adjustment. The elasticity and mass of long belts can cause drive instability and thus increased robot settling time.

A.2.4 Gear Drives

The spur or helical gear drives provide reliable, sealed, low-maintenance power transmission in robot manipulators. They are commonly used in robot wrists, where multiple axes intersect and compact drive arrangements are required. Large-diameter, turnable, gears are used in the base joints of large robot manipulators to handle high torques with high stiffness. Gears are often used in stages and often with long drive shafts, thus enabling physical separation between actuator and the driven joint.

Minimising backlash (free play) in a joint gear drive requires careful design, high precision and rigid support to produce a drive mechanism which does not sacrifice stiffness, efficiency and accuracy for low backlash. The backlash in robots is controlled by a number of methods, including selective assembly, gear centre adjustment and proprietary anti-backlash design.

A.2.5 Worm Gear Drives

For low-speed robot manipulator applications, the worm gear drive is ideal. Its operation features right-angle and offset drive capability, high ratios, simplicity, good stiffness and load capacity.

One of its drawbacks is that it has poor efficiency, which makes them unable to be driven backwards at very high ratios. This causes the joint to hold its position when not powered but also makes it prone to damage by attempts to reposition the robot manipulator manually.

A.2.6 Proprietary Drives

These are widely used in standard industrial robot manipulators. Examples include the very common harmonic drive and the rotary vector (RV) drive, which have compact, low-backlash, high torque capability drives using special gears, cams and bearings. They are commonly applied in situations where there are very small to medium-sized robot manipulators. In general, these drives have low backlash, but the flexspline allows elastic windup and low stiffness during small reversing movements. The RV drives are usually used in larger robots, especially those subject to overloads and shock loading.

A.2.7 Linear Drives

Direct-drive linear actuators incorporate a linear motor with a linkage to a linear axis. This linkage is often merely a rigid or flexure connection between the actuator forcer and the robot link. Alternatively, an already packaged linear motor with its own guide-ways is mechanically connected directly to a linear axis.

Direct linear electromagnetic drives feature zero backlash, high stiffness, high speeds, and excellent performance but the drawback is that they are heavy, have poor energy efficiency and cost more than other types of linear drives.

A.2.8 Ball Screw Drives

Ball-screw-based linear drives efficiently and smoothly convert rotary actuator motion into linear motion. Typically, a recirculating ball nut mates with a ground and hardened alloy steel screw to convert rotary motion into linear motion. Ball screws can be easily integrated into linear axes. Compact actuator/drive packages are also available, as are components for custom integration. Stillness is good for short and medium travel; however, it is lower for long motions because the screw can only be supported at its ends. Low or zero backlash can be obtained with precision-ground screw. Speeds are limited by screw dynamic stability, so rotating nuts enable higher speeds. Low-cost robot manipulators may employ plain screw drives that feature thermoplastic nuts on smooth rolled thread screw.

A.2.9 Rack-and-pinion Drives

These traditional components are useful for long motions where the guide-ways are straight or even curved sometimes. Stiffness is determined by the gear/rack interface and independent of length of travel. Backlash can be difficult to control as rack-to-pinion centre tolerances must be held over the entire length of travel. Dual pinion drives are sometimes employed to deal with backlash by providing active pre-load. Forces are generally lower with screws due to lower ratios. Small-diameter (low teeth count) pinions have poor contact ratios, which result in vibrations. Sliding involute tooth contact requires lubrication to minimise wear. These catalogue stock drive components are often used on large gantry robots and track-mounted manipulators.

A.2.10 Other Drive Components

Splined shafts, kinematic linkages (four-bar, slider-crank mechanism, etc.), chains, cables, flex couplings, clutches, brakes, and limit stops are just a few examples of other mechanical components used in robot drive mechanisms.

The Yaskawa RobotWorld assembly and process automation robots are magnetically suspended, translate on air a planar (two-DOF) bearing, and are powered by a direct electromagnetic drive planar motor with no internal moving parts.

A.3 Motion Sensors and Estimators

The control of a robot manipulator would be much easier if, in addition to the robot model, a complete model of the world environments was also available and if the robot actuator was able to execute motion commands in a perfect order relative to this model. Unfortunately, this perfect ideal model is not available and that is why perfect control of mechanical structures is never a realistic assumption. The introduction and practical application of sensing and estimation mechanism act as a means to compensate for this insufficient information. The role played by the sensor is to provide information about the condition of the environment and the condition of the robot system as a basis for control, decision making, and interaction with other factors in the environment such as humans.

Two very important definitions are necessary at this stage, the first being the proprioception - which is the sensing and estimation to retrieve the state of the robot itself - the second being the exteroception - which is the sensing and estimation to retrieve the state of the external world. The general practice in the industry is to design robot systems to have the proprioception

necessary to estimate and control their own physical states. On the other hand, trying to extract the state of the world from sensor data is a much more cumbersome and complex task.

The sensor-based robot manipulators have been applied in a wide range of scenarios, such as mobile surveillance, medical interventions and high-performance manipulators.

Sensor data can be corrupted in various ways that can complicate the representation of sensory information in a task-oriented model of the world. There is also statistical noise arising from the transducer, discretisation introduced in the digitisation process, and so forth. The estimation methods are necessary to support appropriate consolidation of information into models of the environment and also for the signal-to-noise ratio improvement.

A.3.1 Perception Process

The input to the perception process is typically structured in a twofold manner: the first being accepting digital data from a number of sensors/transducers and, secondly, being a partial model of the environment (this being the world model) which includes information about the state of the robot and other relevant entities in the external world.

The sensor data to be acquired can assume a variety of forms such as scalar or vector value $\mathbf{x}(\alpha, \beta)$ which is acquired over a time series $x(t)$, a scan $x_t(\theta_i)$, a vector field $\mathbf{x}$ or a three-dimensional volume $x(\rho, \theta, \phi)$. In general, a system must accept and consolidate data from several different sensors. An example would be the estimation of the position of a mobile robot, which may consolidate data from axis encoders, vision, global positioning system (GPS) data and inertial sensors.

The first challenge in the analysis of sensory data is data preprocessing and characteristic extraction. The reason preprocessing is necessary is to reduce the noise from the transducer, to remove systematic errors, and to amplify any relevant aspects of the data. There are many ways that data can be preprocessed, the most common approach being model fitting. Once the sensor information is available, it is often necessary to match the data with an existing model. The model being used could even be based on an anterior familiar structure (such as a CAD model of the environment). Following this, is the application of data association methods to estimate the relationship between sensor data and the model of the environment. Finally, once the sensory data has been matched against the world model it is then possible to update the model with fresh information contained in the sensory data.

A.3.2 Sensors

Sensors are generally classified in accordance with what they measure and how they measure it. It has already been established that proprioceptive sensors measure the internal state of a robot, which most likely include the position of the various degrees of freedom, the temperature, voltage of the key components, motor current and force applied to the end-effector, and so forth.

The other distinguishing factor between sensors is whether they are passive or active. The general definition of an active sensor is one that emits energy into the environment and measures the properties of the environment based on the response. A passive sensor is just the opposite.

The thing that qualifies the active sensor as more robust than the passive sensor is that it applies some control over the measured signals. The drawback of active sensors is that the absorption, scattering and/or interference of the emitted signal can affect their performance drastically. Hence, proprioceptive sensors are typically passive and usually measure physical properties of the robot such as joint position, velocity, acceleration, motor torque, and so forth.

A categorisation of typical sensors according to method and typical application is presented in *Table A.1*.

One of the most fundamental factors necessary for the control of robot manipulators is the estimation of the rotational motion. It is also important for estimation of ego-motion for mobile systems. The most common sensor for measurement of rotation is the quadrature encoder, and this sensor is composed of a transparent disc, with two periodic patterns that are out of phase.

For the estimation of force and torque at an end-effector it is possible to use piezoelectric elements. The way these elements operate is that they generate a voltage that is proportional to the introduced deformation. If one is smart about the placement of the transducer, it is possible to measure both force and torque. These sensors are practically offered in a range of sizes and dynamic ranges which includes new flexible arrays that can be mounted on a variety of end-effectors.

Potential problems with force sensors are a dead band on initial contact and noisy data from the basic sensing elements, which then calls for signal processing to clean up the data.

Ego-motion estimation is a crucial aspect of almost all robotic systems, and to this end it is still possible to use inertial measurement units (IMU), which include both accelerometer and gyros. Accelerometers are sensitive to all forms of acceleration, which implies that both translational motion and rotational (centripetal force) motion are measured in combination. Also, joint IMUs allow the estimation of rotation and translation and for the double integration to estimate the velocity, orientation and position of the system.

Table A.1: Classification of sensors commonly used in robotics according to sensing objective [proprioceptive (PC)/exteroception (EC) and method (active (A)/passive (P))]

Classification	**Sensor type**	**Sens**	**A/P**
Tactile Sensors	Switched/bumpers	EC	P
	Optical barrier	EC	A
	Proximity	EC	P/A
Haptic Sensors	Contact arrays	EC	P
	Force/torque	PC/EC	P
	Resistive	EC	P
Motor/axis sensor	Brush encoders	PC	P
	Potentiometer	PC	P
	Resolvers	PC	A
	Optical encoders	PC	A
	Magnetic encoders	PC	A
	Inductive encoders	PC	A
	Capacitive encoders	EC	A
Heading sensors	Compass	EC	P
	Gyroscopes	PC	P
	Inclinometers	EC	A/P
Beacon based	GPS	EC	A
(position wrt	Active optical	EC	A
an inertial	RF beacons	EC	A
frame)	Ultrasound beacons	EC	A
	Reflective beacons	EC	A
Ranging	Capacitive sensor	EC	P
	Magnetic sensor	EC	P/A
	Camera	EC	P/A
	Sonar	EC	A
	Laser range	EC	A
	Structures light	EC	A
Speed/motion	Doppler radar	EC	A
	Doppler sound	EC	A
	Camera	EC	P
	Accelerometer	EC	P
Identification	Camera	EC	P
	Radio frequency		
	Identification		
	RFID	EC	A
	Laser ranging	EC	A
	Radar	EC	A
	Ultrasound	EC	A
	Sound	EC	P

The single problem associated with the use of an IMU is the need for double integration, which can make small biases and noise signals result in significant divergence in the final estimate. This then calls for the use of detailed models and careful calibration and identification of sensor characteristics.

A.3.3 Estimation Process

The selection, from a large variety, of methods to amalgamate data from the sensor depends largely on prior knowledge about the environment and what information is necessary to perform the required task and what models are suitable for the sensing system. A brief recap of some of the most common methods includes the simple voting-based methods, parametric and non-parametric statistical estimation techniques, fuzzy logic-based systems and Dempster-shafer theory.

The localisation problem can be used to further illustrate this point because at the onset of initialisation, if nothing is known about the environment then the robot may acquire a laser scan and attempt to produce an initial model of the environment using segments. Note that since nothing is known prior, the following items need to be estimated before we can continue: (1) the number of line segments, (2) the data association between line segments and observed data values, and (3) the parameters of the line segments themselves. This is a challenging problem, but can be handled by applying the voting techniques such as the Hough transform or RANSAC or even more sophisticated unsupervised clustering algorithms such as $k-$means, expectation maximisation (EM), or GPCA. One should be warned that these are computationally intensive and iterative processes.

If, on the other hand, a prior CAD model for the environment is known, then the problem becomes simplified and about producing a small set of parameters (that is translational and rotational) of the model to match the data. This problem can be tackled by using the iterative closest-point algorithm (ICP) or more efficient algorithms such as the Monte Carlo method.

Once an initial registration is known, new data can take advantage of the fact that secure prior knowledge is present and the predictor-correction methods such as the Kalman filter or sequential importance sampling can be implemented.

The decision-making problem can be seen as a point estimation problem, and a multitude of algorithms have been successfully employed to yield satisfactory solutions. Such algorithms are the estimation techniques for batch and sequential data with linear models. These optimisation-oriented problems also involve the application of the extended version of the Kalman filter. The problem can also be extended to the nonlinear estimation for sequential data.

In the case when dealing with data that contains *outliers* - which are defined as the data points that are either much more highly corrupted or that are spurious, robust estimation approaches need to be taken such as the M-estimators, RANSAC and least median or squares (LMedS).

A.3.4 Data Association

When dealing with a situation where there is no explicitly known relationship between observations and a quantity to be estimated, this correspondence has to be computed in conjunction with the estimation problem. The formal definition of data association is that it yields a correspondence between the observed data and quantities to be estimated.

Two groups of problems can already be classified: (1) the causal (sequential) association methods for time-series data, and (2) non-causal (batch) methods that can be used when the complete data set is available for processing. A wide variety of clustering algorithms have found general wide use in this field, the most common being the Nearest-Neighbour association, recursive filtering, $k-$means clustering, etc.

A.3.5 Sensor Modelling

The development of a sensor model involves some of the following elements: (1) creating a physical model, (2) determining a sensor calibration, (3) determining an error model, and (4) identifying failure conditions. In simpler terms, the physical model is the relationship $f(.)$ between the underlying quantities of interest (x) and the available data (y). This relationship may not always be so obvious.

A.3.6 Representation

Once sensor data has been obtained it can be used directly for control of the robot manipulator, but it can also be used for estimation of the condition of the robot and the world. Recall, that the *pose* of the robot manipulator is a representation in the world coordinates that is characterised by position and orientation with respect to a particular reference frame. In general, the *pose* is represented by the pair ($\mathbf{R}$, $\mathbf{T}$): $\mathbf{R}$ is an orientation matrix and $\mathbf{T}$ is a translational matrix with respect to a reference frame.

The sensory data is acquired in a local sensor reference frame and, if the goal is to combine this information into a common world model, then the data must be transformed into a robot-centred reference frame or just a fixed world (inertia) reference frame. There are four general classes of models for representing the consolidated sensor data:

- Raw sensor data models
- Grid-based models
- Feature-based models
- Symbolic or graphical models

A.4 Inertial Sensors, GPS and Odometry

The most common and general practice for robot manipulators is to exploit the world coordinate properties to develop a model of the robot motion, which is commonly known as *pose* (position and orientation), relationship to some external reference frame. This issue becomes especially crucial when dealing with autonomous robotic systems for many surveillance applications in the industry or academic research studies. The biggest problem is establishing and maintaining a *pose* estimate of a mobile robot agent.

A.4.1 Odometry

The term *odometry* has had a tremendous overall impact in vast applications from civil engineering to military conquest; in fact, its basic underlying principles have been studied for over 2000 years. Its earliest application enabled humans, while sailing by sea, to know how many kilometres of a journey they had travelled. When applying this concept to autonomous vehicles, the concept refers to the utilisation of data from the actuators to estimate the overall motion *pose* of the vehicle. In simplified terms, the idea is to develop a mathematical model of how selected motions of the vehicle's links, joints, etc. induce motion of the vehicle itself, and then integrate these specified motions over time in order to develop a model of the *pose* of the vehicle as a function of time. This process is generally known as *dead reckoning* or *deduction reckoning*.

When applying the concept of odometry to mobile robots, it can be explained and demonstrated much better by the evaluation of a differential drive vehicle in *Figure A.1*.

The characteristics of a differential drive vehicle are that it has two drivable wheels that receive independent control, and are mounted along a common axis. If one assumes that the location of the wheels are fixed on the vehicle, then in order for the wheels to maintain a constant contact with the ground, the two wheels must describe *arcs* on the plane such that the robot rotates around a point (commonly known as the ICC - instantaneous centre of curvature) that lies on the wheel's common axis. If the ground contact speeds of the left and right wheels are v_ℓ and v_r respectively, and the distance between the wheels is $2d$, then:

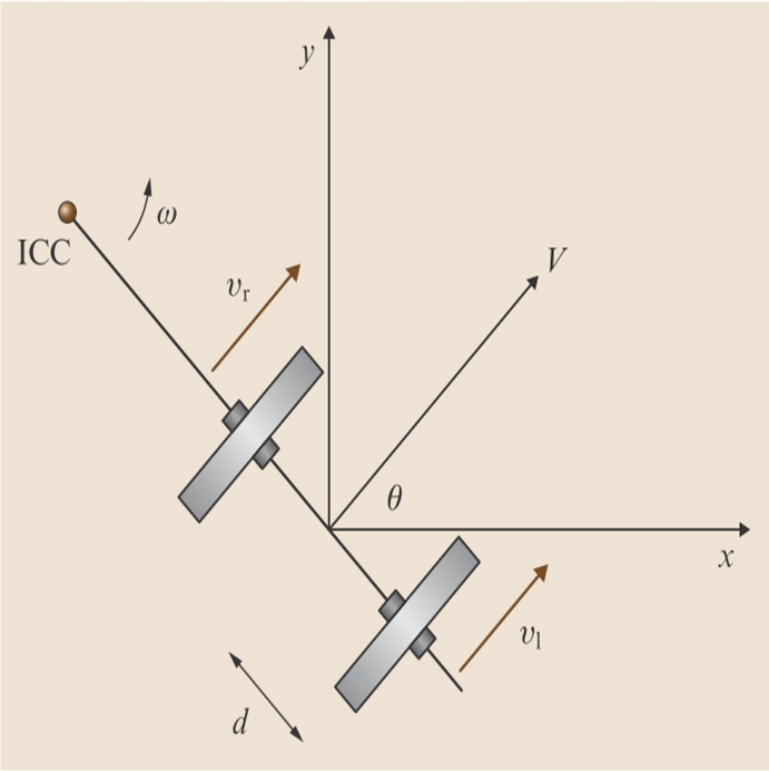

Figure A.1: The differential drive kinematics system

$$v_\ell = \omega(R + d) \tag{A.1}$$

$$v_r = \omega(R - d) \tag{A.2}$$

Rearranging the equations and solving for ω (the rate of rotation about the ICC) and R (the distance from the centre of the robot to the ICC):

$$\omega = \frac{(v_\ell - v_r)}{(2d)} \tag{A.3}$$

$$R = \frac{(v_\ell + v_r)}{(v_\ell - v_r)} \tag{A.4}$$

The instantaneous velocity is given by $V = \omega R$. One can obtain the equations which describe the position and orientation of the robot as a function of time, by using the point midway between the wheels as the origin of the robot and writing θ with respect to the x-axis of a global Cartesian coordinate system; then:

$$\theta(t) = \int \omega(t)dt \tag{A.5}$$

$$x(t) = \int V cos(\theta(t))dt \tag{A.6}$$

$$y(t) = \int V cos(\theta(t))dt \tag{A.7}$$

Equations (A.5), (A.6) and (A.7) give us the solution of a differential drive vehicle on a plane. When provided with the control inputs (υ_ℓ and υ_r) and some initial state estimate, it is possible to estimate the state of the idealised robot at any time t through the use of this motion model.

In a perfect world, all the above promises would be fulfilled, but unfortunately there are many unexpected errors that need to be compensated for, such as:

- Errors in the theoretical modelling (incorrect estimations of vehicle size, etc.);
- Uncertainty about the control inputs;
- Realities of the motor controllers (error between commanded rotation and true rotation); and
- Error in physical modelling of the robot (compaction, slippage, etc.).

These introduce an error between the *dead reckoning* estimate of the vehicle motion and its true motion. The problem of correcting for this error is generally denoted as the problem of *pose* maintenance for the vehicle, and it requires the consolidation of the *dead reckoning* estimates with other estimates obtained from the external sensors.

A.4.2 Gyroscopic System

The main function of a gyroscopic measurement system is to measure the changes in vehicle orientation by using the physical laws which yield predictable effects under rotation. It is important at this stage to remind the reader that a rotating frame is not an inertial frame; in fact, it is commonly denoted as a non-Newtonian frame. The measurement of the deviations from the frames permits the extraction of the underlying self-rotation.

Mechanical System

Mechanical gyroscopes and gyrocompasses have a long history in navigation applications. They rely on the principle of the conservation of angular momentum, which is defined as the tendency of a rotating object to keep rotating at the same angular speed about the same axis of rotation in the absence of an external torque. The angular momentum $\mathbf{L}$ of an object with moment of inertia $\mathbf{I}$ rotating at angular speed ω is given by:

$$\mathbf{L} = \mathbf{I} \times \omega \tag{A.8}$$

Gyroscopes are best suited to perform measurements of the local changes in orientation, which puts them at an ideal position to be applied in vehicular robotic applications. In practice, there are rate gyros (RGs), which are used to measure the vehicle's rotation rate (which is the angular rate of rotation ω), and rate-integrating gyros (RIGs) which use embedded processing to perform integration on the angular rotation rate to yield an approximation of the absolute angular displacement on the vehicle.

A gyrocompass is usually suitable for applications where the orientation is required with respect to an earth reference frame. However, its performance characteristics are affected by the external forces acting on the compass, which also contribute to the precession of the gyroscope. One of their most profound drawbacks is the requirement of an external force to be applied on the mechanical gyrocompass to maintain the rotation of the gyroscope and this introduces undesired forces into the system, which can further corrupt the measurement process.

Mechanical gyrocompasses have been dropped for recent applications because of their drawbacks such as the complexity, size, cost and fragile nature, and they have paved the way for more available less expensive and much more reliable technologies such as optical and micro-electromechanical systems (MEMS).

Optical Gyroscopes

The special attraction of optical gyroscopes is that they rely on the *Sagnac effect* instead of rotational inertia to measure (relative) heading. The complete mechanism is based on the behaviour of an optical standing wave in a rotating frame. In general, they use lasers as their light source.

MEMS Systems

The majority of all MEMS gyroscopes are based on vibrating mechanical elements to sense the rotation. Generally, vibratory gyroscopes rely on the transfer of energy between vibratory modes based on Coriolis acceleration - and by definition the Coriolis acceleration is the apparent acceleration that arises in a rotating frame of reference.

In practice, the early design of MEMS gyroscopes utilised vibrating quartz crystals to generate the necessary linear motion, but more recent designs utilise silicon-based vibrators such as the *tuning-fork* gyroscope, *vibrating wheel* gyroscope and *wire-glass resonant* gyroscopes.

Performance

There are many standards to which the performance of inertial measurement units (IMUs) can be evaluated against, the most common criterion are presented below:

1. Bias repeatability - this is the drift of the readings under ideal conditions.
2. Angle random walk - this is a measurement of noise in the angular rate data coming from the gyro.
3. Scale factor ratio - this is a measurement of the ratio of the output analogue voltage to the sensor parameter of interest (units being $mV/(deg/sec)$).

A.4.3 Accelerometers

In layman terms, an accelerometer is also an IMU which measures external forces which may be acting on the vehicle robot. A very important factor to be understood concerning accelerometers is that they are very sensitive to all external forces acting upon them, including gravitational forces.

Mechanical Accelerometers

A mechanical accelerometer is essentially a basic spring-mass-damper system, as depicted in *Figure A.2* (a), with some mechanism to perform external monitoring. The concept of operation is as follows: when an applied force (which could even be gravity) is presented, this force acts on the mass and displaces the spring. If an assumption is made that the spring is ideal with a force proportional to its displacement, then the external forces must balance the internal one as denoted in equation (A.9):

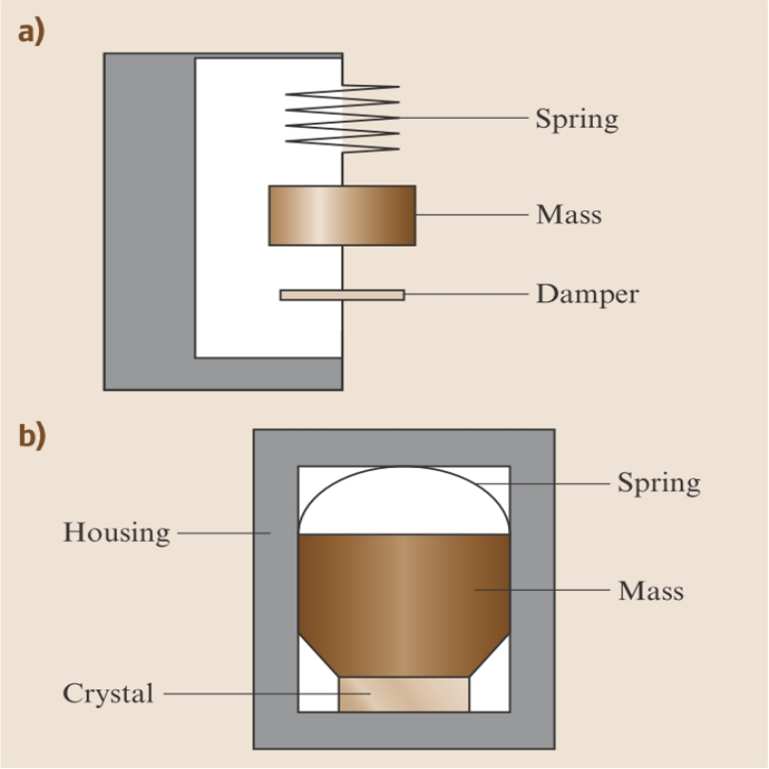

Figure A.2: The mechanical accelerometer basic model structure

$$F_{applied} = F_{inertial} + F_{damping} + F_{spring} \tag{A.9}$$

$$F_{applied} = m\ddot{x} + c\dot{x} + kx \tag{A.10}$$

Where c is the damping coefficient. The biggest drawback of mechanical accelerometers is their sensitivity to vibrations; however, this can be very useful when performing a vibration disturbance test. Their sensitivity suddenly become a strong trait and allows for the accurate measurement of vibration forces or toques.

Another alternative is the piezoelectric accelerometer.

Piezoelectric Accelerometer

Rather than relying on a direct mechanical measurement of the external forces, piezoelectric accelerometers are based on a property exhibited by certain crystals, across which a voltage is generated when they are stressed. This is illustrated in *Figure A.2* (*b*).

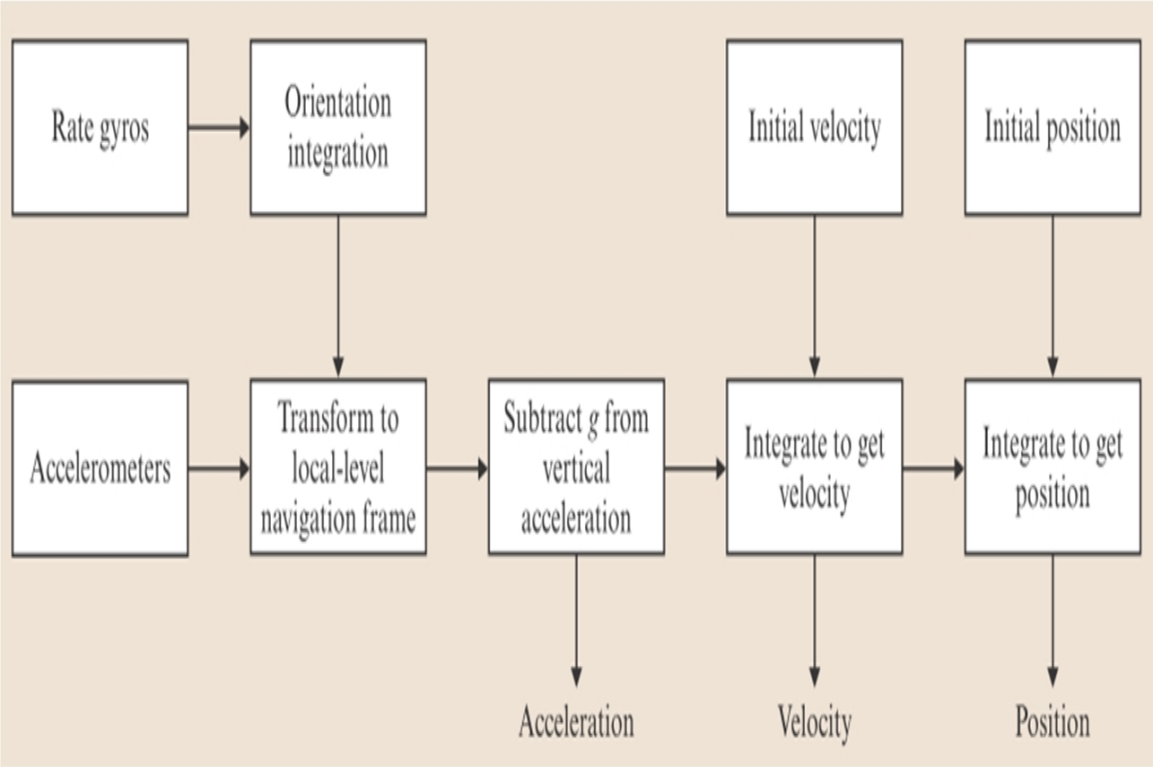

Figure A.3: The basic IMU structure

A.4.4 IMU Packages

In practice, an IMU is a device that utilises measurement system such as gyroscopes and accelerometers to approximate the relative position, velocity, and acceleration of a vehicle in motion. There are two basic IMUs: the gimbaled systems and the strap-down system. The gimbaled IMUs are mounted within complex gimbal structures in order to provide a stable platform from which measurement can be made. The orientation of the gimbaled platform relative to the vehicle is used to map measurements taken within the IMU to the reference frame of the vehicle. Strap-down IMUs, on the other hand, have the IMU rigidly connected to the vehicle (strap down), so no such transformation is required.

Estimating the motion of the robot manipulator needs to be done in realtime. The basic computational task of an IMU is depicted in *Figure A.3*, and this IMU uses three orthogonal accelerometers and three orthogonal gyroscopes in the following manner.

The gyroscope measured data ω is integrated to maintain an ongoing estimate of vehicle orientation θ. At the same time, three accelerometers are used to estimate the instantaneous vehicle acceleration a. This data is then transformed via the current estimate of the vehicle orientation relative to gravity, so that the gravity vector can be estimated and extracted from the measurement. The resulting acceleration is then integrated to obtain vehicle velocity v and integrated again to obtain the position r.

Because it is never possible to eliminate the gravity vector completely, the drift is fundamentally the main issue for the performance of IMUs. To correct this we use a GPS.

A.4.5 Global Position System

The GPS is the single most common used mechanism for location estimation. It basically provides a three-dimensional position estimate in absolute coordinates as well as current time and date and is available anywhere on the earth's surface. The standard commercial GPS provides a position estimate in the horizontal plane to within about 20 m. Its initial development was purposed for military applications, but its increased popularity allowed it to be adapted for civilian applications, including automobile navigation systems, recreational orienteering, and inventory tracking for transportation companies.

The system's operation is based on the received radio signals transmitted by an ensemble of satellites orbiting the earth and by comparing the time delays from the different satellite signals a position fix can be computed.

Performance Characteristics

The GPS performance is not always exact and it depends on several factors, such as satellite transmission accuracy, environmental conditions, interactions with ground-based obstacle, and receiver properties. When applying GPS in robotic applications, the factors that affect the performance of the satellites themselves and the atmospheric conditions are essentially uncontrollable. However, the user should be aware that these issues could be the sources of error and that, most importantly the GPS signal itself may not always be reliable. The list of controllable factors in using GPS for accurate localisation is summarised as follows:

1. It requires an unobstructed line of sight to the satellites;
2. It depends on atmospheric conditions; and
3. It depends on the ability to receive (weak) radio-frequency communication.

GPS-IMU Integration

The promise of high-resolution positioning information offered by the GPS on or about the surface of the earth is great but does not solve all issues associated with robot *pose* estimation. For starters, it does not directly obtain information about vehicle orientation and in order to

determine the orientation of the vehicle yaw, pitch and roll must be estimated by either differentiating the GPS signal or by consolidating with other sensors such as compasses, gyrocompasses and IMUs. Secondly, GPS receivers are generally unable to provide continuous independent estimates of position. Finally, it is not always possible to obtain a GPS fix, because local geography (e.g. mountains, buildings and trees) or an overhead cover that is opaque to radio signals (e.g. indoors, underwater) can block the signal entirely. The consolidation of the GPS with other sensors can deal with these issues at least for short periods of time.

Appendix B

Gimbal Modelling and Performance Characteristics

B.1 DC Motor

Table B.1 below summarises all the variables used for the double gimbal system, including the motor modelling.

Table B.1: PM DC motor label description for model

Symbol	**Description**
M_c	Mass of the gimbal structure
M_w	Mass of the on-board camera (*MultiCam*)
R_a	Armature resistance of the DC motor
L_a	Armature inductance of the DC motor
K_m	DC motor back emf constant
K_t	Torque constant
B_m	Viscous damping coefficient
J	Rotor inertia of the system
i_a	Armature current of the DC motor
$\dot{\theta} = \omega$	Angular velocity
r	Radius of the drive sheave

The method used to model the permanent magnet DC motor is a second order state variable model, and it is implemented on the computer using the Simulink toolbox called SimElectronics. The reason for this is so that the model can reflect the real dynamics of a practical Permanent Magnet (PM) DC motor as closely as possible.

A second order, linear state space approach is considered for modelling the PM DC motor [127].

The ultimate goal is to obtain the torque being generated by the motor and this can be derived from the two states on the modelled motor. The two states are the armature current (i_a) and the rotational speed (ω) of the DC motor from the following equations:

$$T = k_b\dot{\omega} \tag{B.1}$$

$$T = k_t i_a \tag{B.2}$$

There are three well-understood methods regarding the speed control of DC motors: field resistance, armature voltage and armature resistance [128]. For the purpose of this research study, armature voltage was selected as the appropriate method to control the speed of the motor. For any project with many practical considerations, where the motor provides the mechanical drive to bring about mobility to a mechanical platform, accurate modelling of the PM DC motor is paramount [129]. This is also important for robust feedback design of the electric-powered mobility platform.

Most researchers have observed that data plate values are usually either incomplete or missing from the equipment, such as the motor. The PM DC motor has been widely explored and well documented in various relevant engineering text books and articles, and it is mostly treated as an ideal model. However, in a practical motor concerns such as friction losses play a large role in the accuracy of the expected results. The frictional loss of particular concern is represented by the viscous friction coefficient, coulomb and static friction coefficients. These all contribute to what is known as the *frictional torque*.

Using Kirchoff's voltage law, the following equation can be derived:

$$V = R_a i + L_a \frac{di}{dt} + V_{emf} \tag{B.3}$$

Also, when ignoring any load in the system, the torque can be derived as a second order ODE as follows:

$$T = J\ddot{\theta} + B\dot{\theta} \tag{B.4}$$

The electrical and mechanical components are coupled in two ways: firstly, through the relationship between the torque and the current as follows in (B.5):

$$T = k_t i \tag{B.5}$$

Secondly, the motor rotational velocity is related to the back emf through equation (B.6):

$$V_{emf} = k_m \dot{\theta} = k_m \omega \tag{B.6}$$

Equations (B.6) and (B.5) are then substituted in (B.3) and (B.4) as follows:

$$k_t i = J\ddot{\theta} + B\dot{\theta} \tag{B.7}$$

$$V = R_a i + L_a \frac{di}{dt} + k_m \dot{\theta} \tag{B.8}$$

From Kirchof's Voltage Law, the following electrical equations are derived:

$$V = Ri + L\frac{di}{dt} + V_{emf} = Ri + L\frac{di}{dt} + K_m \omega \tag{B.9}$$

$$\begin{bmatrix} \ddot{\theta} \\ \dot{i} \end{bmatrix} = \begin{bmatrix} \frac{-B_m}{J_m} & \frac{K_t}{J_m} \\ \frac{-K_m}{L_a} & \frac{-R_a}{L_a} \end{bmatrix} \begin{bmatrix} \dot{\theta} \\ i \end{bmatrix} + \begin{bmatrix} 0 \\ \frac{1}{L_a} \end{bmatrix} V \tag{B.10}$$

$$\dot{\theta} = \begin{bmatrix} 1 & 0 \end{bmatrix} \begin{bmatrix} \dot{\theta} \\ i \end{bmatrix} \tag{B.11}$$

B.2 Motor Parameters

A general discussion of the experimental determination of the motor parameters for the PM DC motor can be accomplished using the methods as briefly detailed in the following subsections.

B.2.1 Torque Constant

By rearranging equation (B.5) the motor torque constant can be represented in terms of the torque against the current. A test rig can be set up for the PM DC motor, where the torque can be determined via a force measured by a Newton force meter and the current can be measured by a standard off-the-shelf clamp meter (such as digital multi-meter).

Applying a 24 V steady DC voltage at the input terminals of the motor and using a rope to provide a load on the motor, by increasing the load gradually until the motor stalls, the motor will reach a constant speed. Recall that the torque can be calculated from ($T = F \times r$), hence by multiplying the difference between the two measured forces on each end of the rope by the radius of the wheel hub. Also, motor current is measured and recorded at set intervals. A plot of the calculated torque and the measured current can then be generated and from it we can deduce the motor torque constant from the slope of the line.

B.2.2 Speed/Motor Constant

Paying particular attention to the steady state values, it is possible to rearrange equation (B.8) to represent the slope-intercept form in the following manner:

$$\frac{V}{i} = k_m(\frac{\dot{\theta}}{i}) + R_a \tag{B.12}$$

Where $\dot{\theta}$ is the motor shaft rotational speed and from equation (B.12) only steady state values of the input DC voltage, current and motor shaft rotational velocity need to be measured. The digital multi-meter can be used to measure the terminal voltage, and the digital multi-meter clap meter to measure the current. Practically, the motor velocity can be controlled by using a variable resistor to vary the voltage at the motor terminals and a digital rpm gauge can be used to measure the rpm of the wheel, thus providing the shaft velocity. The measurement results can be represented in a plot of ($\frac{V}{i}$) versus ($\frac{\dot{\theta}}{i}$) and the speed constant (k_m) will be the slope of the figure.

B.2.3 Armature Resistance

From equation (B.12) and the results for the speed constant, the armature resistance (R_a) can be estimated from the slope of the line in the figure.

B.2.4 Viscous Friction Coefficient

When the system is under steady state conditions, equation (B.7) becomes:

$$k_t i = B\dot{\theta} \tag{B.13}$$

and from equation (B.13)

$$B = \frac{k_t i}{\dot{\theta}} = \frac{k_t i}{\omega} \tag{B.14}$$

Using the already determined values of (k_t) and the range of steady state current values and rotational velocity values, the speed constant can be determined using equation (B.14). It should be noted that the friction coefficient also takes into account gearing and eddy current losses in the motor iron, which always increase the speed.

B.2.5 Armature Inductance

To be able to measure the armature inductance, the tool required is a digital meter which is capable of capturing and recording instantaneous or real-time changes. Initially, a fixed voltage is supplied to the at-rest motor system on the test rig, with the rotor in a locked position. Using the multi-meter again, the rate of current increase with time is recorded and then, using equation (B.15), the inductance can be calculated.

$$L_a = V/(\frac{di}{dt}) \tag{B.15}$$

It should be noted that the back emf is zero since there is no rotor rotation. The initial current is zero and negligible when compared with the rate of change of current within the first instance of the motor start-up.

B.2.6 Motor/System Inertia

The real-time measurement meter is once again used in the implementation of a means to control voltage input and hence motor current levels. However, in this particular instance the rate of voltage change is required to be measured. The motor rotor is placed in a locked position until a set current is reached, while overcoming the initial effects of rotor inductance, and then released. The rotational velocity is zero at the beginning and subsequently negligible when compared with the rate of rotational acceleration within the first instance of motor release. Equation (B.16) is used to calculate the motor/system inertia, with the initial velocity being negligible.

$$J = (k_t i)/\ddot{\theta} = (k_t i)/\alpha \tag{B.16}$$

B.3 Two-degree of Freedom Gimbal Platform

The analytical derivation of the dynamic model which represents the gimbal platform with all its important properties is presented in this section.

B.4 Lagrangian Model

The derivation considers a single particle.

B.4.1 Deriving Lagrange's Equations

First select an inertial reference frame along x, y and z coordinates. The force along the different axes can be expressed as follows:

$$F_x = m\ddot{x} \tag{B.17}$$

$$F_y = m\ddot{y} \tag{B.18}$$

$$F_z = m\ddot{z} \tag{B.19}$$

Consider coordinates q_1 and q_2 (or θ and ϕ) which are independent variables. When considering completely arbitrary infinitesimal displacement δs (which has components of δx, δy, δz) which results when F is applied to produce the virtual work δW. The virtual work is represented as follows:

$$\delta W = F\delta s \cos(F, \delta s) = F_x\delta x + F_y\delta y + F_z\delta z \tag{B.20}$$

It needs to be mentioned that the directionality for F and δs may not be the same.

Multiplying equation (B.17) to (B.19) by δs and then adding produces the following:

$$m(\ddot{x}\delta x + \ddot{y}\delta y + \ddot{z}\delta z) = F_x\delta x + F_y\delta y + F_z\delta z \tag{B.21}$$

The left hand side of (B.21) represents the slight change in kinetic energy and the right hand side represents the virtual work done by the force applied. Equation (B.21) is called the D'Alembert's equation.

Since coordinates q_1 and q_2 are independently variable, we can focus our attention on δW_{q_1}, which is the work done when only δq_1 is allowed to vary ($\delta q_2 = 0$).

First derive the virtual displacements in the following manner:

$$\delta x = \frac{\partial x}{\partial q_1}\delta q_1 \tag{B.22}$$

$$\delta x = \frac{\partial y}{\partial q_1}\delta q_1 \tag{B.23}$$

$$\delta z = \frac{\partial x}{\partial q_1}\delta q_1 \tag{B.24}$$

Substituting all the virtual displacements in D'Alembert's equation (B.21) and grouping terms we obtain:

$$\delta W_{q_1} = m(\ddot{x}\frac{\partial x}{\partial q_1} + \ddot{y}\frac{\partial y}{\partial q_1} + \ddot{z}\frac{\partial z}{\partial q_1})\delta q_1 = (F_x\frac{\partial x}{\partial q_1} + F_y\frac{\partial y}{\partial q_1} + F_z\frac{\partial z}{\partial q_1})\delta q_1 \tag{B.25}$$

Before continuing, it is critical to state the following proof:

$$\ddot{x}\frac{\partial x}{\partial q_1} = \frac{d}{dt}(\dot{x}\frac{\partial x}{\partial q_1}) - \dot{x}\frac{d}{dt}(\frac{\partial x}{\partial q_1}) \tag{B.26}$$

$$\frac{\partial x}{\partial q_1} = \frac{\dot{x}}{\dot{q_1}} \tag{B.27}$$

$$\frac{d}{dt}(\frac{\partial x}{\partial q_1}) = \frac{\partial \dot{x}}{\partial q_1} \tag{B.28}$$

Substituting equation (B.27) and (B.28) in (B.26):

$$\ddot{x}\frac{\partial x}{\partial q_1} = \frac{d}{dt}(\dot{x}\frac{\partial \dot{x}}{\partial \dot{q_1}}) - \dot{x}\frac{\partial \dot{x}}{\partial q_1} \tag{B.29}$$

Equation (B.29) can be re-written in the following manner, with a minor consideration:

$$\ddot{x}\frac{\partial x}{\partial q_1} = \frac{d}{dt}(\frac{\partial(\dot{x}^2/2}{\partial \dot{q_1}}) - \frac{\partial(\dot{x}^2/2)}{\partial q_1} \tag{B.30}$$

We can also develop similar relations involving x, y and z and substituting equation (B.30) in (B.25) we obtain:

$$\delta W_{q_1} = \left[\frac{d}{dt}(\frac{\partial}{\partial \dot{q_1}}\frac{m(\dot{x}^2+\dot{y}^2+\dot{z}^2)}{2}) - \frac{\partial}{\partial q_1}\frac{m(\dot{x}^2+\dot{y}^2+\dot{z}^2)}{2}\right]\delta q_1 = (F_x\frac{\partial x}{\partial q_1} + F_y\frac{\partial y}{\partial q_1} + F_z\frac{\partial z}{\partial q_1})\delta q_1 \tag{B.31}$$

But, we know that $\frac{1}{2}m(\dot{x}^2+\dot{y}^2+\dot{z}^2)$ is the kinetic energy, T, of the particle being considered.

Hence:

$$\frac{d}{dt}(\frac{\partial T}{\partial \dot{q_1}}) - \frac{\partial T}{\partial q_1} = F_x\frac{\partial x}{\partial q_1} + F_y\frac{\partial y}{\partial q_1} + F_z\frac{\partial z}{\partial q_1} \tag{B.32}$$

Equation (B.32) is the Lagrangian equation, that can be re-written conveniently as follows:

$$F_x\frac{\partial x}{\partial q_1} + F_y\frac{\partial y}{\partial q_1} + F_z\frac{\partial z}{\partial q_1} = F_{q_r} \tag{B.33}$$

Whereby q_r is one of the chosen coordinates appearing in T and F_{q_r} is referred to as the *generalized force*. The Lagrangian equation can be compacted to take the following general form:

$$\frac{d}{dt}(\frac{\partial T}{\partial \dot{q_r}}) - \frac{\partial T}{\partial q_r} = F_{q_r} \tag{B.34}$$

Important things to be noted with Equation (B.34):

- For a rotational system, the left hand side accounts for all the inertial forces.
- The right hand side accounts for all the driving forces/generalised forces.
- The are as many Lagrangian equations of motion as there are degrees of freedom, a system that has two degrees of freedom will have two Lagrangian equations.
- When forces are conservative, it is usually more convenient to determine F_{q_r} from a potential energy function.

The work done can be finally represented as follows:

$$\delta W_{q_r} = F_{q_r} \delta q_r \tag{B.35}$$

Conservative Systems - Potential Functions

In general analysis of work done for a particle, the work done does not depend on the length or shape of the path taken by the particle moving from (x_0, y_0) to (x, y). When the system is displaced from one configuration to another, the work done by the forces depends only on the initial and final coordinates of the particles. This behaviour of forces is commonly referred to as conservative. An example of conservative forces is as follows:

- Gravitational forces between masses
- Forces due to all types of springs and elastic bodies
- Forces between stationary electric charges

Examples of non-conservative forces:

- Frictional forces
- The drag on an object moving through fluid
- Externally applied forces/torques on an object

The work done by conservative forces in a transfer of the system from a general configuration A(where coordinates of the particles are x_1, y_1, z_1 ... etc.) to a reference configuration B(coordinates now ${}_0x_1$, ${}_0y_1$, ${}_0z_1$, ... etc.) is defined as the potential energy $V(x_i, y_i, z_i)$ which the system as point A has with respect to point B.

The Lagrange's equations for conservative systems, and this is only where motion is as a result of conservative forces acting is:

$$\frac{d}{dt}\left(\frac{\partial T}{\partial \dot{q_r}}\right) - \frac{\partial T}{\partial q_r} = -\frac{\partial V}{\partial q_r} \tag{B.36}$$

Which can also be rearranged as follows:

$$\frac{d}{dt}(\frac{\partial T}{\partial \dot{q_r}}) - \frac{\partial (T-V)}{\partial q_r} = 0 \tag{B.37}$$

By introducing the *Lagrangian function* L, which is defined to be $L = T - V$, then equation (B.37) can be modified as follows:

$$\frac{d}{dt}(\frac{\partial L}{\partial \dot{q_r}}) - \frac{\partial L}{\partial q_r} = 0 \tag{B.38}$$

It is permissible to replace T with L in $\frac{\partial T}{\partial \dot{q_r}}$, because in the usual mechanical problem, V is not a function of $\dot{q_r}$.

When some of the forces acting on the system are non-conservative, the Lagrangian equation can be written in the following way:

$$\frac{d}{dt}(\frac{\partial L}{\partial \dot{q_r}}) - \frac{\partial L}{\partial q_r} = F_{q_r} \tag{B.39}$$

Where F_{q_r} accounts for the non-conservative forces.

For a system with p-particles with conservative forces $F_1, F_2, ...F_p$, the potential energy can be calculated using the following formula:

$$V = \int_{x_i, y_i, z_i}^{{}^0x_i, {}^0y_i, {}^0z_i} \sum_{i=1}^{p} (F_x dx_i + F_y dy_i + F_z dz_i) \tag{B.40}$$

This can also be written as follows:

$$V = -\int_{{}^0x_i, {}^0y_i, {}^0z_i}^{x_i, y_i, z_i} \sum_{i=1}^{p} (F_x dx_i + F_y dy_i + F_z dz_i) \tag{B.41}$$

Note:

$$F_{x_i} = -\frac{\partial V}{\partial x_i} \tag{B.42}$$

$$F_{y_i} = -\frac{\partial V}{\partial y_i} \tag{B.43}$$

$$F_{z_i} = -\frac{\partial V}{\partial z_i} \tag{B.44}$$

In general, the generalised forces can be expressed as follows, when V is expressed in generalised coordinates:

$$F_{x_i} = -\frac{\partial V}{\partial q_r} \tag{B.45}$$

Note, it can also be shown that for conservative forces, the following is true:

$$\frac{\partial F_{q_r}}{\partial q_s} = \frac{\partial F_{q_s}}{\partial q_r} \tag{B.46}$$

B.5 Gimbal Performance Characteristics

In this section the parameters affecting the gimbal's performance characteristics are discussed and some general notes are made based on gimbal manufacturers observations and conclusions based on various experiments and an extensive experience.

An important parameter to be monitored is the acceleration of the gimbal, which is often measured in units of (*degrees per second*^{2}), and it is generally combined with the payload inertia in order to establish how much torque is required to increase or decrease the speed of the payload. When we consider the required *continuous* azimuth rotation, the gimbal can sweep continuously in one direction, however, it is worth mentioning that special hardware (such as slip rings and rotary joints) is required to prevent damage to the gimbal and payload wiring. The elevation travel range is defined as rotational travel in the elevation axis, and zero degrees typically represents horizontal.

In general, the inertia is defined as the object's resistance to changing its speed or direction. For most applications, the payload inertia is a critical factor in the gimbal performance. The reader is reminded that inertia is a function of the object's size, weight, and the location of the centre of gravity relative to the axis of rotation. As can be seen from Appendix A, an inertial sensor can be used to stabilise the gimbal platform, however, it must be noted as well that this sensor can be influenced by the earth's motion as well as the motion of the gimbal itself. This results in the slow and cumulative error in pointing, which is formally referred to as *drift*. When selecting the sensor, attention needs to be paid to the fact that its quality is often directly related to the amount of drift. Also, the drift in many *inexpensive* sensors is a function of temperature, hence the drift can be mitigated by applying temperature-compensating software or simply by maintaining the sensor at a constant temperature.

Pointing accuracy is formally defined as the absolute error between the reference pointing position and the actual pointing position. This pointing accuracy is a function of the gimbal

structure, its drive train, position instruments, the control software and the payload. Another factor which is also relevant to gimbals that have installed position measuring instruments (such as encoders or resolvers) is the *position resolution*, which is thought of as the smallest increment of a degree of angular motion that has to be measured by the instrument.

Repeatability is generally the gimbal's ability to point to exactly the same point in space when it is commanded to point to a specific position. The reader must be aware that a gimbal that possesses perfect repeatability will always point to the same point in space when it is provided with the same coordinates, but the point it goes to may still be off-target by the value of the pointing accuracy.

Another important measure is the *settling time*, which is a function of the mechanical stiffness of the gimbal and payload structures, the control software and the structure that the gimbal is mounted on. Settling time is formally defined as a measure of how long it takes for the gimbal and payload to come to rest after moving from one point to another. An industry rule of thumb is that weight has an equivalent effect to stiffness, meaning that a lightweight gimbal with heavy payload will have a higher settling time than a heavy gimbal with the same payload.

The *slew rate*, which is typically measured in *degrees per second*, is commonly known as the angular velocity of the gimbal and payload. The slew rate can also be used to determine the type of actuation (servo or stepping motors required) and the ratio of the maximum and minimum slew rates is an indicator of the variation in required speed. Industrial gimbals generally use either servo or DC motors or a stepping motor. The operational range of voltages is from 12 V DC and 48 V DC. The voltage is dictated by the size of the gimbal and its torque requirements. This is also linked to the maximum power requirements, which in general depend on the payload mass and inertia, system slew rates and accelerations.

When it comes to the airborne applications of gimbals, issues to be taken very seriously during the assembling stage or even design stage is whether it is going to be operating in a pressurised or unpressurised aircraft environment. If the environment is unpressurised, then from the given operating altitude, the temperature and air pressure can be obtained from the standards related to aircraft equipment. Also, when wind load or wind disturbances outside the aircraft begin to affect the gimbal, the operating air speed and altitude become crucial to the structural requirements of the gimbal and the actuator torque requirement to overcome the disturbances.

Other disturbances can arise from the aircraft vibration and rotor vibration. Wind loads can produce high frequency vibrations in the gimbal, and it has been observed that unless the vibrations are low frequency ones, it is usually not economical to attempt to stabilise a gimbal against wind loads. Often, it is better to use a heavier, stiffer gimbal with a much more rigid interface between the gimbal and the payload in an effort to *damp* out the vibrations.

The orientation of the gimbal platform with respect to its axes is one of the most important structural considerations. In a typical application, a pan/tilt gimbal is designed to be oriented with the pan axis below the tilt axis. This then results in the following motion operation, when the pan axis moves, the payload and the tilt axis are also turned, but when the tilt axis moves, only the payload is turned.

B.5.1 Parameter Specifications

Acceleration

Most standard industrial/commercial gimbal products are designed for accelerations in the range of 1-2 *radians per seconds*^{2}. Ideally, the payload inertia is matched to the rotor inertia of the motor in order to obtain the best performance.

Slew rate

Generally, for long-range surveillance system applications, the minimum slew rate is more critical, because the field of view is very narrow, and high slew rates result in the user being unable to see objects as they flash across the lens. As a general rule of thumb, the human eye is able to easily track objects at up to 12 degrees per second, provided that the field of view is wide enough that the object is in view for several seconds. As the field of view narrows, the slew rate also must be reduced to give a person time to recognise and follow an object. Slew rates of a fraction of degrees per second can be achieved with proper actuator drive ratios and/or control electronics. On the other hand, very high slew rates with a heavy payload can become limited by the speed/torque curve of the motor or simply by the power supply. As an example, a system using a high drive ratio to obtain a very slow slew rate will then have the top speed limited by the maximum *rpm* of the motor, or by a loss of torque at high motor speeds. Similarly, motors can be voltage limited at high speeds because the power supply is inadequate to overcome the back EMF generated at the motor.

B.5.2 Control Regulator Problem

When considering a stabilised system, the corollary to pointing accuracy is line-of-sight stability, which is the ability to maintain a specific pointing vector in response to base motion in the mounting platform. The selection of the instrument for position measurement becomes even more complex because in addition to having to resolve motion less than the specified stability, the gimbal must also be able to react quickly enough to correct for the motion before the error

becomes too large. As the magnitude and frequency of the errors increase, the demand on the instruments, control system, and drive trains will increase.

Appendix C

Project Management

C.1 Time Lines

Figure C.1 illustrates the projected time line for the major milestones of the project. The progress took many forms in order to comply with the proposed timelines. Various delays were encountered and dealt with in various ways, some included improvising by deserting certain routes completely. Overall, the projected time frame for completion was met.

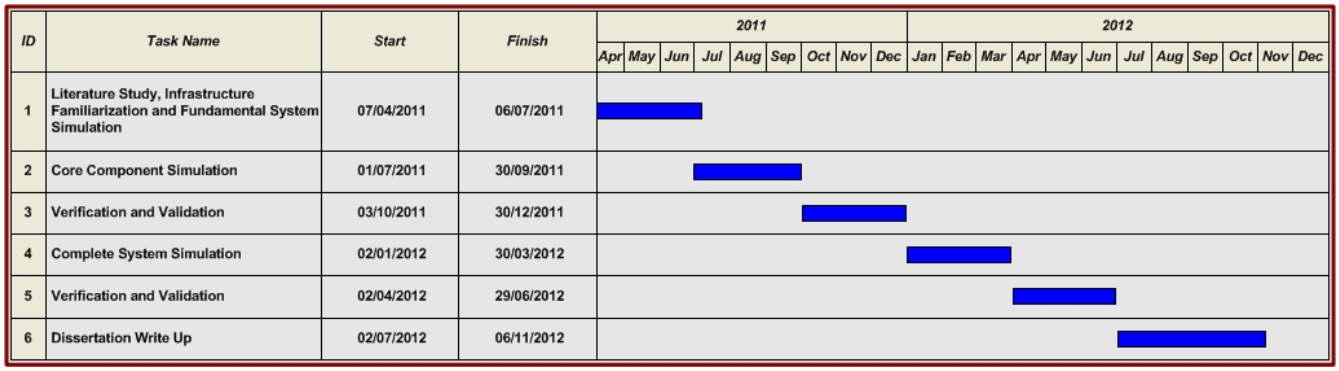

ID	Task Name	Start	Finish
1	Literature Study, Infrastructure Familiarization and Fundamental System Simulation	07/04/2011	06/07/2011
2	Core Component Simulation	01/07/2011	30/09/2011
3	Verification and Validation	03/10/2011	30/12/2011
4	Complete System Simulation	02/01/2012	30/03/2012
5	Verification and Validation	02/04/2012	29/06/2012
6	Dissertation Write Up	02/07/2012	06/11/2012

Figure C.1: Gantt Chart indicating original projected time line of the project

Appendix D

Financial Considerations

Often the budget for a positioning system (gimbal) is overlooked in the planning phase of a project. It is generally assumed that the gimbal will be an off-the-shelf solution or very inexpensive solution, regardless of the performance requirements. When developing an integrated system, there is a tendency to establish a price point based on the payload cost, only to discover that the budget no longer has room for the appropriate gimbal system. When planning a project budget, the major cost drivers for the gimbal platform are the pointing accuracy, positional resolution, payload capacity, and, for stabilised systems, the line-of-sight stability.

D.1 Gimbal Cost

The **RIEtech Global** gimbals are available from $6800 USD (R60 920.52) to $70000 USD (R627 123), depending on specification and complexity requirements.

D.2 Experimental Equipment Cost

1. Micropilot AutoPilot (R100 000)[**never purchased**]
2. Arduino starter kit R914.85.
3. Optical incremental encoder (Agilent AEDA-3200-Txx series) R1437.34.

D.3 Denel Dynamics Test Cost

The total cost for the **Denel Dynamics** test required to extract an accurate model of the system and a vibration disturbance performance is R29 700, and the break down is as follows:

- The initial test (2 day duration) was going to be the **modal test** to be carried out on the aircraft costs R19 800,
- The seconds test (1 day duration) was going to be the aircraft & gimbal assembly **vibration test** costs R9 900.

D.3.1 Resources

The resources that the Denel Dynamics personnel where planning to use to concuct the test are summarized below.

- To conduct the modal test on the aircraft, the plan was to suspend the aircraft in bungee's hanging about 300 mm from the ground and place about 20 accelerometers. The aircraft was to be excited using a 220 N shaker, using sine sweeps and random noise for generality. The transfer function was to be measured from the input to the accelerometers, and mode shapes would be inferred from the results.
- To excite the modal frequencies, they were planning to used the LMS TESTLAB V11.00 software, LMS SCADA III front end, and MB DYNAMICS MB50 shaker and amplifier.
- To measure the response, they were planning on using the PCB load cells and ADXL accelerometers, and the LMS TESTLAB V11.00 software, LMS SCADA III front end.
- To inject the vibration on the shaker, they planned on using the LING dynamic shaker using spectral dynamics PUMA control system.

D.4 Overall UAV Project Cost

The roughly estimated development cost of the UAV project (including the gimbal platform and multi-sensor camera on-board) is **R1.5 Million**, and the helicopter UAV contributes about **R650 000** towards that total estimated cost. After a considerable amount of conversations with the project team, especially all those who began with the project back in the mid-1990's, they all have an estimated cost of about **R100 000** for the whole system when it finished, fully integrated and placed on the store shelves for purchase. Obviously, since the system is not there yet, this projected cost will change. It all depends on the final costing of everything that was used and at the relevant market price.

D.5 Projected Control Cost

The robust controller implemented for the gimbal assembly and its accompanying hardware is therefore projected to cost around ±R10 000, this is also taking into account the design and assembling fee. Once again, this is a rough, inexperience figure, which will depend on the consultation with the marketing/commercialising experts, and an accurate account of the resources used.

Appendix E

List of Abbreviations

AHRS - Attitude and Heading Reference System
CAD - Computer Aided Design
CG - Center of Gravity
CSIR - Council for Scientific and Industrial Research
DC - Direct Current
D-H - Denavit-Hartenberg
DOF - Degree of Freedom
FOV - Field of View
FOPDT - Frst-Order Plus Dead Time
FOPTD - First-Order Plus Time Delay
GA - Genetic Algorithm
GMVC - Generalised Minimum Variance Control
GPS - Global Positioning System
HV - High Voltage
IAE - Integral Absolute Error
IMU - Inertial Measurement Unit
IR - Infrared
ISE - Integral Square Error
ISP - Inertial Stabilised Platform
ITAE - Integral Time Square Error
ITSE - Integral Time Square Error
LFT - Linear Fractional Transform
LHP - Left Hand Plane
LOS - Line of Sight
LQR - Linear Quadratic Regulator
LQG - Linear Quadratic Gaussian
LTI - Linear Time Invariant
LTR - Loop Transfer Recovery

MIMO - Multiple Input Multiple Output
MISO - Multiple Input Single Output
MSM - Material Science and Manufacturing
MRAC - Model Reference Adaptive Control
MV - Medium Voltage
MW - MegaWatt
NN - Neural Network
UAV - Unmanned Aerial Vehicle
PID - Proportional Integral Derivative
PTZ - Pan Tilt Zoom
PWM - Pulse Width Modulation
QFT - Quantitative Feedback THeory
R-UAV - Rotary Unmanned Aerial Vehicle
SA - South Africa
SISO - Single Input Single Output
RC - Radio Control
SST - Sensor Science Technology
UV - Ultraviolet

References

[1] M. Garcia-Sanz. *"Quantitative Robust Control Engineering: Theory and Applications"*. RTO-EN-SCI-166, May 12-14 2006. Educational Notes RTO-EN-SCI-166.

[2] V.S. Murthy, K. Tarakanath, D.K. Mohanta, and S. Gupta. *"Insulation Condition Analysis for Overhead Distribution Lines Using Combined Wavelet Support Vector Machine"*, volume 17. IEEE Transaction on Dielectrics and Electrical Insulation, 2010.

[3] S. Montambault and N. Pouliot. *"The HQ LineROVer: Contribution to Innovation in Transmission Line Maintenance"*. IEEE, 2003. 03ESMO0070.

[4] G. Earp. *"Condition Based Risk Assessment of Electricity Towers Using High Resolution Images from a Helicopter"*. 18th International Conference on Electricity Distribution, 6-9 June 2005. CIRED, Session No. 3.

[5] D. Jones, I. Golightly, J. Roberts, and K. Usher. *"Modeling and Control of a Robotic Power Line Inspection Vehicle"*. IEEE International Conference on COntrol Applications, Munich, Germany, October 4-6 2006. WeB08.4.

[6] D.I. Jones. *"Power Line Inspection - An UAV Concept"*. The IEE Systems Engineering Professional Network. University of Wales, Bangor.

[7] J. Sawada, K. Kusumoto, T. Munakata, Y. Maikawa, and Y. Ishikawa. *"A Mobile Robot for Inspection of Power Transmission Lines"*, volume 6(No. 1. IEEE Transactions on Power Delivery, January 1991. Tokyo Electric Power Inc. and Toshiba Corporation, Japan.

[8] R.K. Aggarwal, A.T. Johns, and J.A.S.B. Jayasinghe. *"An Overview of the Condition Monitoring of Overhead Lines"*, volume 53. 2000. Electric Power Systems Research, Elsevier.

[9] D.I. Jones. *"Aerial Inspection of Overhead Power Lines Using Video: Estimation of Image Blurring Due to Vehicle and Camera Motion"*, volume 147. April 2000. IEE Proc-Vis. Image Signal Process.

[10] G. Jaensch, H. Hoffmann, and A. Markees. *"LOcating Defects in High Voltage Transmission Lines"*. IEEE, 1998. 9837-C-ESMO-16.

[11] IOL. *"IOL Business Report"*. Independent Online. http://www.iol.co.za/business/business-news/.

[12] ESKOM. ESKOM SOC. http://www.eskom.co.za/.

[13] M.K. Masten. *"Inertially Stabilized Platform for Optical Imaging Systems : Tracking Dynamic Targets with Mobile Sensors"*. Control Systems Magazine, IEEE, 2008.

[14] J. Hilkert. *"Inertially Stabilized Platform Technology: Concepts and Priciples"*. Control Systems Magazine, IEEE, 2008.

[15] H.G. Wang and T.C. Williams. *"Strategic Inertial Navigation Systems: High-Accuracy Inertially Stabilized Platforms for Hostile Environments"*. IEEE Control Systems Magazine, February 2008. Digital Object Identifier 10.1109/MCS.2007.910206.

[16] J.L. Weston and D.J. Titterton. *"Modern Inertial Navigation Technology and Its Application"*. Electronic and Communication Engineering Journal, April 2000.

[17] C.J. von Klemperer and V.E. Verijenko. *"Design, Analysis and Construction of a Composite Camera GImbal"*, volume 54. ELSEVIER, Composite Structures, 2001.

[18] K.J. Astrom H. Panagopoulos and T. Hagglund. *"Design of PID controllers based on constrained optimisation"*. IEE Proceedings online No. 20020102, 2002.

[19] P. Cominos and N. Munro. *"PID Controllers: recent tuning methods and design to specification"*. Number 1. IEEE proceeding, control theory application, 149 2002.

[20] P. Mhaskar, N. H. El-Farra, and P. D. Christofides. *"A Method for PID Tuning Using Nonlinear Control Techniques"*. American Control Conference, Boston, 30 2004.

[21] S. Puntunan and M Parnichkun. *"Online Self-Tuning Precompensation for a PID Heading Control of a Flying Robot"*. International Journal of Advanced Robotic Systems, 2006. last accessed 02-08-13.

[22] DOLEZEL, Pert, MARES, and Jan. *"Self-Tuning PID Control using Genetic Algorithm and Artificial Neural Networks"*. University of Pardubice, Faculty of Electrical Engineering and Informatics. last accessed 12/04/11.

[23] S. Omatu and M. Yoshioka. *"Self-Tuning Neuro-PID Control and Applications"*. Department of computer and System Science, College of Engineering, Osaka Prefecture University, Sakai, Japan. last accessed 12/04/11.

[24] F. Lin, R.D. Brandt, and G. Saikalis. *"Self-Tuning of PID Controllers by Adaptive Interactions"*. Proceedings of the American Control Conference, Chicago, Illinois, 2000.

[25] C.L.S. Carari, D. Vrabie, and M. Kloetzer. *"Neuro-Predictive Control Based Self-Tuning of PID Control"*. ESANN 2004 Proceedings European Symposium on Artificial Neural Networks, 2004.

[26] D. Vrancic, J. Kocijan, and S. Strmcnik. *"Simplified Disturbance Rejection Tuning Method for PID Controllers"*. Department of Systems and Control, J. Stefan Inistitute, Jamova 39, Slovenia. last accessed 12/04/11.

[27] B.R. Copeland. *"The Design of PID COntrollers using Ziegler Nichols Tuning"*. 2008. last accessed 12/04/11.

[28] K. Seong, H. Kang, B. Yeo, and H. Lee. *"The Stabilization Loop Design for a Two-Axis Gimbal System Using LQG/LTR Controller"*. SICE-ICASE International Joint Conference, October 10-21 2006. Bexco, Busan, Korea.

[29] J. Rocha and J. Sequeira. *"The Development of a Robotic System for Maintenance and Inspection of Power Lines"*. Institute for Systems and Robotics, Torre Norte, Av. Rovisco Pais 1, Portugal.

[30] D.I. Jones, C.C. Whitworth, G.K. Earp, and A.W.G. Duller. *"A Laboratory Test-Bed for an Automated Power Line Inspection System"*, volume 13 (2005). Control Engineering Practice, Elsevier, 2004. www.elsevier.com/locate/conengprac.

[31] L. Ma and Y. Chen. *"Aerial Surveillance System for Overhead Power Line Inspection"*. Center for Self-Organizing and Intelligent Systems (CSOIS), Department of Electrical and Computer Engineering, College of Engineering, Utah State University, USA, December 2004.

[32] H.B.S. Segundo, V. Fuster, L. Perez, and P. Mayorga. *"Automated Inspection of Electric Transmission Lines: The Power Supply System"*. IEEE, 2006.

[33] I. Golightly and D.I. Jones. *"Visual Control of an Unmanned Aerial Vehicle for Power Line Inspection"*. IEEE, 2005.

[34] C.C. Whitworth, A.W.G. Duller, D.I. Jones, and G.K. Earp. *"Aerial Video Inspection of Overheard Power Lines "*. Power Engineering Journal, February 2001.

[35] M. Williams, D.I. Jones, and G.K. Earp. *"Obstacle Avoidance During Aerial Inspection of Power Lines"*, volume 73 (No. 5). Aircraft Engineering and Aerospace Technology, 2001. MCB University Press.

[36] L. Mejias, J.F. Correa, I. Mondragon, and P. Campoy. *"COLIBRI: A Vision-Guided UAV for Surveillance and Visual Inspection"*. IEEE International Conference on Robotics and Automation, 10-14 April 2007. ThC12.2.

[37] D.I. Jones and G.K. Earp. *"Camera Sightline Pointing Requirements for Aerial Inspection of Overhead Power Lines"*, volume 57. Electric Power Systems Research, Elsevier, 2001. PII: S0378-7796(01)00100-6.

[38] K. Kawada, T. Shiino, T. Yamamoto, M. Komichi, and T. Nishioka. *"Data-Driven PD Gimbal Control"*. Hiroshima University, Hiroshima, Japan: CIMCA 2008, 2008.

[39] U.B. Hald, M.V. Hesselbaek, J.T. Holmgaard, C.S. Jensen, S.L. Jakobsen, and M. Siegumfeldt. *"Autonomous Helicopter - Modelling and Control"*. Department of Control Engineering, Aalborg University, May 2005.

[40] M. Draper, G. Calhoun, and J. Nelson. *"Evaluation of Synthetic Vision Overlay Concepts for UAV Sensor Operation: Landmark Cues and Picture-in-Picture"*. Human Effectiveness Directorate, Warfighter Interface Division, Air Force Research Laboratory, February 2006.

[41] C. Urmson, J. Anhalt, M. Clark, T. Galatali, J.P. Gonzalez, J. Gowdy, A. Gutierrez, S. Harbaugh, M. Johnson-Robertson, Y.H. Kato, P. Koon, K. Peterson, B. Smith, S. Spiker, E. Tryzelaar, and W. Wittaker. *"High Speed Navigation of Unrehearsed Terrain: Red Team Technology for Grand Challenge 2004"*. The Robotics Institute Carnegie Mellon University, 5000 Forbes Avenue, Pittsburgh, June 1 2004. CMU-RI-TR-04-37.

[42] R.T. Rudin. *"Strapdown Stabilization for Image Seekers"*. 2nd Annual AIAA SDIO Interceptor Technology Conference, June 6-9 1993.

[43] F.N. Barnes. *"Stable Member Equations of Motion for a Three-Axis Gyro Stabilized Platform"*, volume AES-7 (No. 5). IEEE Transaction on Aerospace and Electronic Systems, September 1971. Lockheed Electronics, Houston.

[44] J. Osborne, G. Hicks, and R. Fuentes. *"Global Analysis of the Double-Gimbal Mechanism: Dynamics and Control on the Torus"*. IEEE Control Systems Magazine, August 2008. Digital Object Identifier: 10.1109/MCS.2008.924794.

[45] T.L. Vincent. *"Stabilization for Film and Broadcast Cameras"*. Application of Control, IEEE Control Systems Magazine, February 2008. Digital Object Identifier: 10.1109/MCS.2007.911392.

[46] B. Michini. *"Modeling and Adaptive Control of Indoor Unmanned Aerial Vehicles"*. Department of Aeronautics and Astronautics, Massachusetts Institute of Technology, September 2009. Master of Science in Aeronautics and Astronautics.

[47] C. Lidstone. *"The Gimballed Helicopter Testbed: Design, Build and Validation"*. System Control Group, Department of Electrical and Computing Engineering, University of Toronto, 2003. Msc Dissertation.

[48] W.S. Griffin and M. Beach. *"Stabilized Sighting Device for Vehicles"*. United States Patent, July 19 1983.

[49] W.S. Griffin and M. Beach. *"Two-Axis Optical Inertial System Using A Gyro Rotor As A Stable Reference"*. United States Patent, May 5 1987.

[50] N. Yonemoto, K. Yamamoto, K. Yamada, H. Yasui N. Tanaka, C. Migliaccio, J-Y. Dauvignac, and C. Pichot. *"Performance of Obstacle Detection and Collision Warning System for Civil Helicopters"*. Electronic Navigation Research Institute (ENRI), Japan and Electronics, Antennas and Telecommunication Laboratory (LEAT), France. Last Accessed 13-12-2012.

[51] B.B. Bederson, R.S. Wallace, and E.L. Schwartz. *"Two Miniature Pan-Tilt Devices"*. International Conference on Robotics and Automation, IEEE, May 1992. France.

[52] D.R. Otlowski, K. Wiener, and B.A. Rathbun. *"Mass Properties Factors in Achieving Stable Imagery from a Gimbal Mounted Camera"*, volume 6946. Society of Photo-Optical Instrumentation Engineers (SPIE), Airborne Intelligence, Surveillance, Reconnaissance (ISR) System and Application V, 2008. Space Electronics LLC, 81 Fuller Way, Berlin, CT, USA 06037.

[53] K. Tiimus and M. Tamre. *"Camera Gimbal Control System for Unmanned Platforms"*, volume 7. 7th International DAAAM Baltic Conference, 22-24 April 2010. Tallinn, Estonia.

[54] J.Nygards, P. Skoglar, M. Ulvklo, and T. Hogstrom. *"Navigation Aided Image Processing in UAV Surveillance: Preliminary Results and Design of an Airborne Experimental System"*, volume 21(2). Journal of Robotic System, Wiley InterScience, 2004. www.interscience.wiley.com.

[55] F.M. Broilo. *"Modeling of a Gimbal Azimuth Drive and Simulation of Control Techniques"*. B.S. Electrical Engineering, New Mexico Institute of Mining and Technology, 2010. RIEtech Global and Sagebrush Technology Project.

[56] P. Skoglar. *"Modelling and control of IR/EO-gimbal for UAV surveillance applications"*. Linkoping Institute of Technology, Applied Physics and Electrical Engineering (SIREOS Project), June 06 2002.

[57] M.J. Monda, C.A. Woolsey, and C.K. Reddy. *"Ground Target Localization and Tracking in Riverine Environment from a UAV with a Gimbaled Camera"*. American Institute of Aeronautics and Astronautics Guidance, Navigation and Control Conference and Exhibition, August 2007. 20-23 Aug, Hilton Head, South Carolina.

[58] S. Stolle and R. Rysdyk. *"Flight Path Following Guidance for Unmanned Air Vehicles with Pan-Tilt Camera for Target Observation"*. IEEE, 2003.

[59] V.N. Dobrokhodov, I.I. Kaminer, K.D. Jones, and R. Ghabcheloo. *"Vision-Based Tracking and Motion Estimation for Moving Targets using small UAVs"*. American Control Conference, IEEE, June 14-16 2006. Minneapolis, Minnesota, USA.

[60] M. Quigley, M.A. Goodrich, S. Griffiths, A. Eldredge, and R.W. Beard. *"Target Acquisition, Localization, and Surveillance Using a Fixed-Wing Mini-UAV and Gimbaled Camera"*. International Conference on Robotics and Automation, IEEE, April 2005. Barcelona, Spain.

[61] J.D. Redding, T.W. Mclain, R.W. Beard, and C.N. Taylor. *"Vision-Based Target Localization from a Fixed-Wing Miniature Air Vehicle"*. American Control Conference, IEEE, June 14-16 2006. Minneapolis, Minnesota, USA.

[62] F. Rafi, S. Khad, K. Shafiq, and M. Shah. *"Autonomous Target Following by Unmanned Aerial Vehicles"*. Computer Vision Lab, Department of computer science, University of Central Florida, Orlando FL, USA.

[63] A. Harris, J.J. Sluss, and H.H. Refai. *"Alignment and Tracking of a Free-Space Optical Communication Link to a UAV"*. IEEE, 2005. University of Oklahoma, USA.

[64] Z. Hurak and M. Rezac. *"Combined Line-of-Sight Inertial Stabilization and Visual Tracking: Application to an Airborne Camera Platform"*. Joint 48th IEEE Conference on Decision and Control and 28th Chinese Control Confernece, December 16-18 2009.

[65] F. Rafi, S. Khan, K. Shafiq, and M. Shah. *"Autonomous Target Following by Unmanned Aerial Vehicles"*. Computer Vision Lab, Department of Computer Science, University of Central Florida, USA.

[66] J.L. Cooper and M.A. Goodrich. *"Integrating Critical Interface Elements for Intuitive Single-Display Aviation Control of UAVs"*. Brigham Young University, USA.

[67] D. Antolovic, B. Himebaugh, and S.D. Johnson. *"SKEYEBALL: Real-Time Vision System for an Autonomous Model Airplane"*. IEEE, 2003.

[68] M. Quigley, B. Barber, S. Griffiths, and M.A. Goodrich. *"Towards Real-World Searching with Fixed-Wing Mini-UAVs "*. Computer Science Department and Mechanical Engineering Department, Brigham Young University, Provo, USA.

[69] O. Amidi, T. Kanade, and R. Miller. *"Vision-Based Autonomous Helicopter Research at Carnegie Mellon Robotics Intitute"*, volume T7-3. Carnegie Mellon University, Robotics Institute, School of Computer Science, 1998. American Helicopter Society.

[70] C.S. Sharp, O. SHakernia, and S.S. Sastry. *"A Vision System for Landing an Unmanned Aerial Vehicle"*. International Conference on Robotics and Automation, IEEE, May 21-26 2001.

[71] E.N. Johnson and D.P. Schrage. *"The Georgia Tech Unmanned Aerial Research Vehicle: GTMax"*. School of Aerospace Engineering, Georgia Institute of Technology, Atlanta, GA 30332-0150, May 2002.

[72] O.C. Jakobsen and E.N. Johnson. *"Control Architecture for a UAV-Mounted Pan/Tilt/Roll Camera Gimbal"*. American Institute of Aeronautics and Astronautics, September 2005. 26-29 Sept Arlington, Virginia.

[73] C. Chen and Y. Teng. *"Multirate Digital Servo Drive Based on Acceleration Observer and Disturbance Compensator"*. Proceedings of the 17th world congress The International Federation of Automatic Control (IFAC), July 6-11 2008. Seoul, Korea.

[74] T. Shiino, K. Kawada, T. Yamamoto, M. Komichi, and T. Nishioka. *"Gimbal Control wiht the Camera for Aerial Photography in RC Helicopter"*. International Conference on Control, Automation and System, October 14-17 2008. COEX, Seoul, Korea.

[75] K. Kawada, T. Shiino, T. Yamamoto, M. Komichi, and T. Nishioka. *"Data-Driven PD Gimbal Control"*. CIMCA 2008, IAWTIC 2008 and ISE 2008, IEEE Computer Society, 2008. DOI 10.1109/CIMCA.2008.184.

[76] M.J.L. Tiernego and J.J. van Dixhoorn. *"Three-Axis Platform Simulation: Bond Graph and Lagrangian Approach"*. Journal of The Franklin Institute, Pergamon Pres. Ltd. Twente University of Technology, Department of Electrical Engineering, The Netherlands.

[77] J.M. Hilkert and M. Jonas. *"A Unique Three-Axis Gimbal Mechanism"*, volume 6971 (69710E). Proceedings of SPIE, 2008.

[78] M. Baumker, F.J. Heimes, H. Hahn, W. Klier, R. Brechtken, and T. Richter. *"Mathematical Modeling, Computer Simulation, Control and Applications of a Stabilized Platform of an Airborne Sensor"*, volume XXXIII (Part B2). International Archives of Photogrammetry and Remote Sensing, 2000. Amsterdam.

[79] J. Fang, S. Zheng, and B. Han. *"AMB Vibration Control for Structural Resonance of Double-Gimbal Control Moment Gyro with High-Speed Magnetically SUspended Rotor"*. IEEE/ASME Transaction of Machatronics, 2011. Digital Object Identifier: 10.1109/TMECH.2011.2161877.

[80] R. Singh, M. Hanmandlu, S. Khatoon, and V.K. Madsu. *"Modeling and Simulation of the Dynamics of a Large Size Stabilized Gimbal Platform Assembly"*, volume 1(2). Asia International Journal of Science and Technology in Production and Manufacturing, 2008.

[81] O.J. Hernandez and J.A. Alamia. *"Precision Stabilization Simulation of a Ball Joint Gimbal Mirror Using Advanced MATLAB Techniques"*. IEEE, 2009.

[82] H. Khodadadi, M.R.J. Motlagh, and M. Gorji. *"Robust Control and Modeling a 2-DOF Inertial Stabilized Platform"*. International COnference on Electrical, Control and Computer Engineering, June 21-22 2011. Pahang, Malaysia.

[83] L.A. Ingham, T. Jones, and A. Maneschijn. *"Certification of Unmanned Aerial Vehicles in South African Airspace"*, volume 22 (1). R and D Journal, incorporated into The SA Mechanical Engineer, 2006.

[84] B. Siciliano and O. Khatib. *"Springer Handbook of Robotics"*. Springer-Verlag Berlin Heidelberg, 1st edition, 2008.

[85] D.A. Wells. *"SCHAUM'S OUTILES - Theory and Problems of Lagrangian Dynamics"*. McGraw-Hill, University of Cincinnati, 1 edition, October 1967.

[86] K.S. Fu, R.C. Gonzalez, and C.S.G. Lee. *"ROBOTICS: Control, Sensing, Vision and Intelligence"*. McGraw-Hill Book Company, 1987.

[87] I.J.M. Besselink. *"Vehicle Dynamic Analysis Using SimMechanics and TNO Delft-Tyre"*. TNO Automotive - Eindhoven University of Technology, The Netherlands.

[88] *"Matlab function reference"*. Mathworks. http://www.mathworks.com.

[89] G. Zames. *"Feedback and Optimal Sensitivity: Model Reference Transformations, Multiplicative Seminorms, and Approximate Inverses"*, volume AC-26, No. 2. IEEE Transaction On Automation Control, April 1981.

[90] I. Horowitz. *"Quantitative Feedback Theory"*, volume Vol. 129 Pt. D, No. 6. IEE Proceedings, November 1982.

[91] P. Skoglar. *"Modelling and control of IR/EO-gimbal for UAV surveillance applications"*. Linkoping Institute of Technology, Applied Physics and Electrical Engineering (SIREOS Project), 2002. ISRN LITH-ISY-EX-3258-2002.

[92] *"RIEtech Global - Gimbal Selection guide"*. RIEtech Global.

[93] L.v. Wenge, L. Deyuan, C. Siyuan, L. Shaoming, Z. Xiangwei, and Z. Linhai. *"Research on PID Control Parameters Tuning Based on Election-Survey Optimization Algorithm"*. IEEE Computer Society, 2010 International Conference on Computing, Control and Industrial Engineering, 2010. Supported by National Science Foundation (50676022).

[94] A.E.A Awouda and R.B Mamat. *"Refine PID Tuning Rule using ITAE Criteria"*, volume 5. IEEE, 2010.

[95] J.D Mohammad, S.G. Kambiz, S.M.H. Seyedkashi, and M. Behnam T. *"Novel Simulated Annealing Algorithm in Order to Optimal Adjustment of Digital PID Controller"*. IEEE, 11th International Conference on Control, Automation, Robotics and Vision, Singapore, 7-10th December 2010. ICARCV2010.

[96] J.P. Hespanha. *"Undergraduate Lecture Notes on LQR/LQG controller design"*. April 1 2007. Last accessed:30-08-2012.

[97] S. Hossain. *"Design of a Robust Controller for a Magnetic Levitation System"*. Last accessed:30-08-2012.

[98] S.P. Bhattacharyya, H. Chapellat, and L.H. Keel. *"ROBUST CONTROL: The Parametric Approach"*. Prentice Hall PTR, January 1995.

[99] K.J. Astrom and R.M. Murray. *"FEEDBACK SYSTEMS: An Introduction for Scientists and Engineers"*. Princeton University Press, January 2011. http://www.cds.caltech.edu/ murray/amwiki.

[100] B.A. Francis. *"Lecture Notes in Control and Information Science: A Course in H-infinity Control Theory"*, volume 88. Springer-Verlag, May 1986. Edited by M. Thoma and A. Wyner.

[101] L. Brezina and T. Brezina. *"H-Infinity Controller Design for a DC Motor Model with Uncertainty Parameters"*, volume 18. Engineering MECHANICS, May 5 2011. No. 5/6.

[102] A. Kruezek and A. Stribrsky. *"H-Infinity Control of Automotive Active Suspension with Linear Motor"*. CTU, Faculty of Electrical Engineering, Department of Control Engineering, Karlovo namesti.

[103] N. Nawash. *"H-Infinity Control of an Autonomous Mobile Robot"*. Cleveland State University: Bachelor of Science in Electrical Engineering, May 2005. Msc Thesis.

[104] H. Kwakernaak. *"Robust Control and H-Infinity Optimization - Tutorial Paper"*. IFAC Symposium, 1993. Last accessed:30-08-2012.

[105] S.S. Nair. *"Automatic Weight Selection Algorithm for Designing H-Infinity Controller for Active Magnetic Bearing"*, volume Vol. 3, No. 1. International Journal of Engineering Science and Technology (IJEST), January 2011. ISSN:0975-5462.

[106] R.W. Beaven, M.T. Wright, and D.R. Seaward. *"Weighting Function Selection in the H-Infinity Design Process"*, volume Vol. 5, No. 5. Control Eng. Practice, Elsevier Science Ltd., 1996. PII:S0967-0661(96)00044-5.

[107] J.E. Bibel and D.S. Malyevac. *"Guidlines for the Selection of Weighting Functions for H-Infinity Control"*. Naval Surface Warfare Center: Dahlgren Division, January 1992. NSWCDD/MP-92/43.

[108] W. Chen and D.J. Ballance. *"Stability Analysis On the Nichols Chart and its Application in QFT"*. Centre for Systems and Control, Department of Mechanical Engineering, University of Glasgow, UK., August 1997.

[109] C.H. Houpis. *"Fundamentals of the Quantitative Feedback Theory Technique"*, volume Vol IX. Control Systems, Robotics and Automation.

[110] M. Garcia-Sanz, A. Mauch, C. Philippe, and C.H. Houpis. *"The QFT Control Toolbox (QFTCT) for MATLAB: User's Guide"*. Case Western Reserve University, 2011. http://cesc.case.edu.

[111] W. Chen, D.J. Ballance, and Y. Li. *"Automatic Loop-Shaping in QFT Using Genetic Algorithms"*. Centre for Systems and Control, Department of Mechanical Engineering, University of Glasgow, UK., May 7 1998.

[112] A.A. Akbari, M.R. Gharib, and E. Karrabi. *"Comparison QFT Controller Based on Genetic Algorithm with MIMO Fuzzy Approach in a Robot"*. 5th SASTech, Khavaran Higher-education Institute, Mashhad, Iran, May 12-14 2011.

[113] V.S. Bokharaie and A. Khaki-Sedigh. *"Optimal Design of Robust Quantitative Feedback Controllers Using Linear Programming and Genetic Algorithms"*. K.N. Toosi University of Technology.

[114] H. Mansor, S.B.M. Noor, R.K.R. Ahmad, and F.S. Taip. *"Online Quantitative feedback theory (QFT) -based self-tuning controller for grain drying process"*, volume Vol. 6(31). Scientific Research and Essays, December 16 2011. http://www.academicjournals.org/SRE.

[115] J.C. Moreno, A. Banos, and M. Berenguel. *"The Design of QFT Robust Compensators with Magnitude and Phase Specifications"*, volume Vol. 2010. Hindawi Publishing Corporation, Mathematical Problems in Engineering, December 27 2010. Research Article.

[116] G. Happawana. *"Quantitative Feedback Theory and Sliding Mode Control"*. Department of Mechanical Engineering,California State University, Fresno, California, USA.

[117] E. Boje. *"Quantitative Feedback Design for Systems with Probabilistic Parameterisations"*. Proceedings of the First African Control Conference.

[118] S.M. Mahdi Alavi and Martin J. Hayes. *"Quantitative Feedback Design for a Benchmark Quadruple-Tank Process"*. ISSC 2006, Dublin Institute ofTechnology, June 28-30 2006.

[119] M. Barbu and S. Caraman. *"QFT Robust Control of Wastewater Treatment Processes"*. Dunarea de Jos University of Galati, Romania.

[120] Q.T. Dinh, K.K. Ahn, and J.I Yoon. *"Introduction to Quantitative Feedback Theory For Robust Force Control of Load Simulator"*. IEEE, 2008. 1-4244-2426-9/08.

[121] M.R. Gharib, A.A.A. Moghadam, and M. Moavenian. *"Optimal Controller Design for Two Arm Manipulators using Quantitative Feedback Theory Method"*. 24th International Symposium on Automation and Robotics in Construction (ISARC 2007), 2007. Construction Automation Group, I.I.T, Madras.

[122] H. Mansor, A.H. Zaeri, S.B.M. Noor, R.K.R. Ahmad, F.S. Taip, and H.I Ali. *"Design Of Qft Controller For A Bench-Top Helicopter System Model"*, volume Vol. 11, No. 5. IJSSST.

[123] W.D. Phillips. *"SELECTION OF A FREQUENCY SENSITIVE QFT WEIGHTING MATRIX USING THE METHOD OF SPECIFIED OUTPUTS"*. AIR FORCE INSTITUTE OF TECHNOLOGY, AFIT/GAE/ENG/88D-01, December 1988. THESIS.

[124] J.J.E. Slotine and W. Li. *"Applied Nonlinear Control "*. Prentice Hall, Englewood Cliffs, New Jersey 07632, 1991. Chapter 1, 3, 7 and 8.

[125] W. Chen and D.J. Ballance. *"Stability Analysis On the Nichols Chart and Its Application in QFT"*. Centre for Systems and Control, Department of Mechanical Engineering, University of Glasgow, UK., August 1997.

[126] C. ADRIAN, A. CORNELIU, and B. MIRCEA. *"The simulation of the adaptive systems using the MIT rule"*. 10th WSEAS International Conference on Mathematical Methods and Computational Techniques in Electrical Engineering (MMACTEE), May 2-4 2008. Sofia, Bulgaria.

[127] S. Padmakumar, V. Agarwal, and K. Roy. *"A Tutorial on Dynamic Simulation of DC Motor and Implementation of Kalman Filter on Floating Point DSP"*. World Academy of Science, Engineering and Technology 53, 2009.

[128] S. Ayasun and G. Karbeyaz. *"DC Motor Speed Control Methods Using Matlab/Simulink and their Intergration into Undergraduate Electric Machinery Courses"*. Wiley Perioicals Inc., 2007. http://www.interscience.wiley.com.

[129] P. Wolm, X.Q. Cheng, J.G. Chase, W. Pettigrew, and C.E. Hann. *"Analysis of a PM DC Motor Model for Application in Feedback Design for Electric Powered Mobility Vehicles"*. 15th International Conference on Mechatronics and Machine Vision in Practice (M2VIP08), 2-4 December 2008.